2013

POLYMER MICELLES FOR TUNABLE DRUG RELEASE AND ENHANCED ANTITUMOR EFFICACY

Andrei G. Ponta
University of Kentucky, Andrei1800@gmail.com

STUDENT AGREEMENT:

I represent that my thesis or dissertation and abstract are my original work. Proper attribution has been given to all outside sources. I understand that I am solely responsible for obtaining any needed copyright permissions. I have obtained and attached hereto needed written permission statements(s) from the owner(s) of each third-party copyrighted matter to be included in my work, allowing electronic distribution (if such use is not permitted by the fair use doctrine).

I hereby grant to The University of Kentucky and its agents the non-exclusive license to archive and make accessible my work in whole or in part in all forms of media, now or hereafter known. I agree that the document mentioned above may be made available immediately for worldwide access unless a preapproved embargo applies.

I retain all other ownership rights to the copyright of my work. I also retain the right to use in future works (such as articles or books) all or part of my work. I understand that I am free to register the copyright to my work.

REVIEW, APPROVAL AND ACCEPTANCE

The document mentioned above has been reviewed and accepted by the student's advisor, on behalf of the advisory committee, and by the Director of Graduate Studies (DGS), on behalf of the program; we verify that this is the final, approved version of the student's dissertation including all changes required by the advisory committee. The undersigned agree to abide by the statements above.

Andrei G. Ponta, Student

Dr. Younsoo Bae, Major Professor

Dr. Jim Pauly, Director of Graduate Studies

POLYMER MICELLES FOR TUNABLE DRUG RELEASE AND ENHANCED ANTITUMOR EFFICACY

DISSERTATION

A dissertation submitted in partial fulfillment of the
requirements for the degree of Doctor of Philosophy in the
College of Pharmacy
at the University of Kentucky

By

Andrei Gheorghe Ponta

Lexington, Kentucky

Director: Dr. Younsoo Bae, Professor of Pharmaceutical Sciences

Lexington, Kentucky

2013

ABSTRACT OF DISSERTATION

POLYMER MICELLES FOR TUNABLE DRUG RELEASE AND ENHANCED ANTITUMOR EFFICACY

Cancer remains a leading cause of death in the United States. The most common treatment options include chemotherapy, but poor solubility, adverse side effects and differential drug sensitivity hamper clinical applications. Current chemotherapy generally aims to deliver drugs at the limit of toxicity, assuming that higher dosage increases efficacy, with little attention paid to potential benefits of tunable release. Growing evidence suggests that releasing drugs at a constant rate will be as effective as a single bolus dose. To test this hypothesis, it is critical to develop drug delivery systems that fine-tune drug release and elucidate the impact of tunable drug release rates on chemotherapeutic efficacy.

Block copolymer micelles, spherical nanoassemblies with a core-shell structure, are widely used in recent research. Micelles for this study were engineered to release a model drug (doxorubicin: DOX) at differential rates under acidic conditions, corresponding to tumor tissue (pH < 7). Three specific aims were pursued: to develop drug carriers capable of tuning drug release rates; to determine activity of developed carriers *in vitro*; and to elucidate effects of tunable drug release rates *in vivo*.

Block copolymers with covalently linked DOX were synthesized and self-associated, forming micelles. Drug binding linkers (glycine, aminobenzoate, or hydrazide) were used to tune release of DOX. Micelles were characterized to determine physicochemical properties such as particle size, drug entrapment yields, and drug release parameters. Characterization revealed that drug release profiles were modulated by interchanging drug binding linkers.

Micelles were evaluated *in vitro* to elucidate the effect of tunable drug release. Micelles delivered drugs at a slower, prolonged rate compared to free DOX. Cytotoxicity and cellular internalization analysis revealed that by slowing release rates, micelles kill cells more efficiently.

Biodistribution studies showed that micelles decrease DOX accumulation in peripheral tissue while increasing the maximum tolerated dose. Antitumor activity studies

verified that micelles with slower release rates better suppressed tumor growth. This further confirms that release rates play a key role in chemotherapeutic efficacy.

Therefore, this thesis provides better insights into the effects of tunable drug release in tumors, leading the way for improved chemotherapy treatments in the future.

Key words: Cancer, Chemotherapy, Drug Delivery Systems, Polymer Micelles, Tunable Drug Release

Andrei Ponta

12/13/13

POLYMER MICELLES FOR TUNABLE DRUG RELEASE AND ENHANCED ANTITUMOR EFFICACY

By

Andrei Gheorghe Ponta

Dr. Younsoo Bae
Director of Dissertation

Dr. Jim Pauly
Director of Graduate Studies

12/13/13

Dedicated To

My Wife and Family

ACKNOWLEDGEMENTS

I would like to express my thanks to a number of people who have helped and supported me throughout the course of my graduate studies. This would not have been possible without you.

First and foremost, I would like to thank my mentor and research advisor Dr. Younsoo Bae for the opportunity to work under his guidance. Over the past several years, I have evolved as an independent scientist with his help. I would also like to thank my committee members, Dr. Anderson, Dr. Bummer, and Dr. Hilt for sharing their valuable time, knowledge, and experience throughout my graduate studies. From Dr. Anderson's laboratory, I would like to recognize Kyle Fugit's efforts, as our collaboration solidified the dissertation herein. I would be remiss not to mention the Pharmaceutical Sciences Graduate Program staff for their support - especially Catina Rossol for guiding me through this arduous process. She has been available every step of the way, and if she didn't already know the solution to any issue that arose, she would make sure to point me in the right direction.

My former and current colleagues in Dr. Bae's lab have also aided me in this journey. From Dr. Hyun Jin Lee who helped me as I was just beginning to learn what it means to be a scientist, to Dr. Pengxiao Cao who was instrumental in preparing me to conduct *in vivo* studies. Dr. Daniel Scott, Dr. Matt Dickerson, Steven Rheiner, Amber Jerke, and Derek Reichel have all made long days in the laboratory a more pleasant and constructive experience. From other labs I would like to acknowledge Nayon Kang, Shanjida Akter, Allison Eckman, and JiAe Kim for the work we did together. Every

shared idea, collaboration, and late-night discussion helped pave the way for this dissertation, the culmination of my doctoral work.

Beyond the laboratory I would like to thank my friends. They were always there to listen and support me through everything. Deepest thanks go to my family - Aurora, Gheorghe, and Alice Ponta, who encouraged me to purse a PhD, furthering my education to the highest level possible. Last but certainly not least, I would like to extend my thanks to my wife, Lindsay (wove). She has been amazing and extremely understanding through even the hardest of times. I could not have done this without you. I love you.

Thank you all!

TABLE OF CONTENTS

LIST OF TABLES

LIST OF FIGURES

CHAPTER ONE

1 STATEMENT OF AIMS

Chemotherapy continues to play a major role in cancer therapy as viable cancer treatment options remain scarce (1). In an effort to improve current chemotherapeutic regimens, the nanotechnology field has developed a variety of nanotechnology-based drug delivery systems (NDDSs) including polymer micelles (2, 3), liposomes (4, 5), crosslinked nanoassemblies (6), and dendrimers (7). In preclinical and clinical studies, NDDSs have shown promise by increasing bioavailability, lowering toxicity, and enhancing solubility of chemotherapeutic agents (8-10). Because of these benefits, researchers have continued to develop more complex NDDSs with a myriad of capabilities, such as combination therapy (11), active targeting (12, 13), and imaging (14). Additionally, NDDSs have been designed to respond to environmental stimuli, releasing drug payloads in specific conditions (15-17). The design of this environmental responsive release is based on changes in pH (18-21), temperature (22, 23), redox potential (24-26), or enzymes (27).

While these factors provide a rationale for the use of NDDSs, recent developments in the field have focused on toxicity reduction (28, 29). Treatments often overlook the potential benefits of controlled drug release, and in most cases, chemotherapeutic agents are delivered at the limit of toxicity with the assumption that more drug equates to successful treatment (30). It has been observed that delivering drugs at a constant rate can be as effective, if not more so, than a single bolus dose (31-33). It is crucial to clarify the effects of controlled drug release to provide optimal treatment paradigms. It is therefore hypothesized that the elucidation of drug release effects will lead to enhanced antitumor efficacy.

To elucidate the antitumor effects of tunable drug release *in vivo*, three specific aims are proposed:

1.1 To Tune Drug Release Rates

To observe the effects of tunable drug release rates *in vitro* and *in vivo*, the tools capable of modifying drug release rates must first be developed. Polymer micelles have been selected as the NDDS of choice because of their promising results in clinical trials (21). Polymer micelles are typically composed of amphiphilic block copolymers. Based on concentration, block copolymers spontaneously form spherical nanoassemblies capable of carrying a drug payload (34). Herein, micelles will be prepared using modified poly(ethylene glycol)-poly(β-benzyl-L-aspartate) [PEG-p(BLA)] block copolymers. Through facile chemical modifications, drug binding linkers (HYD, ABZ-HYD, or GLY-HYD) will be introduced to the polymer backbone. The model drug doxorubicin (DOX) will be conjugated to the block copolymers using a hydrazone bond. Reconstituting final block copolymers in aqueous solution will produce polymer micelles. The hydrazone bond has been studied extensively in literature. The hydrolysis of the hydrazone bond has been shown to be pH-sensitive, as the bond is cleaved more rapidly in acidic conditions (35). A hydrazone bond enables polymer micelles to release DOX based on pH changes. Tuning release rates will be accomplished in one of two ways: adjusting hydrophobic unit chain length or inserting drug binding linkers. Drug release studies will confirm modified release rates. Initially, an all-encompassing drug release model will be used to determine the optimal method for tuning drug release rates (chain length versus drug binding linker). An in-depth analysis of drug release will be performed once a method for developing a polymer micelle system is established. A mathematical model describing

drug release will identify key differences between micellar formulations. Polymer micelles will be characterized thoroughly by determining their particle size, surface charge, and drug loading.

1.2 To Determine Activity of Carriers Modulating Drug Release in Vitro

Prepared polymer micelles will be tested *in vitro*. The human cancer cell lines DU145, A549, and HT29 will be used for cytotoxicity assays. The cytotoxicity of block copolymers will be determined, ensuring that only one active pharmaceutical ingredient is present in the micelle formulations. Additionally, the activity of DOX released from polymer micelles will be confirmed. Once the activity of DOX is established, the effects of drug release rates on cytotoxicity will be observed. Cells will be exposed to DOX, either as a free drug or in micellar formulations, for two different lengths of time: 48 and 72 hours. The half-maximal inhibitory concentration will then be determined for each treatment period. To better understand the impact of differential drug release, cellular internalization of free DOX will be compared to the internalization of DOX from polymer micelles. The uptake of block copolymers will also be examined.

1.3 To Elucidate Effects of Tunable Drug Release in Vivo

In vivo studies are required not only to further understand the effects of tunable drug release, but also to provide guidance to improve chemotherapeutic treatment. Xenograft models will be used for biodistribution and antitumor studies. The biodistribution of DOX, either from polymer micelles or as free DOX, will be analyzed. Polymer micelle treatment is expected to minimize DOX accumulation in peripheral tissue relative to treatment with free drug. The accumulation of polymer micelles at the tumor site will also be a key factor. With the exception of drug release rates, prepared polymer micelles

will be designed to have similar properties and will therefore be expected to accumulate similarly at the tumor site. Antitumor activity of polymer micelles and DOX will be evaluated. The efficacy of polymer micelles will elucidate the effect of tunable drug release. Depending on micellar treatment, the efficacy will vary as the drug release parameters change; providing a guide to optimize future treatments.

CHAPTER TWO

2 BACKGROUND

2.1 Cancer Chemotherapy

Cancer is the second leading cause of mortality in the United States, accounting for nearly one in every four deaths (36). Treatment options generally include surgery, radiation, chemotherapy, or, most commonly, a combination of the three (37). In the majority of cases, chemotherapy is used in some degree but is limited by toxic side-effects and drug resistance hindering the potential of most available drugs (38, 39). The differential drug sensitivity of cancer cells, depending on disease stages and lesions, also makes chemotherapy challenging (40-42). There are neither successful dosage forms nor therapeutic paradigms currently available to resolve these issues simultaneously.

2.2 Nanotechnology-Based Drug Delivery Systems

Recently, NDDSs using carriers such as water-soluble polymers, liposomes, and polymer micelles have been developed to circumvent issues associated with chemotherapeutic treatments (43, 44). These nanoparticle drug carriers have numerous advantages, including higher solubility, increased bioavailability, enhanced tumor accumulation, and lower adverse toxicity in comparison to free drug formulations (45-47). NDDSs generally contain both a hydrophobic and a hydrophilic component. Poorly-soluble drugs are incorporated into the hydrophobic section, while the hydrophilic segments enhance solubility (15). Particle size and surface modifications play key roles in the design of NDDSs. Carefully designed NDDSs exhibit reduced uptake by mononuclear phagocytes and prolonged circulation times. NDDSs with a poly(ethylene glycol) (PEG) shell are capable of avoiding the reticuloendothelial system (48, 49). At the same time, particles

larger than ~10 nm can circumvent renal clearance (50). It is important to note that tumor vasculature forms rapidly and irregularly, leaving fenestrations in the tumor blood vessels ranging from 100 nm to 1.2 μm, with the majority falling in the 380-780 nm range (51, 52). NDDSs are too large to penetrate healthy blood vessels but can accumulate intratumorally via these fenestrations (53). Therefore, NDDSs preferentially accumulate at tumor sites. This accumulation minimizes distribution of cancer therapeutics to peripheral tissue (54, 55). Additionally, tumors have poor lymphatic drainage, enhancing retention of NDDSs (56). This phenomenon is known as the enhanced permeation and retention (EPR) effect (51, 57). NDDSs can take advantage of the EPR effect, simultaneously decreasing the toxicity and enhancing intratumoral accumulation of chemotherapeutics. Drug accumulation at the tumor site after NDDSs treatment varies, ranging from a small percentage to upwards of 10% of the dose, while the uptake treatment with free drug is typically only around one percent (58). Several factors affect the drug accumulation from NDDSs treatment, including tumor size, tumor type, and physicochemical properties of the NDDS (58).

2.3 Tunable Drug Release

The development of NDDSs is typically focused on delivering chemotherapeutic agents as close to the maximum tolerated dose as possible. The potential benefits of rate of drug delivery are often overlooked. Studies have shown that chemotherapeutic efficacy *in vivo* depends both on drug dose and therapeutic schedules (59, 60). Growing evidence suggests that releasing chemotherapeutic agents at a slow rate will be as effective as a single bolus dose (61-63). Nevertheless, the primary focus of NDDSs research has been to improve solubility and tumor-specific accumulation of drugs (64-66). Targeted drug

delivery in conjunction with reduced toxicity can achieve considerable therapeutic efficacy, yet therapeutic potential of drug carriers is often over- or underestimated by the extent of tumor-specific drug delivery (67, 68). Recent studies have demonstrated that cancer cells exposed to smaller amounts of drug over longer periods appear to be at least as sensitive to chemotherapy as cells incubated with a higher drug dose for a shorter period (69). This supports the rationale that controlling the temporal distribution of anticancer drugs would significantly impact the therapeutic response of relative to conventional chemotherapy, potentially optimizing treatment methods. As such, it is critical to elucidate the effects of drug release rates on chemotherapeutic efficacy. To accomplish this goal, it is essential to develop nanoparticle drug carriers that are capable of fine-tune drug release.

2.4 Block Copolymer Micelles

Block copolymer micelles are attractive candidates as nanoparticle drug carriers. Polymer micelles have high drug loading capacity and high water solubility. Additionally, polymer micelles are easily modified (70, 71). Polymer micelles are composed of amphiphilic block copolymers that self-associate to form spherical nanoassemblies through an entropy-driven process (72, 73). Polymer micelles consist of a hydrophilic shell and a hydrophobic core. The core environment can play an important role in particle stability (74). Furthermore, poorly-soluble drug molecules can be incorporated into micelles by physical entrapment or chemical conjugation (75, 76). Hydrophobic and ionic interactions have also been used to facilitate physical drug entrapment. The early burst release of drugs is always a concern with physically-entrapped drugs (77-79). Burst release can be prevented by chemically conjugating therapeutic agents to the block

copolymer backbone (80, 81). The shell is frequently composed of a hydrophilic polymer such as PEG which can enhance drug solubility (82). An additional benefit to the core-shell structure is the resulting polymer micelle size, typically ranging from 10 to 100 nm. This size range enables polymer micelles to take advantage of the EPR effect (9, 83, 84). Animal studies show that polymer micelles can circumvent the body's defense system *in vivo*, leading to prolonged plasma retention time (12, 85-87).

2.5 PEG-poly(β-benzyl-L-aspartate) Block Copolymer Micelles

In this study, biocompatible block copolymer micelles were used to delineate the *in vitro* and *in vivo* effects of tunable drug release. Facile chemical modifications can be made to the core domain of polymer micelles without changing physicochemical properties (21). Herein, polymer micelles were prepared from block copolymers based on a PEG-p(BLA) scaffold. Modifications to the hydrophobic portion (BLA) of block copolymers led to differential drug release.

The overall design of block copolymers is shown in Figure 1. One of three drug binding linkers (HYD, ABZ-HYD, or GLY-HYD) was introduced into the PEG-p(BLA) scaffold (Figure 1A). The drug binding linkers were composed of hydrazide groups and spacers. The hydrazide groups were used to covalently attach the model drug DOX to block copolymers through a hydrazone bond. Final block copolymers were used to prepare micelles.

DOX was used as the model drug in this study due to its chemical characteristics. DOX contains a ketone group at its C13 position, allowing for facile hydrazone bond formation. It also possesses spectrometric advantages, as it is detectable by color and fluorescence. Additionally, the hydrazone linkage permits the release of the actual drug,

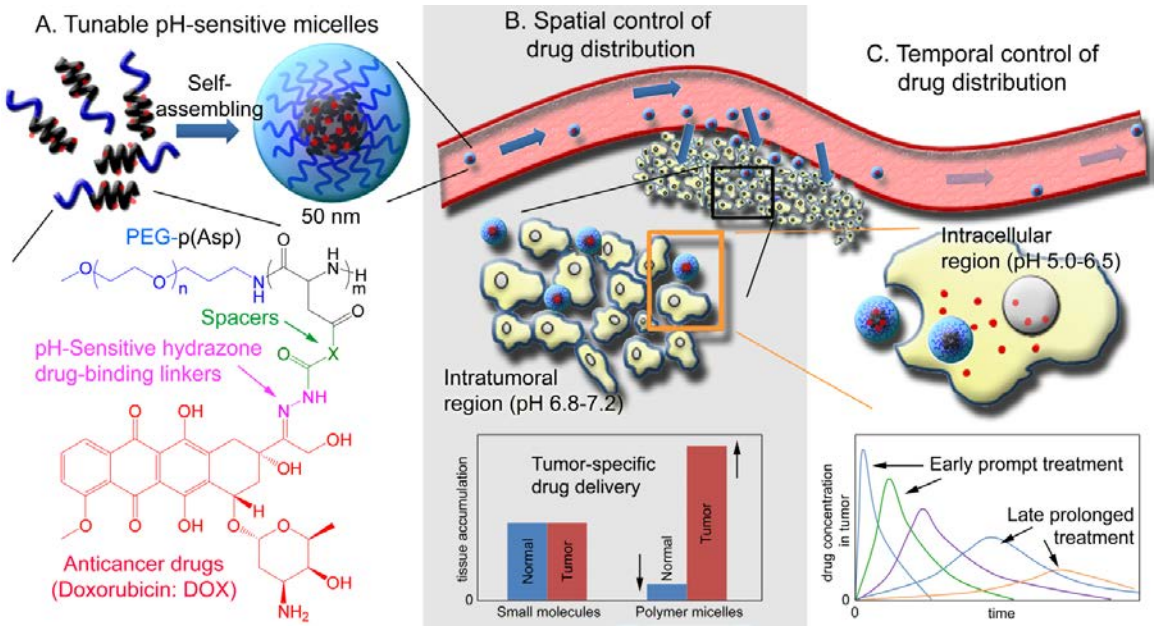

Figure 1. Spatial and Temporal Control of Drug Distribution Using Tunable pH-Sensitive Polymer Micelles

not an analogue while maintaining the structure of the block copolymer scaffold (88).

Hydrazone bonds are relatively stable at physiological pH but cleaved more rapidly in acidic conditions (89, 90). This Schiff base bond has been used extensively and the mechanism of hydrolysis has been established (91-93). It should be noted that the hydrolysis rates of hydrazone bonds vary depending on the functional groups adjacent to the hydrazide group (94, 95). By inserting a spacer prior to the hydrazide group, the hydrolysis rate of the hydrazone bond can be modified (35). In this study, the effects of ABZ and GLY spacers were explored.

It is known that the intratumoral pH is more acidic (6.8-7.2) than physiological pH (7.4). Intracellular pH in certain organelles is even lower, falling to 5.0 in endosomes and lysosomes (96). These pH variations permit hydrazone bound DOX to be released differentially (97, 98). This acidic pH-triggered release is key to observing the effects of release rates *in vitro* and *in vivo*. Herein, synthesized block copolymers contained hydrazone bound DOX. These block copolymers were used to prepared polymer micelles, which were expected to show differential drug release rates based on changes in pH. The hydrophobic portion of block copolymers was altered to further tune the release rates of DOX.

Developed polymer micelles herein served as a means to observe the effects of differential drug release rates on cells. The efficacy of DOX as a free drug was compared to DOX in a micellar formulation in an *in vitro* cell culture system. Efficacy was investigated in multiple cancer cell lines including colon, prostate, and lung cancer. Additionally, total DOX internalization was observed after treatment with free drug or micellar formulations. The combined results of efficacy and internalization studies

provided critical information on the effects of differential drug release. Results shed light on the potential benefits of tunable drug release.

Though *in vitro* analysis guided polymer micelle preparation, *in vivo* studies provided further information on the effects of tunable drug release. The antitumor efficacy of micellar treatments was compared to free drug treatment. Polymer micelles were expected to preferentially accumulate at the tumor site due to the EPR effect (Figure 1B). Polymer micelles herein were prepared from block copolymers with an identical number of hydrophilic repeating units; only the hydrophobic portions of block copolymers were modified. Block copolymer scaffolds underwent simple drug binding linker modification and covalent attachment of DOX. Therefore, micelles prepared from block copolymers were expected to have similar physicochemical properties. Preparing micelles with similar characteristics was expected to lead to comparable micellar tumor accumulation. Holding everything constant, the primary factor impacting antitumor efficacy was differential drug release. The antitumor efficacy of micellar formulations was observed, with each micelle formulation representing a different drug release profile (Figure 1C).

**Portions of Chapter 2 were previously published in (21). Reproduced with kind permission from Springer Science and Business Media: Pharmaceutical Research, Volume 27, 2010, pages 2330-2342, PEG-poly(amino acid) Block Copolymer Micelles for Tunable Drug Release, Andrei Ponta and Younsoo Bae, Figure 1, Copyright 2010 is given to the publication in which the material was originally published.

CHAPTER THREE

3 MODULATING DOXORUBICIN DRUG RELEASE UTILIZING POLYMER MICELLES BASED ON MODIFIED PEG-P(AMINO ACID) BLOCK COPOLYMERS

3.1 Introduction

This work focuses on the development and characterization of polymer micelles because of their versatility and prior success in preclinical and clinical atmospheres (99-103). Polymer micelles are spherical nanoassemblies generally prepared from amphiphilic block copolymers (104). Depending on concentration, block copolymers spontaneously form a characteristic core-shell structure. The core consists of the hydrophobic portion of block copolymers while the shell is composed of the hydrophilic portion. This structure enables polymer micelles to protect drug payloads and functional groups from the external environment (105, 106). It is hypothesized that drug release rates could be modulated by modifying the polymer micelle core. Herein, two factors affecting drug release are analyzed simultaneously: hydrophobic repeating unit chain length and drug binding linker modification.

Three block copolymer scaffolds based on PEG-p(BLA) were synthesized to prepare polymer micelles. Each scaffold has an increasing number of hydrophobic repeating units: 5, 15, and 35. The hydrophobic portion of these block copolymers was modified through the introduction of drug binding linkers; two such linkers were inserted into the scaffold: glycine-hydrazide (GLY-HYD) and aminobenzoate-hydrazide (ABZ-HYD). DOX, an FDA-approved chemotherapeutic, was subsequently conjugated to block copolymers through a hydrazone bond. The final block copolymers were then used to prepare micelles.

Literature shows that hydrazone bonds are relatively stable at physiological pH, whereas the bond can be cleaved in more acidic conditions (107, 108). The rate of hydrolysis can be altered by inserting a spacer (glycine or aminobenzoate) prior to the hydrazide moiety. Designing block copolymers with spacers adjacent to the hydrazide group was expected to modify drug release. This approach is one possible method of tuning drug release.

Block copolymers with an increasing number of hydrophobic repeating units (BLA) were synthesized. Preparing micelles from block copolymers with a greater number of BLA units was expected to produce a more hydrophobic core than micelles prepared from shorter chain length block copolymers. The change in hydrophobicity could in turn alter the stability of polymer micelles, thereby affecting drug release. This approach is a second possible method of tuning drug release.

A collection of six block copolymers with different compositions was synthesized to prepare polymer micelles. Drug release studies were analyzed to investigate the effects of drug-binding linkers and hydrophobic unit chain length. Furthermore, the efficacy of DOX, as a free drug or as a micellar formulation, was determined in two human cancer cell lines: DU145 and A549 (prostate cancer and non-small cell lung cancer, respectively). The cellular internalization of free DOX was also observed and compared to the internalization of DOX from micellar treatment. This critical information can provide insight on the impact of differential drug release rates.

3.2 Materials and Methods

3.2.1 Materials

L-aspartic acid β-benzyl ester, anhydrous hydrazine, benzene, blue dextran, N,N-dimethylformamide, triphosgene, anhydrous N,N-dimethylformamide (DMF), anhydrous dimethylsulfoxide (DMSO), doxorubicin hydrochloride (DOX), dimethylsulfoxide-d6 (DMSO-*d6*), anhydrous ethyl ether, anhydrous hexane, anhydrous tetrahydrofuran (THF), acetate buffer solution, phosphate buffer solution, methyl 4-aminobenzoate, O-benzotriazole-N,N,N',N'-tetramethyl-uronium-hexafluoro-phosphate (HBTU), and sodium hydroxide (NaOH) were purchased from Sigma-Aldrich (USA). Glycine-OMe was purchased from Novabiochem (SUI). α-Methoxy-ω-amino poly(ethylene glycol) [PEG-NH_2, molecular weight (MW) =12,266] was purchased from NOF Corporation (Japan). Regenerated cellulose dialysis bags [6,000-8,000 molecular weight cut off (MWCO)], Slide-A-Lyzer® dialysis cassettes (10,000 MWCO), Sephadex LH-20 gels, sterile filters (0.22 μm), and other cell culture supplies (e.g. 96-well culture plates, pipettes, and flasks) were purchased from Fisher Scientific (USA). Amicon-Ultra centrifugal ultrafiltration devices (30,000 MWCO) were purchased from Millipore (USA). Kaighn's modification of Ham's F-12 medium (F12-K), Dulbecco's modified Eagle's medium (DMEM), fetal bovine serum (FBS), trypsin-EDTA (0.25% trypsin and 2.21 mM EDTA) and the cell lines DU145 and A549 were purchased from ATCC (USA).

3.2.2 Monomer Synthesis

The Fuchs-Farthing method was used to prepare β-benzyl-L-aspartate N-carboxy anhydride (BLA-NCA) (109). Triphosgene (2.88 g, 9.7 mmol) was added to β-benzyl-L-

aspartate (BLA) (5.0 g, 22.4 mmol) in dry THF (100 mL) under N_2 at 45°C with constant stirring at 45°C under N_2. When the solution became clear, anhydrous hexane was slowly added until BLA-NCA crystals appeared and disappeared quickly. The final solution was stored in -20°C for BLA-NCA to produce needle-like BLA-NCA crystals which were used for block copolymer synthesis.

3.2.3 PEG-p(BLA) Block Copolymer Scaffold Synthesis

Three compositions of PEG-p(BLA) block copolymers were synthesized, each consisting of 12,000 MW PEG and an increasing number of BLA repeating units (5, 15, and 35). The number of BLA repeating units was precisely controlled by increasing the amount of BLA-NCA used in the reaction. PEG was freeze-dried prior to the reaction. Amine-activated PEG was used as an initiator for the ring-opening polymerization of BLA-NCA (15, 110). BLA-NCA monomer (0.46 µmol, 183 µmol, 361 µmol) and PEG (42 µmol, 183 µmol, 183 µmol) were placed in separate flasks and dissolved with anhydrous DMSO at a 50 mg/mL concentration. Dissolved monomers were then added to the PEG solution, and the polymerization was carried out with constant stirring at 45°C under N_2. Pure PEG-p(BLA) block copolymers were collected after repeated ether precipitation to remove DMSO. Briefly, polymer solution was added to excess ether in a conical tube. Contents were mixed and centrifuged. Supernatant was discarded, removing DMSO and other impurities. Solubility tests confirmed that PEG-p(BLA) precipitates in ether, while unreacted BLA readily dissolves in ether. The resulting polymer precipitate was dissolved in benzene and freeze-dried, producing a pure white polymer powder. Any remaining BLA was removed in the subsequent step of the synthesis process as block

copolymers were later dialyzed. Amine-activated PEG was no longer present since BLA-NCA was added in excess.

3.2.4 Drug Binding Linker Insertion and DOX Conjugation

Carbazate drug binding linkers were introduced to PEG-p(BLA) scaffolds. The BLA side chains were modified according to the following steps: deprotection, spacer coupling, and end-group functionalization with hydrazine (Figure 2). Benzyl groups of PEG-p(BLA) block copolymers were deprotected with 0.1 N NaOH, resulting in PEG-p(Asp) block copolymers. Freeze-dried PEG-p(Asp) (12 μmol) was coupled with methyl 4-aminobenzoate (ABZ-OMe) (130 μmol, 450 μmol, 680 μmol) or glycine methyl ester (GLY-OMe) (129 μmol, 400 μmol, 700 μmol) spacers. This reaction used HBTU to couple spacers to the Asp portion of block copolymers. The reaction was performed in DMF overnight with constant stirring at 45°C. The amount of spacers added to the reaction mixture was increased based on the number of Asp repeating units (5, 15, or 35). Side-chain modified block copolymers [PEG-p(Asp-ABZ) or PEG-p(Asp-GLY)] were thoroughly purified to remove unreacted ABZ-OMe and GLY-OMe. Products were first precipitated in ether and then dialyzed in a deionized water/methanol (50:50) solution. Finally, any remaining precipitates were removed by filtration.

An aminolysis reaction in DMF was used to replace methyl esters of the spacers with hydrazide. PEG-p(Asp-ABZ) (5.4 μmol, 6.8 μmol, 4.9 μmol) and PEG-p(Asp-GLY) (5.9 μmol, 6.5 μmol, 5.1 μmol) were reacted with fivefold excess hydrazine (134 μmol, 515 μmol, 856 μmol, and 145 μmol, 490 μmol, 890 μmol for the ABZ and GLY modified block copolymers, respectively). The reaction proceeded for one hour with constant stirring at 40°C. PEG-p(Asp-GLY-HYD) and PEG-p(Asp-ABZ-HYD) final

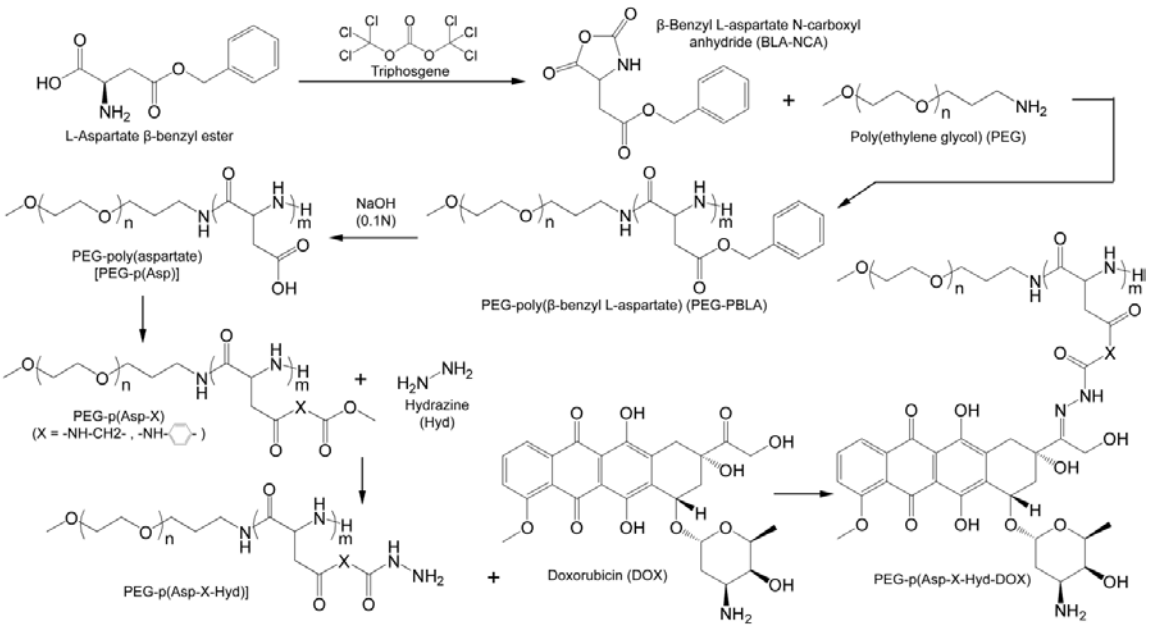

Figure 2. Synthesis Scheme for 12-5, 12-15, and 12-35 Block Copolymers with ABZ-HYD and GLY-HYD Drug Binding Linkers

products were collected. Impurities were removed through repetitive ether precipitation. Products were collected by freeze-drying.

PEG-p(Asp-GLY-HYD) and PEG-p(Asp-ABZ-HYD) block copolymers were conjugated with DOX in DMSO for two days at 30°C. Unreacted drug and DMSO were removed using ether precipitation. The resulting products were further purified by a Sephadex LH-20 column eluted with methanol to remove drug molecules physically bound to block copolymers. Block copolymers with shorter hydrophobic chain lengths (5 or 15) readily dissolved in methanol. Small amounts of DMSO were added to completely dissolve block polymers with longer hydrophobic chain lengths (35 repeating units) in methanol. The block copolymer fraction from the column was collected in a round-bottom flask. Methanol was removed by rotary evaporation. A thin film was produced after rotary evaporation. For block copolymers with five and 15 hydrophobic repeating units, the film was directly dissolved in benzene and subsequently freeze-dried. Block copolymers with 35 hydrophobic repeating units were poorly soluble in benzene and were therefore redissolved in DMSO. Products were precipitated in ether and collected by freeze-drying from benzene/methanol mixed solvents. UV-Vis colorimetric analysis at 480 nm was used to determine the degree of DOX conjugation for these block copolymers.

3.2.5 Polymer Micelle Preparation

Preparation of polymer micelles was carried out in one of two ways depending on the solubility of the final block copolymers. Irrespective of drug binding linker, shorter block copolymers were dissolved in deionized water and sonicated to prepare polymer micelles. Block copolymers containing 35 repeating units were found to be insoluble in deionized

water, so polymer micelles were prepared using a dilution method. Final block copolymers were dissolved in DMSO (<5 mg/mL) and subsequently titrated into a deionized water solution reaching a 0.5 mg/mL maximum concentration. DMSO was completely removed by repeated centrifugal ultrafiltration (30,000 MWCO) from deionized water. A clear concentrated polymeric micelle solution was obtained. UV-Vis colorimetric analysis at 480 nm was used to determine the drug loading content of the polymer micelles.

Each of the polymer micelles are referred to by the MW of PEG x 10^3 followed by the number of hydrophobic repeating units and the spacer used in the reaction. 12-5 GLY micelles refer to polymer micelles formed from block copolymers containing a GLY spacer with five hydrophobic repeating units. If the spacer was omitted, both ABZ and GLY polymer micelles are discussed. For example, 12-5 micelles refer to both 12-5 GLY and 12-5 ABZ micelles.

3.2.6 Analytical Methods

^{1}H-NMR measurements of block copolymers were performed in DMSO-*d6* at 300 MHz normal proton frequencies. The spectrometer was equipped with an FTS Systems preconditioning device. The device included an internal temperature controller, refrigerating unit, and inclusion transfer line. Measurement conditions were set at a temperature of 25°C for all samples.

Dynamic light scattering (DLS) was used to characterize polymer micelle size. Polymer micelles mean diameters were determined with a Zetasizer Nano-ZS (Malvern, UK) equipped with a He-Ne laser (4mW, 633 nm) light source and 173° angle scattered light collection configuration. The hydrodynamic diameter of polymer micelles was

calculated based on the Stokes-Einstein equation. The correlation function was curve-fitted by a cumulant method to calculate mean size. Block copolymers were dissolved in deionized water at a 2 mg/mL concentration and measurements were taken at room temperature. Three separate polymer micelle solutions were prepared for each block copolymer composition to provide a precise analysis. Particle size based on number average distributions was presented as the average diameter ± standard deviation.

Drug conjugation and loading were determined using a SpectraMax M5 (Molecular Devices, USA) equipped with variable spectrum filters and SoftMax Pro software. Absorbance was measured in aqueous solutions using a 96 well plate at 25 ºC. It was determined that DOX has a fingerprint peak at 480 nm by taking the absorbance spectra of DOX from 400 to 800 nm. PEG-p(Asp-GLY-HYD-DOX) and PEG-p(Asp-ABZ-HYD-DOX) spectra confirmed that the absorbance profile of DOX does not change after chemical modification. With DOX standards (0.98 to 250 μM), a calibration curve was prepared using the fingerprint peak at 480 nm. Drug loading and drug release were measured using this standard curve.

3.2.7 Drug Release Study

In preparation for release experiments, polymer micelle solutions (0.5 mL) were loaded into two Slide-A-Lyzer® (Thermo Scientific, USA) dialysis cassettes (10,000 MWCO). There were six sampling intervals so two cassettes were used for each individual experiment. The cassettes containing micellar solutions were placed in 4.0 L of 10 mM buffer solutions at two different pH conditions. For pH 5.0, sodium acetate buffer solution (0.01 M ionic strength) was used while potassium phosphate monobasic buffer solution (0.02 M ionic strength) was used for pH 7.4. The outer buffer solution pH was

measured periodically, verifying no pH drift. Additionally, manufacturer specifications indicated that sodium acetate buffer solution pH ranged from 5.00 to 5.02 at 37°C. Temperature was held constant at 37ºC throughout the drug release study to mimic physiological conditions. Similar to pH, the temperature of the buffer was measured regularly to ensure constant temperature. Samples were taken at 0, 0.5, 1, 3, 6, 24, and 48 hours. At each interval, at least 50 µL were withdrawn from dialysis cassettes and collected in microtubes to be stored for analysis. The first cassette was used for sampling up to the three hour time point, with the remainder of the samples taken from the second cassette. This experiment was done in triplicate.

3.2.8 In Vitro *Cytotoxicity*

Cytotoxicity of drug loaded polymer micelles and free DOX was observed in two cancer cell lines: DU145 and A549. Cells were cultured in a humidified atmosphere with 5% CO_2 at 37ºC. Cell culture media contained 10% FBS. DU145 cells were cultured in DMEM while A549 cells were cultured in F-12K. Cytotoxicity experiments were performed identically irrespective of cell line. Five thousand cells were seeded in 96-well plates and incubated for 24 hours. Cells were subsequently treated with solutions of free drug or micellar formulations at DOX-equivalent concentrations ranging from 10^{-5} µM to 100 µM. The highest attainable DOX-equivalent concentration of 12-5 micelles was 10 µM due to lower drug loading. The stability of block copolymers in media was not directly studied in this work, but similar systems reported no issues with stability in *in vitro* and *in vivo* studies (12, 86, 111). After 72 hours the number of viable cells was determined using a Resazurin assay (112). Each experiment was done in triplicate. The

half-maximal inhibitory concentration (IC50) was determined using Prism. The log (DOX concentration) versus response was fitted using nonlinear regression.

The solubility of free DOX was not an issue in the concentration range used for the *in vitro* studies. The highest concentration used herein was 58 µg/mL, while in the literature, DOX was used at higher concentrations in cell culture media (113). Furthermore, precipitates were not seen upon visual inspection.

3.2.9 DOX Cellular Uptake

DOX uptake was determined in the A549 cell line. The cell culturing conditions from cytotoxicity experiments were maintained in cellular uptake studies. Uptake studies were performed using 96-well plates. Ten thousand cells were plated in 96-well plates which were subsequently placed in an incubator. After 24 hours, media was removed and replaced with drug-containing media. Drug containing media was the same as cell culture media. Internalization of free DOX was first observed. Cells were treated with a 100 µM DOX solution. After 30 minutes, cell culture medium was removed and cells were washed with PBS three times. Any free DOX remaining in plate wells was removed by the PBS wash. DOX binding to the cells was not analyzed specifically but the PBS wash was expected to minimize binding. Additional experiments performed in chapter six confirmed free DOX removal after PBS washing. After the last wash, any remaining PBS was removed and cells were lysed with 100 µL of DMSO. This procedure was repeated for the following time intervals: 1, 3, 6, 24, 48, and 72 hours. DOX fluorescence was measured spectrometrically with an excitation at 490 nm and emission at 590 nm to determine DOX concentration. The excitation wavelength was selected at the absorbance

peak of DOX. Holding the excitation wavelength at 490 nm, the emission spectra showed a DOX peak at approximately 590 nm.

A calibration curve was prepared to quantify DOX concentration. DOX stock solutions were prepared in DMSO. A serial dilution was used to obtain a range of DOX concentrations (0.01-1000 μM). The fluorescence was measured and the results were plotted versus concentration to create a calibration curve. The linear range was from 0.1 to 20 μM DOX. These concentrations were used as the lower and higher limits of detection. The response factor was confirmed with a second set of standards. DOX concentration in the lysed cellular solution was determined based on this calibration curve.

DOX internalization in the presence of micelles was similarly observed. Experiments were conducted identically to studies of free DOX uptake. Cells were treated with solutions containing 12-15 GLY, 12-15 ABZ, and 12-35 GLY micelles at 100 μM DOX-equivalent concentrations. At the predetermined time points cells were lysed and the fluorescent signal related to DOX was measured (excitation at 490 nm and emission at 590 nm). These measurements included both free DOX and DOX conjugated to block copolymers. Conjugated DOX had a similar fluorescent spectrum to free DOX, thus the resulting fluorescent signal was the combined total of free DOX and conjugated DOX.

3.2.10 Statistics

Statistical analyses were performed using two-way ANOVA at 5% significance level combined with Bonferroni Multiple Comparison Test. Data were recorded as mean ±

standard deviation or standard error, as indicated. Experiments were repeated at least three times. GraphPad Prism (GraphPad Software, USA) was used for all data analysis.

3.3 Results

3.3.1 Denotation

Block copolymer compositions are in the form of X-Y, where X and Y denote PEG MW×10^3 and number of BLA repeating units, respectively. Modifications to the hydrophobic section of block copolymers are described sequentially, following Asp within the parenthesis. For example, PEG-p(Asp-GLY-HYD) describes PEG-p(Asp) block copolymers modified with a GLY spacer and a hydrazide moiety. ABZ and GLY micelles refer to micelles prepared from PEG-p(Asp-ABZ-HYD-DOX) and PEG-p(Asp-GLY-HYD-DOX) block copolymers, respectively.

3.3.2 Monomer and Block Copolymer Scaffold Synthesis

BLA-NCA monomers were synthesized successfully using a previously described protocol (72). Needle-like BLA-NCA crystals were collected after purification. Three PEG-p(BLA) block copolymer scaffolds were synthesized, with 5, 15, or 35 BLA repeating units. The number of BLA repeating units on each scaffold was altered by changing the amount of BLA-NCA monomers added to the reaction mixture. Increasing monomer concentration used in the reaction resulted in an increased number of BLA units on the block copolymer scaffold.

The number of BLA repeating units on each block copolymer scaffold was determined with ^{1}H-NMR. PEG (12,000 MW) had a prominent peak at 3.5 ppm (Figure 3A, denoted by letter a). The peak observed at 7.3 ppm represented the benzyl groups of BLA (Figure 3A, denoted by letter b). The number of BLA repeating units was

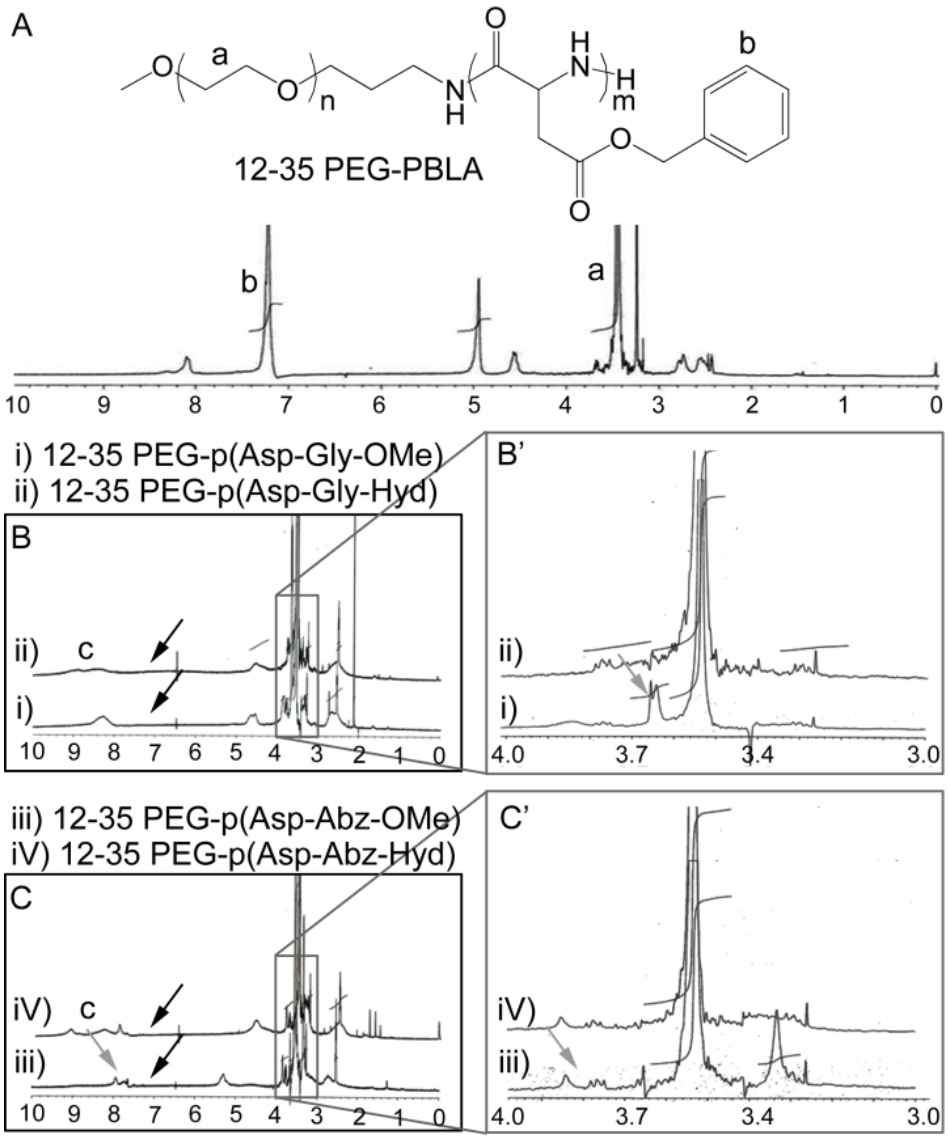

Figure 3. [1]H-NMR Spectra Confirming PEG-p(BLA) Synthesis (A) and ABZ-HYD or GLY-HYD Insertion (B and C)

determined using the ratio of the PEG peak area to the BLA peak area. The integral ratios, in the form of PEG:BLA, of the three block copolymers synthesized were 1091:25, 1091:77, and 1091:172. These ratios correspond to 5, 15, and 35 BLA repeating units. Final products yielded three PEG-p(BLA) block copolymer scaffolds which were subsequently modified with drug binding linkers.

3.3.3 Drug Binding Linker Insertion and DOX Conjugation

PEG-p(BLA) benzyl esters were removed after deprotection, producing PEG-p(Asp) block copolymers. GLY-OMe or ABZ-OMe spacers were coupled to the carboxyl groups of PEG-p(Asp) (Figure 3). A variety of methods and reaction conditions was tested in the coupling reaction until a protocol was established. DIC, NHS, and DMAP were used initially without success. Coupling with HBTU yielded the most promising results. The conjugation of GLY-OMe and ABZ-OMe to PEG-p(Asp) was confirmed using ^{1}H-NMR (Figure 3). Successful spacer conjugation, in either case, resulted in the insertion of methyl ester groups. It should be noted that unreacted GLY-OMe and ABZ-OMe were removed after dialysis. A portion of the ^{1}H-NMR spectra from 3 to 4 ppm was magnified to clearly see the appearance of methyl ester peaks. The peak related to GLY-OMe appeared at 3.7 ppm (Figure 3B', denoted by a gray arrow). The methyl ester peaks of ABZ-OMe at 3.8 ppm (Figure 3C', denoted by a gray arrow) were less prominent than their GLY-OMe counterparts, but ABZ benzyl peaks related to ABZ-OMe were observed at 7.8 ppm (Figure 3C, denoted by a gray arrow). In addition to confirming spacer insertion, ^{1}H-NMR spectra showed successful PEG-p(BLA) deprotection. The benzyl peak which originally resulted from BLA groups (Figure 3A) was not present in the ^{1}H-

NMR spectra of PEG-p(Asp-ABZ-OMe) or PEG-p(Asp-GLY-OMe) (Figure 3B and 3C, denoted by black arrows).

Block copolymer end-groups were functionalized by replacing methyl esters with hydrazine. ^{1}H-NMR spectra of hydrazide groups are represented by broad peaks at ~9 ppm. Methyl ester peak absence in conjunction with the appearance of broad peaks at 9 ppm in both ^{1}H-NMR spectra signified a successful reaction (Figure 3B and 3C, denoted by letter c). Specifically, PEG-p(Asp-GLY-OMe) ^{1}H-NMR spectra clearly showed the methyl ester peak disappearance 3.7 ppm after the hydrazide reaction (Figure 3B').

Though PEG-p(Asp) block copolymers were successfully modified with GLY-OMe and ABZ-OMe, quantification of the extent of reaction was not possible by ^{1}H-NMR due to peak overlap and broadening. Similarly, hydrazide insertion was not quantifiable. For these reasons, the minimal number of conjugation sites on each block copolymer was estimated by quantifying the drug molecules bound to block copolymers.

DOX was conjugated to PEG-p(Asp-ABZ-HYD) or PEG-p(Asp-GLY-HYD) block copolymers through a hydrazone bond (Figures 2 and 4). In previous studies, the reaction conditions for DOX conjugation have been optimized through extensive testing of different solvents, temperatures, and concentrations. These studies determined that the drug conjugation reaction between DOX and hydrazide groups does not require an acid catalyst in DMSO. Successful DOX conjugation produced PEG-p(Asp-ABZ-HYD-DOX) or PEG-p(Asp-GLY-HYD-DOX) block copolymers. Ether precipitation removed free DOX. Afterwards, a Sephadex LH-20 column eluted with methanol removed remaining unreacted drug molecules. Briefly, dissolved block copolymers were added to the column for separation. Two red bands were observed, each with its own distinct color. The darker

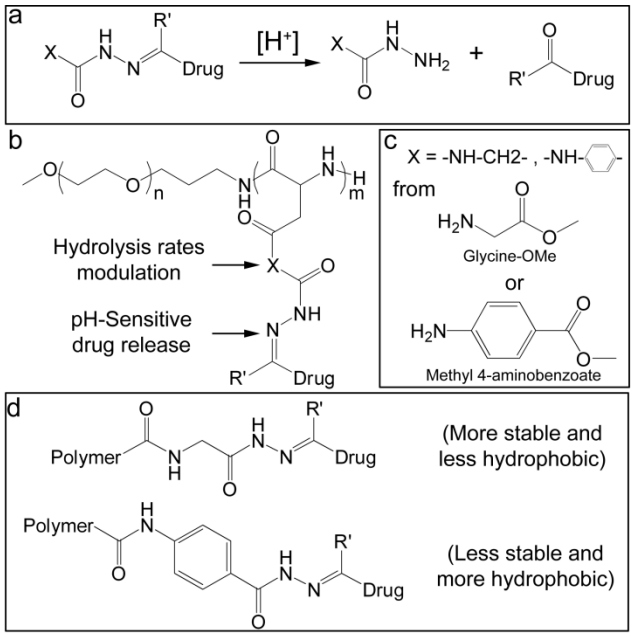

Figure 4. Proposed Mechanism of pH-Sensitive Drug Release

band passed through the column more quickly than the lighter band. The first, darker band contained polymer-drug conjugates. This fraction was collected in a round bottom flask. Rotary evaporation removed methanol and final products were collected after freeze-drying. Solubility of block copolymers in benzene varied, hampering product collection by simple reconstitution and freeze-drying. 12-5 and 12-15 block copolymers were dissolved in benzene and freeze-dried. However, 12-35 block copolymers were insoluble in benzene and were therefore dissolved in DMSO. Ether precipitation was used to remove DMSO. Resulting polymers were then freeze-dried from benzene/methanol mixed solvents.

DOX loading of final block copolymers was determined using UV-Vis spectrometry (Table 1). Drug loading was reported as weight/weight percent. For further analysis, the number of DOX molecules per block copolymer and the percentage of DOX molecules conjugated in proportion to available linkers were also calculated. DOX was successfully conjugated to all six block copolymers. With regard to weight/weight percent, drug loading increased as the number of hydrophobic repeating units increased. The drug loading of PEG-p(Asp-ABZ-HYD-DOX) and PEG-p(Asp-GLY-HYD-DOX) block copolymers increased from 4.0% to 11% and from 2.8% to 32%, respectively. It was apparent that increasing the hydrophobic chain lengths increased the number of DOX molecules conjugated to each block copolymer chain. The drug loading per conjugation site of PEG-p(Asp-GLY-HYD-DOX) block copolymers steadily increased from 13% to 44% as the chain length was extended from five to 35 repeating units. The same phenomenon was observed in 12-5 and 12-15 PEG-p(Asp-ABZ-HYD-DOX) block copolymers. Here, the drug loading per conjugation site increased from 20% to 23%.

Table 1. Drug Loading of 12-5, 12-15, and 12-35 Micelles

Compound	Composition	Drug loading weight %	DOX molecule/ block copolymer	Drug loading/ conjugation site (%)
PEG-p(Asp-GLY-HYD-DOX)	12-5	2.80 ± 0.1	0.7 ± 0.1	13 ± 0.2
	12-15	10.4 ± 0.4	3.0 ± 0.2	20 ± 0.9
	12-35	31.7 ± 0.1	15 ± 0.1	44 ± 0.1
PEG-p(Asp-ABZ-HYD-DOX)	12-5	4.10 ± 0.2	1.0 ± 0.1	20 ± 1.0
	12-15	10.9 ± 0.7	3.4 ± 0.2	23 ± 1.5
	12-35	11.5 ± 0.2	4.8 ± 0.1	14 ± 0.2

Data were obtained by triplicate measurements and shown as average ± standard deviation.

Interestingly, drug loading per conjugation site decreased to 14% for the 12-35 PEG-p(Asp-ABZ-HYD-DOX) composition. This result indicated that DOX was only conjugated to five out of a possible 35 drug binding sites. Increasing the number of Asp-ABZ-HYD repeating units increased the number of DOX conjugation sites, but this had a negligible effect on drug loading. The introduction of ABZ spacers prior to the hydrazone may have induced steric hindrance, hampering DOX conjugation. Other factors, including charge density, length of spacers, and lipophilicity of the micelle core may have played a crucial role not only in drug loading but also in drug release.

3.3.4 Polymer Micelle Preparation and Characterization

Polymer micelles were prepared from polymer-drug conjugates as described in the experimental section. Intriguingly, simply dissolving 12-5 and 12-15 block copolymers in aqueous solution readily produced uniform micelles. However, block copolymers with 35 repeating units precipitated in aqueous solution. For this reason, 12-35 micelles were prepared by an alternate method: block copolymers were dissolved in DMSO and then titrated in aqueous solution. DMSO was removed by centrifugal ultrafiltration.

Prepared micelles were thoroughly characterized. Micelle particle size was determined using DLS. The number average distribution was reported. This measurement accounted for effects of large particle outliers by reporting the particle size of each individual population. In all DLS measurements, more than 99% of particles fell into a single population. Each of the six block copolymer compositions formed micelles with a diameter less than 50 nm (Table 2). Notably, GLY micelles showed no significant difference among the three different compositions, maintaining a particle size between 40 and 45 nm. On the other hand, the particle size of ABZ micelles increased as the

Table 2. 12-5, 12-15, and 12-35 Micelle Particle Size Distribution

Compound	Composition	Particle size (nm)
PEG-p(Asp-GLY-HYD-DOX)	12-5	44 ± 9
	12-15	45 ± 11
	12-35	40 ± 5
PEG-p(Asp-ABZ-HYD-DOX)	12-5	11 ± 2
	12-15	24 ± 6
	12-35	43 ± 6

Data were obtained by triplicate measurements and shown as average ± standard deviation.

hydrophobic chain lengths increased. Particle sizes of 12-5, 12-15, and 12-35 ABZ micelles were 11, 24, and 43 nm, respectively. A similar particle size was observed with 12-35 ABZ and GLY micelles.

3.3.5 Drug Release Study

DOX release from micelles was observed over 48 hours. Seven measurements were taken during that period (0, 0.5, 1, 3, 6, 24, and 48 hours). There was unexpected drug release at pH 7.4 for all micellar formulations. At least 15% of DOX was released at 48 hours in every case (Figure 5). However, irrespective of micelle composition, DOX release was greater at pH 5.0 than at pH 7.4. 12-5 and 12-15 GLY micelles showed very similar drug release patterns at both pH 5.0 and pH 7.4. The extension of the hydrophobic chain length seemed to have had little effect on the release patterns for these two compositions. However, 12-35 GLY micelles had a different release profile, releasing the least amount of drug in both pH conditions. A similar pattern was observed with ABZ micelles. There was almost no difference in the release profiles of 12-5 and 12-15 ABZ micelles, while 12-35 ABZ micelles released DOX the least. A trend was observed, with shorter chain length micelles maintaining similar release profiles, while longer chain length micelles released DOX more slowly.

The total DOX release over a 48 hour period was analyzed to clarify pH effects (Figure 6). At pH 7.4, 12-5 GLY micelles released 30% of DOX, which increased to 40% at pH 5.0. The 12-15 GLY formulation had similar drug release, with 44% of DOX released at pH 7.4 and 57% at pH 5.0. Overall, 12-35 GLY micelles released the lowest amount of DOX. At pH 7.4 17% of DOX was released while only 37% was released at pH 5.0. 12-5 and 12-15 ABZ micelles had larger differences in total drug release between

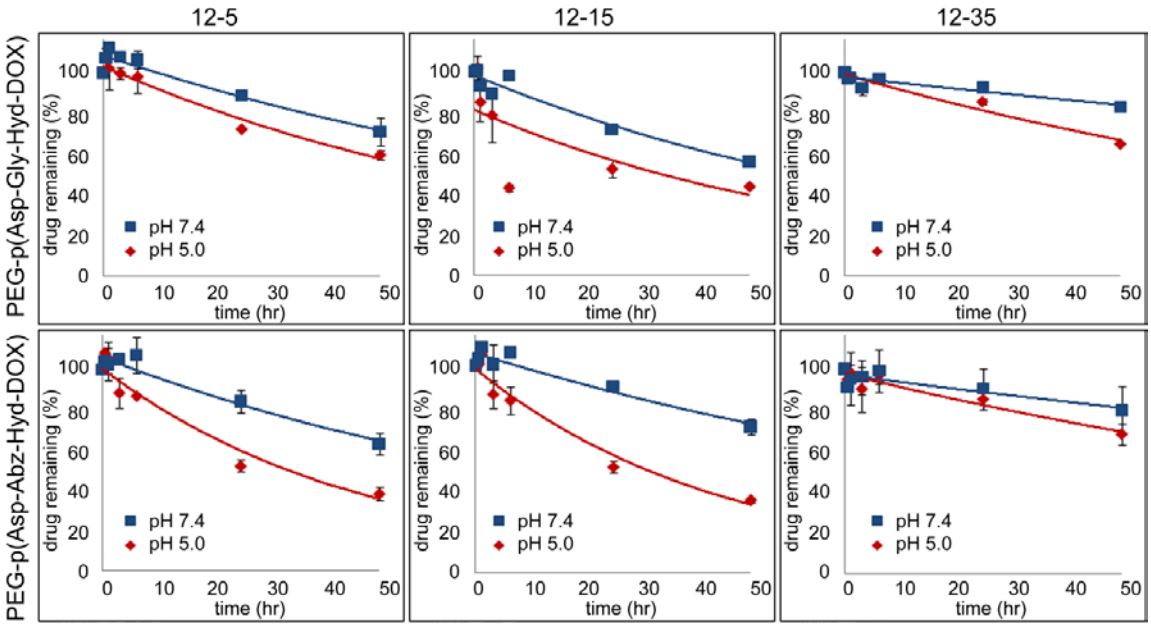

Figure 5. Drug Release Analysis: Block Copolymer Chain Length and Spacer Effect. Lines Represent 1st Order Drug Release Model Fitting

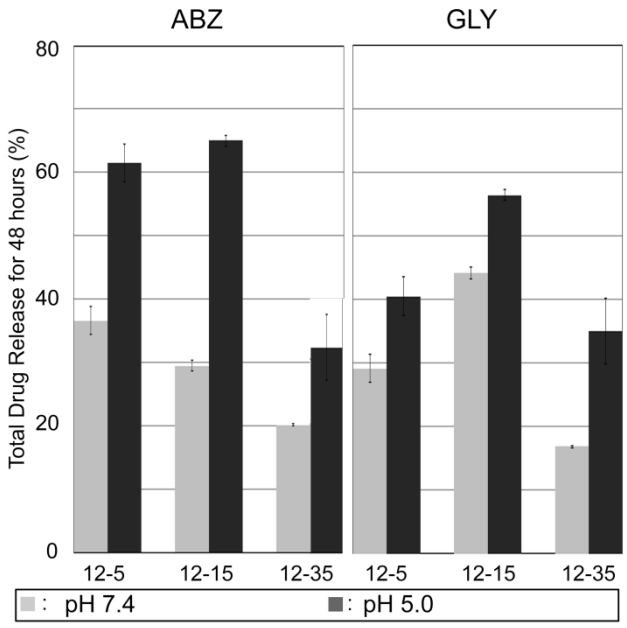

Figure 6. Quantification of Total Drug Release after 48 hours. Error Bars Represent Standard Deviation

pH 5.0 and pH 7.4. 12-5 ABZ micelles released 60% of DOX at pH 5.0 but only 36% at pH 7.4. Almost identical values were seen for 12-15 ABZ micelles. At pH 5.0, 65% of DOX was released. This dropped to 30% at pH 7.4. DOX release from 12-35 ABZ micelles was minimized at both pH 5.0 and pH 7.4, with the maximum amount of DOX released being 30%.

Differences in total drug release were not only observed when comparing micelles with the same spacer, but also when comparing those with different spacers. The total amount of drug released from ABZ and GLY micelles at pH 5.0 was significantly different. In 48 hours, 12-5 ABZ micelles released 60% of DOX, while 12-5 GLY micelles only released 40% of DOX. This trend continued for 12-15 micelles: ABZ micelles released 65% of DOX and GLY micelles released 55%. Interestingly, both 12-35 GLY and ABZ micelles released similar amounts of DOX after 48 hours. Total drug release was 32% and 35% for 12-35 ABZ and GLY micelles, respectively. At pH 7.4, ABZ and GLY micelles released similar amounts of drug. Approximately 30-40% of DOX was released from 12-5 and 12-15 micelles. For the 12-35 composition, both ABZ and GLY released slightly less than 20% of drug.

The release rates of DOX from micelles were determined at both pH 5.0 and pH 7.4. Drug release was fitted to zero and first order models (Table 3). At pH 7.4, drug release rates of 12-5 and 12-15 micelles were not affected by either linker or hydrophobic chain length. All four of the micelles had zero order release rate constants between 0.66 and 0.86 %*hour^{-1}. First order release rate constants were between 0.007 and 0.011 hour^{-1}. 12-35 micelles had the lowest rate of DOX release. Based on the zero order release model, rate constants were 0.28 %*hour^{-1} for GLY micelles and 0.36 %*hour^{-1} for ABZ

Table 3. Drug Release Analysis from Micelles Varrying Block Copolymer Chain Length

Spacer	Composition	pH 5.0		pH 7.4	
		k_0 (%/hour)	k_1 (hour^{-1})	k_0 (%/hour)	k_1 (hour^{-1})
ABZ	5	1.42 ± 0.12	0.024 ± 0.0035	0.86 ± 0.08	0.010 ± 0.0011
	15	1.43 ± 0.11	0.025 ± 0.0031	0.74 ± 0.10	0.008 ± 0.0012
	35	0.60 ± 0.07	0.007 ± 0.0010	0.36 ± 0.11	0.004 ± 0.0006
GLY	5	0.98 ± 0.10	0.013 ± 0.0018	0.66 ± 0.18	0.007 ± 0.0023
	15	1.04 ± 0.22	0.019 ± 0.0072	0.80 ± 0.20	0.011 ± 0.0030
	35	0.70 ± 0.04	0.008 ± 0.0011	0.28 ± 0.03	0.003 ± 0.0006

Drug release kinetic parameters were estimated with zero-order (k_0) and first-order (k_1) models. Release rates are reported as the best fit values with their standard error. % represents the drug remaining percent.

micelles. First order release rate constants were 0.004 and 0.003 hour^{-1} for ABZ and GLY micelles, respectively. The release rates at pH 5.0 were analyzed to further evaluate the effect of spacers. Neither type of spacer nor chain length affected 12-5 and 12-15 micelle release rates. Conversely, release rates from 12-35 micelles were slower than 12-5 and 12-15 micelles.

Comparing the release rates at pH 5.0 and pH 7.4 for each micelle composition revealed a dramatic contrast. Zero order and first order release rates from 12-5 and 12-15 GLY micelles increased at least 20% in pH 5.0. ABZ micelles showed an even greater change. Release rates of 12 -5 ABZ micelles were 40% higher in pH 5.0, while there was a twofold increase in release rates from 12-15 ABZ micelle. The release rates from 12-35 micelles almost doubled in acidic conditions.

3.3.6 In Vitro *Cytotoxicity*

Cytotoxicity of DOX, either as a free drug or a micellar formulation, was determined in two cell lines, a lung cancer cell line (A549) and a prostate cancer cell line (DU145). The IC50 of each micellar treatment was compared to the IC50 of free DOX treatment (Figure 7, Table 4). In the A549 cell line, the IC50 values after treatment with 12-5 ABZ, 12-15 ABZ, and 12-35 ABZ micelles were 3.89, 2.95, and 3.80 μM, respectively. The IC50 of free DOX treatment was 2.95 μM. ABZ micellar treatment was statistically equivalent to treatment with free DOX. In order of increasing repeating units, treatment with GLY micelles resulted in IC50s of 5.35, 2.08, and 17.7 μM. Only treatment with the 12-35 GLY formulation was statistically different than free DOX treatment. For the DU145 cell line, all micellar treatments had cytotoxic effects comparable to that of free DOX treatment, with the sole exception of 12-35 GLY micelles. ABZ formulations had an

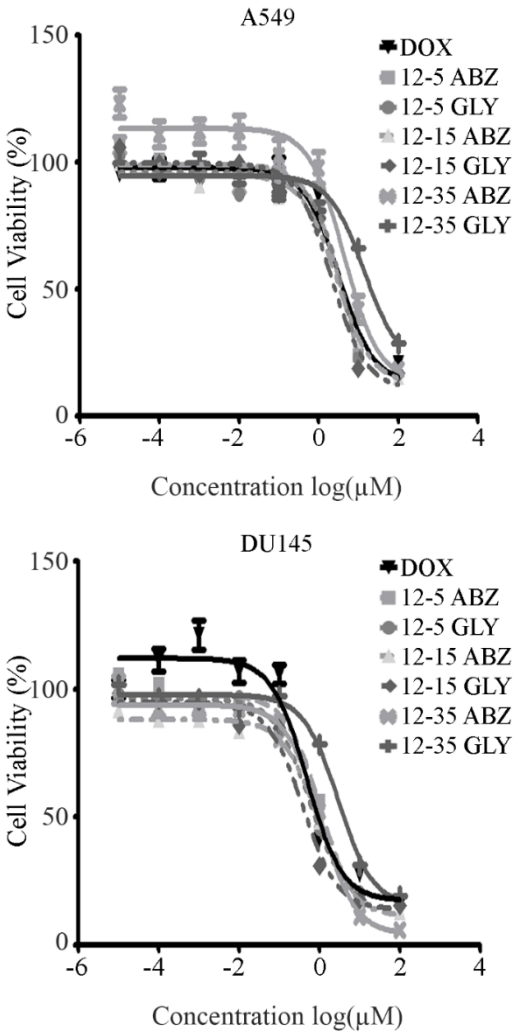

Figure 7. Cytotoxicity Compariston of Treatments with 12-5, 12-15, 12-35 Micelles or Free DOX

Table 4. Cytotoxicity Determination after Treatments with 12-5, 12-15, 12-35 Micelles or Free DOX in A549 and DU145 Cells

Cell Line	Spacer	Cytotoxicity	DOX	12-5	12-15	12-35
A549	ABZ	log (IC50)	0.47 ± 0.05	0.59 ± 0.11	0.47 ± 0.08	0.58 ± 0.19
		IC50 (μM)	2.95	3.89	2.95	3.80
	GLY	log (IC50)	0.47 ± 0.05	0.73 ± 0.15	0.32 ± 0.15	1.25 ± 0.28*
		IC50 (μM)	2.95	5.35	2.08	17.7*
DU145	ABZ	log (IC50)	-0.30 ± 0.08	0.014 ± 0.02	-0.077 ± 0.13	0.037 ± 0.27
		IC50 (μM)	0.51	1.03	0.84	1.09
	GLY	log (IC50)	-0.30 ± 0.08	-0.27 ± 0.19	-0.44 ± 0.13	0.44 ± 0.14**
		IC50 (μM)	0.51	0.65	0.36	2.75**

IC50 values are described in two ways: as log (IC50 concentration) ± the standard deviation; and as the corresponding IC50 concentration in μM. Statistical significance is indicated by * ($p < 0.05$), ** ($p < 0.01$).

IC50 of approximately 1.0 μM. Treatment with 12-5 and 12-15 GLY micelles resulted in lower IC50s of 0.65 and 0.36 μM, respectively. Treatment with the 12-35 GLY formulation resulted in an IC50 of 2.75 μM, the highest of any treatment.

3.3.7 DOX Cellular Uptake

The intracellular uptake of DOX was observed in the A549 cell line to elucidate the cytotoxic effects of drug loaded micelles. Cells were treated with solutions containing either free DOX or a micellar formulation. The three micellar formulations studied were 12-15 GLY, 12-15 ABZ, and 12-35 GLY micelles. Cells were exposed to drug-containing media for a set time period, after which the fluorescent signal of DOX was measured. This signal was thereafter converted to DOX concentrations. As previously stated, the DOX concentration measured from micellar treatment represents the combined total of free DOX and DOX conjugated to block copolymers. Cellular uptake results are reported as the percent DOX internalized (concentration of DOX internalized/concentration of DOX dose) (Figure 8). At each time point, free DOX was taken up by cells to a greater extent than DOX after micellar treatments. Initially, there was up to a 30-fold difference between free drug internalization and DOX internalization from micellar formulations. After 30 minutes, total DOX uptake from 12-15 ABZ and GLY micelle treatment was 0.02% and 0.08%, respectively, while DOX uptake from the 12-35 GLY formulation was negligible. DOX uptake continually increased through the first 24 hours. At this point, DOX uptake from 12-15 GLY micellar formulations reached 0.66%. DOX from 12-15 ABZ micelles was similarly taken up, but DOX uptake after 12-35 GLY treatment remained minimal. DOX related internalization slowed regardless of therapeutic agent used after 24 hours.

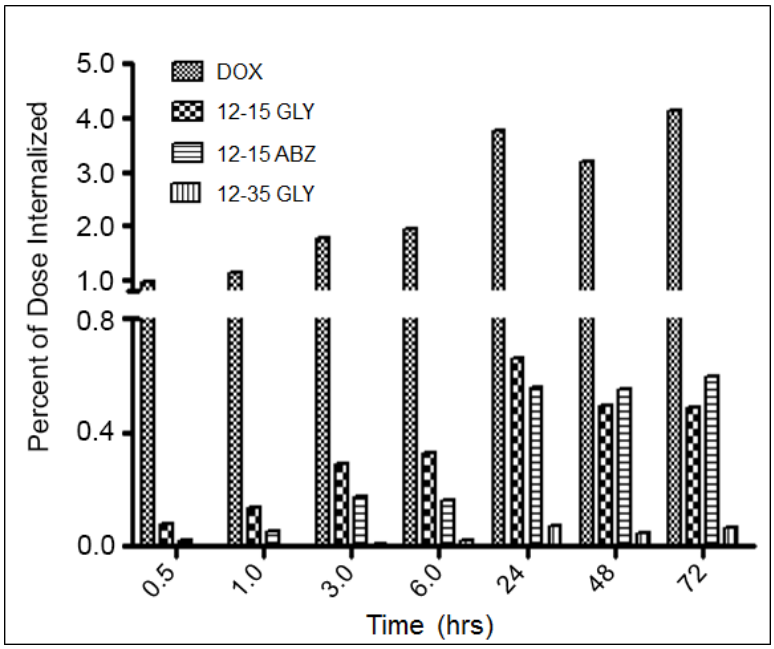

Figure 8. Cellular Internalization of Micelle Related DOX (Conjugated and Free DOX) and Free DOX in A549 Cells

Area under the curve (AUC) analysis was performed over the 72 hours of the internalization study (Figure 9). The AUC of free DOX treatment approached 250 %dose*hours, more than six times the AUCs of 12-15 ABZ and GLY treatments. The AUC of 12-15 treatments did not reach 50 % dose*hours. AUC analysis confirmed that treatment with 12-35 GLY micelles produced the lowest amount of DOX internalization.

3.4 Discussion

A NDDS platform from polymer micelles was designed to tune drug release rates. Polymer micelles were prepared from block copolymers based on poly(ethylene glycol)-poly(amino acid) (Figure 1A). In previous works, NDDSs were developed primarily to improve the solubility and tumor-specific accumulation of chemotherapeutic agents, focusing on the spatial control of drug distribution (Figure 1B). The novel delivery system proposed in this study was expected to achieve controlled drug release through modifications of the micelle core (Figure 1C). Herein, the effects of the hydrophobic chain length and drug binding linkers are described.

3.4.1 Monomer and Block Copolymer Scaffold Synthesis

Three compositions of PEG-p(BLA) block copolymers were synthesized as scaffolds. Synthesis of PEG-p(BLA) was successful and replicable. By controlling the monomer ratio added, synthesis was predictable. Initially, polymers with 10, 20, and 40 hydrophobic repeating units were targeted. Comparable block copolymers were synthesized, containing 5, 15, or 35 BLA repeating units. The slight deviation in synthesized block copolymer chain length was attributed to partially inactive BLA-NCA. The number of repeating units was increased from five to 35 to observe effects of the number of hydrophobic repeating units.

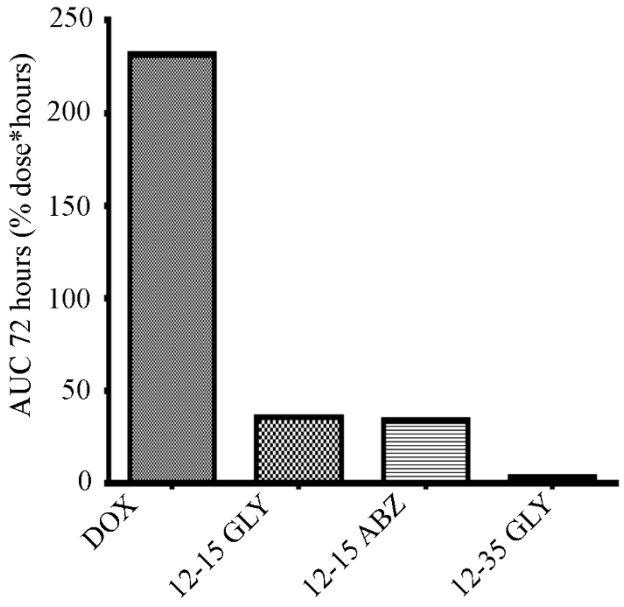

Figure 9. DOX Cellular Internalization AUC after Micellar and Free DOX Treatments

3.4.2 Drug Binding Linker Insertion and DOX Conjugation

PEG-p(BLA) scaffolds were deprotected producing PEG-p(Asp). One of two drug binding linkers (GLY-HYD or ABZ-HYD) was then attached to the Asp moiety. A GLY or ABZ spacer was first inserted onto PEG-p(Asp) using a coupling reaction typically used in solid phase peptide synthesis (Figure 4). Different coupling methods were initially attempted without success. Using HBTU as the coupling agent proved key to inserting spacers. It was therefore surmised that the single molecule-mediated coupling mechanism of HBTU seemed to be least influenced by intramolecular steric hindrance at the PEG-p(Asp) side chain. Other coupling agents such as DCC, DIC, and EDC contain bulky active esters, which were involved in the coupling reaction. Another factor that made the coupling reaction challenging was the solubility of block copolymers, which changed as coupling reactions proceeded. After spacer insertion, block copolymers were modified with hydrazide groups. In the last step of synthesis, DOX was attached to block copolymers using a hydrazone bond.

Acid-labile hydrazone linkages were employed in this study to modulate drug release from polymeric micelles. Carbazate drug binding linkers were used leading to hydrazone linkages of drug molecules possessing a ketone group. In addition to the hydrazine linkage, GLY or ABZ spacers were introduced prior to the hydrazine bond. The hydrazone bond is pH-sensitive, and previous work showed that the insertion of an ABZ spacer increased release rates, while GLY spacers decreased release rates (95, 114).

To properly elucidate the relationship between linker design and drug release patterns, the selection of the model drug was considered to be an important factor. DOX, an anthracycline antibiotic, was proven effective against a wide range of cancers, but

adverse cytotoxicity kept it from reaching its full potential. Additionally, DOX proved useful due to its detectability by fluorescence and absorbance, hydrophobic nature, and well-defined physicochemical properties. Moreover, the clinically-proven therapeutic efficacy of DOX was expected to help elucidate the effects of tunable drug release on tumor chemotherapy. Lastly, studies constantly showed that developing a NDDS for DOX can improve the therapeutic index of DOX (49, 115).

Each polymer composition synthesized revealed a different degree of drug conjugation (Table 1). In terms of weight/weight percent, drug loading increased as the hydrophobic chain length increased, presumably due to the increasing number of conjugation sites. Unsurprisingly, block copolymers with the shortest chain length had the lowest amount of conjugated DOX, with only one drug molecule attached per block copolymer. Drug loading for the 12-15 compositions increased to about three DOX molecules per block copolymer. In terms of drug loading per conjugation site, 12-5 and 12-15 block copolymers were similar (~20%). Comparing spacer effects, 12-35 block copolymers had the largest difference in drug loading per conjugation site. GLY modified block copolymers contained between 15 and 16 DOX molecules per block copolymer, while ABZ micelles contained just five DOX molecules per block copolymer. Compared to GLY micelles, DOX conjugation was less efficient in ABZ micelles. It was surmised that the extension of the drug binding linker allowed the ABZ benzyl ring to cause steric hindrance.

Micelles with shorter chain lengths proved less promising than those with longer chain lengths. For 12-5 micelles only one drug molecule was bound per block copolymer. Multiple drug molecules per block copolymer were conjugated onto 12-15 and 12-35

block copolymers. This high drug loading capacity maximizes the benefits of micellar treatment. In regard to the potential conjugation sites, overall drug conjugation was relatively low. Only the 12-35 GLY block copolymer showed conjugation greater than 22%, leaving room for improvement. Results suggested that optimizing both the coupling reactions of spacers and the hydrazide insertion could lead to more effective drug conjugation.

3.4.3 Polymer Micelle Preparation and Characterization

PEG-poly(amino acid) block copolymers have been shown to readily form micelles, as was the case with the six block copolymers synthesized in this study. 12-5 and 12-15 block copolymers were reconstituted in aqueous solution, forming micelles with a hydrodynamic diameter less than 50 nm. Longer chain length block copolymers were not directly soluble in solution. The 20 repeating-unit difference from 12-15 to 12-35 block copolymers changed the hydrophobic portion's MW by approximately 5,000 g/mol. It was unsurprising that an effect on solubility was observed considering that total block copolymer MW of ranges from 13,000 to 25,000 g/mol. A dilution approach was used to prepare micelles with 12-35 block copolymers. Similar to 12-5 and 12-15 micelles, 12-35 micelles had a diameter of approximately 40 nm.

3.4.4 Drug Release Study

Drug release studies were used to observe the effects of differential drug binding linkers (GLY-HYD or ABZ-HYD) and hydrophobic repeating unit length (5, 15, or 35) on DOX release. DOX was attached to block copolymers with a hydrazone bond. The hydrazone bond was shown to undergo hydrolysis more quickly in acidic intratumoral or intracellular environments (pH 5.0-6.8) (85). Therefore, DOX release was expected to be

pH-sensitive. To confirm this hypothesis, DOX release from micelles was observed under sink conditions in environments intended to mimic physiological and intracellular settings (Figure 5).

Quantification of total drug release showed that more DOX is released in acidic conditions, regardless of spacer type and hydrophobic chain length. Depending on formulation, differences in amount of drug released were observed as early as the one hour time point. In addition to comparing drug released at individual time points, zero and first order release rates were determined and compared. Results indicated that DOX was released more quickly at pH 5.0. Zero order release rates were at least 20% slower at pH 7.4. There were greater differences in first order release rates, as drug release rates were two to three times lower at pH 7.4. The differences in release rates can be partially attributed to the use of the hydrazone bond. It was previously shown that hydrolysis of the hydrazine bond is pH-sensitive (116, 117). Literature showed that small molecules with hydrazone bonds have greater than tenfold differences in hydrolysis rates going from neutral to acidic conditions (35, 95, 118). It was surmised that DOX release from block copolymer micelles was also influenced by other factors. Core properties (i.e. steric hindrance, hydrophobicity) may have played a role in DOX release. This phenomenon was previously observed with polymeric carriers (90, 114).

The hydrophobic chain length of polymer micelles was varied in an effort to tune drug release rates. 12-5 and 12-15 micelles released more DOX than 12-35 micelles at pH 7.4. This was also observed at pH 5.0. Interestingly, there were minimal differences between the amount of DOX released from 12-5 and 12-15 micelles. Release rate analysis confirmed that 12-5 and 12-15 micelles had equivalent release rates. This held

true in both pH 5.0 and pH 7.4. Though release rates from shorter chain length block copolymers were similar, extending the hydrophobic chain length to 35 slowed release significantly. It appeared that extending the chain length beyond a certain point significantly slows drug release rates.

The secondary method to tune drug release rates was attempted by inserting a spacer prior to the hydrazone bond. Hydrolysis release rates are altered due to neighboring substituent effects (119, 120). More specifically, earlier works with ABZ and GLY spacers show that the insertion of ABZ leads to greater drug release at a faster rate than the insertion of GLY (114). In this study, total DOX release was statistically different when comparing 12-5 micelles with different spacers. Similarly, a difference was observed with 12-15 micelles but this difference was no longer evident with the 12-35 micelles. Spacers had no effect on total DOX release when the hydrophobic chain length was increased to 35 units. More surprising was the fact that release rates of DOX were not statistically different when comparing micelles containing the same number of hydrophobic repeating units, but different spacers (GLY or ABZ).

Modeling the drug release based on zero and first order release kinetics gave insight to DOX release from micelles, but both models oversimplified the drug release process. For DOX to be released from micelles, a minimum of three factors must be considered: hydrazone bond cleavage, DOX escape from micelle, and DOX partitioning within the micelle. Additionally, dynamic dialysis studies should account for the effects of the dialysis membrane. The rates reported herein are all-encompassing, combining all of the factors into a single observed rate constant.

The first order model was expected to describe the drug release more accurately, as hydrazone hydrolysis is often expressed as a first order process (118, 120). This only holds true under the assumption that hydrazone hydrolysis is rate limiting, and that remaining factors play minimal roles. In this study, first order release models produced better fits, specifically in terms of coefficient of determination. But even with the first order drug release model, there was room for improvement as drug release fitting at pH 7.4 was poor. Additionally, determined rate constants had large variability. Determining spacer effects was thus inconclusive. However, there were significant differences in total drug release when comparing 12-5 and 12-15 GLY to their ABZ counterparts. The variability in release rates and poor fitting at pH 7.4 highlighted the need for a more complete drug release model. This would not only better describe DOX release from micelles, but also give insight into which factors impact drug release.

3.4.5 In Vitro *Cytotoxicity*

Cytotoxicity of micellar formulations was determined in the A549 and DU145 cell lines to evaluate micellar efficacy and to shed light on the effects of drug release rates *in vitro*. It is important to note that DOX conjugated to block copolymers through an ester linkage was not cytotoxic (121). Therefore, it was hypothesized that DOX must first to be cleaved from block copolymers to produce an active pharmaceutical ingredient. The cytotoxic effects of micellar DOX consisted of two possible routes. Entrapped DOX could be released extracellularly, at which point the free drug is internalized by the cells. Alternatively, micelles can be taken up by cells and release DOX intracellularly. The most likely scenario is that a combination of the two occurred *in vitro*. Nanoparticles, including micelles, have been shown to be taken up by cells through endocytosis (18,

122-125). During the endocytic cycle, pH drops as low as 4.5 in lysosomes (126, 127). At this low pH, DOX release from micelles was accelerated. Though drug release studies in media were not performed, it was expected that drug release in buffer would correlate with drug release in media. Additionally, cellular internalization studies showed very low DOX uptake due to micellar treatment, confirming slow drug release.

Cytotoxicity experiments were performed over 72 hours. When determining efficacy, cells were treated with an equal amount of DOX in every study. Taking into account differential DOX release rates from micelles, the amount of free DOX available differed depending on the micelle formulation. Initially DOX was completely conjugated to block copolymers and was not available in its free active form. Over a 72 hour period, the concentration of free DOX from micellar treatments increased as more DOX was released. Micelles developed herein had two distinct release profiles, one from 12-5 and 12-15 micelles and another from 12-35 micelles. Overall, 12-35 micelles released DOX at a slower rate than 12-5 and 12-15 micelles. In addition to micellar treatments, the cytotoxicity of free DOX was determined. Free DOX treatment represented a single bolus dose, as cells were instantaneously exposed to a large amount of DOX in the active form.

In A549 cells, micellar treatments were equipotent to free DOX with the sole exception being the 12-35 GLY formulation (Figure 7, Table 4). Similar results were observed in DU145 cells, with micellar treatments having comparable IC50s to free DOX (Figure 7, Table 4). The 12-35 GLY formulation was again the exception, having a statistically higher IC50. Overall cytotoxicity results were intriguing. The amount of free DOX available for cells changed depending on treatment, but this change generally did

not hamper efficacy. Releasing DOX at a slow rate appeared to be as efficacious as exposing cells to a single large dose of free DOX.

The exception to the rule was 12-35 GLY micelles. Cells treated with 12-35 micelles yielded the least free DOX due to slow DOX release. The high IC50 in both A549 and DU145 cells after 12-35 GLY treatment was attributed to low free DOX availability. There appeared to be a point where slow release ceased to be beneficial. Additional factors such as intracellular uptake may have also played a role in efficacy. This could explain why 12-35 ABZ micelles were cytotoxic, even though they also released DOX at a slow rate.

The effectiveness of micellar treatment with prolonged release showed that not only does dosage matter, but so does the rate of release. This was especially apparent when comparing 12-5 and 12-15 micelles to free DOX treatment. These micelles released DOX at a slow, prolonged rate yet were as efficacious as free DOX.

3.4.6 DOX Cellular Uptake

A549 cells were treated with DOX in micellar formulation or as a free drug. At specific intervals, the intracellular DOX concentration was measured (Figure 8). The intracellular concentration measured from micellar treatment included both free DOX and conjugated DOX, as the two could not be differentiated. The uptake of DOX from 12-5 micelles was not analyzed due to low drug loading. A 100 μM DOX-equivalent concentration was required for internalization studies and this was not attainable with 12-5 micelles. 12-35 ABZ and 12-35 GLY micelles had similar physicochemical properties and released DOX at similar rates; thus only the 12-35 GLY formulation was studied. As described earlier, micelle treatment was expected to have two modes of DOX internalization: diffusion as a

small molecule and endocytosis of micelles. Extracellular release of DOX followed by diffusion was less likely due to the pH-dependent DOX release from micelles.

High intracellular DOX concentrations were observed very quickly after free DOX treatment. Directly available as a small molecule, DOX was readily internalized. As early as the 30 minute time point DOX was detected intracellularly at high levels. At each subsequent time point, measured DOX concentrations increased equating to greater free DOX uptake. DOX related uptake was significantly slower in the case of micelles. However, intracellular DOX concentrations steadily increased through the first 72 hours in each case. The lower DOX uptake from micellar treatments was related not only to the slower uptake of micelles, but also to slow DOX release from micelles.

DOX release from micelles was compared to the cellular internalization of DOX after micellar treatment (Figure 10). DOX release as a percentage at either pH 5.0 or pH 7.4 was plotted on the left y-axis, while percent dose internalized was plotted on the right y-axis. The drug release profile from 12-15 GLY micelles at pH 5.0 was in line with cellular internalization of DOX. This correlation was replicated with the 12-15 ABZ but was not observed with 12-35 GLY micelles. In block copolymers with shorter hydrophobic chain length, the rate of release appears to directly influence cellular internalization.

3.5 Conclusions

Experimental results demonstrated that modified PEG-p(Asp) block copolymers readily formed micelles regardless of chain length. Previously, short block copolymers have been shown to form unstable micelles or to be incapable of self-assembling. The insertion of spacers seemed to stabilize micelles by retaining sufficient hydrophobicity for self-

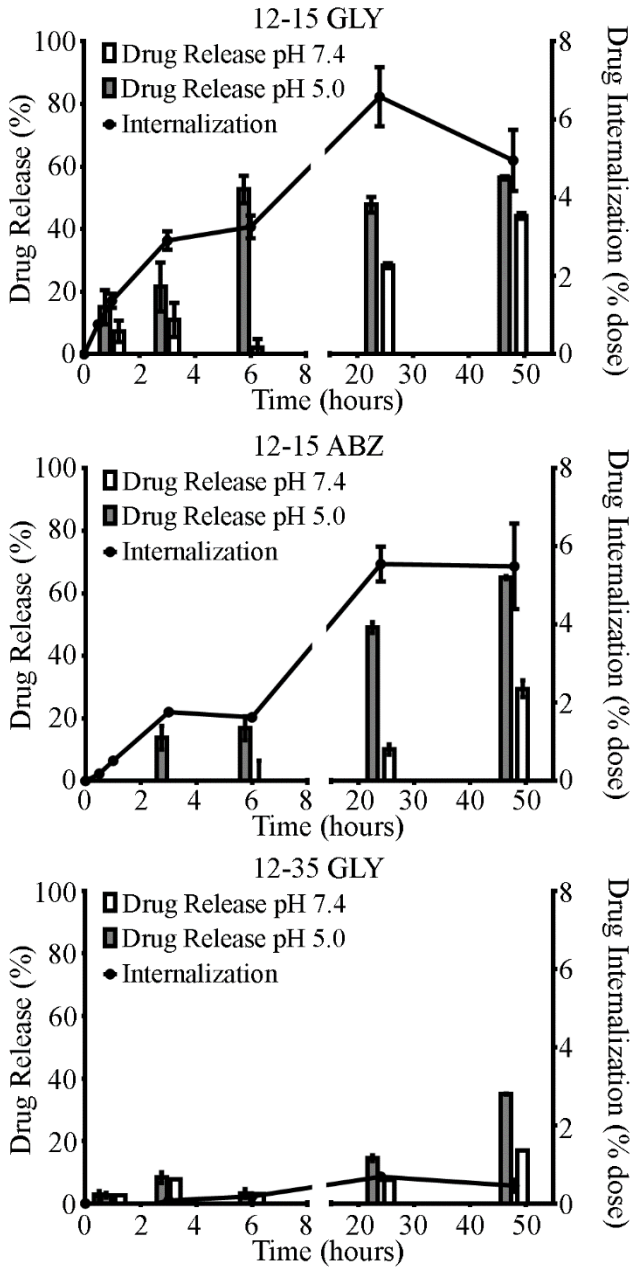

Figure 10. Comparative Analysis of DOX Release from Micelles at pH 5.0 (Closed Bars) and pH 7.4 (Open Bars) Versus Cellular Uptake of DOX (Closed Circles)

assembly. Moreover, the results of this study elucidated the effects of chain length and core modifications on drug release. The use of a hydrazone linkage led to pH-dependent release of DOX, as the DOX release rate was faster in pH 5.0 than in pH 7.4 for all micellar formulations.

Results from drug release studies indicated that block copolymers with longer chain lengths (35 repeating units) have slower drug release rates compared to those with shorter chain lengths (5 and 15 repeating units). Micelle cores composed of longer chain length polymers seemed to more efficiently protect drug binding linkers (GLY-HYD or ABZ-HYD) from hydrolysis. Intriguingly, the effect of drug binding linkers was not evident in terms of drug release rates. However, total drug release from GLY micelles was significantly different from ABZ micelles. The drug release model used apparent drug release rates, which oversimplified the drug release process. This oversimplification caused high variability in determined release rates, and therefore only very large differences in release rates could be differentiated. As total drug release results indicated, the use of spacers may still lead to fine-tuned drug release.

Effects of differential drug release rates were observed *in vitro* through cytotoxicity experiments. Treatment with micelles that released DOX slowly was found to be equipotent to a single large dose of free DOX. However, treatment with 12-35 GLY micelles showed that there was a limit to the benefits of slow drug release. Cellular uptake studies revealed that DOX was internalized after micellar treatments, but to a low degree. The combined results of cytotoxicity and cellular internalization experiments indicated that delivering smaller amounts of DOX at a slow rate is equivalent to administering a single high dose of DOX. Focusing on dosing schedule rather than

delivering drugs at the maximum tolerated dose could pave the way to more efficient chemotherapeutic treatments.

**Portions of Chapter 3 were previously published in (21). Reproduced with kind permission from Springer Science and Business Media: Pharmaceutical Research, Volume 27, 2010, pages 2330-2342, PEG-poly(amino acid) Block Copolymer Micelles for Tunable Drug Release, Andrei Ponta and Younsoo Bae, Figures 2-5, Copyright 2010 is given to the publication in which the material was originally published.

CHAPTER FOUR

4 Block Copolymer Micelle Preparation and Characterization: Developing a Micellar System Containing Differential Drug Binding Linkers

4.1 Introduction

Initial micelle development laid the foundation for the remainder of the study, guiding subsequent block copolymer synthesis and micelle preparation. PEG-p(Asp-X-HYD-DOX) (X = ABZ or GLY) block copolymers were previously synthesized and used to prepare micelles. Findings regarding drug loading, drug release, and *in vitro* efficacy revealed the effects of hydrophobic repeating units (5, 15, or 35) and type of drug binding linker (GLY-HYD or ABZ-HYD).

Drug loading analysis showed that extending the hydrophobic chain length led to higher drug loading. Specifically, block copolymers containing 35 hydrophobic repeating units had the greatest drug loading. Furthermore, drug release analysis revealed that 12-35 micelles released DOX at slower rates than 12-5 and 12-15 micelles. Though release rates decreased by extending the chain length, these rates could not be fine-tuned. There appeared to be a breaking point within the range of hydrophobic chain length beyond which release rates decreased with little room for adjustment. Drug release studies also showed that total DOX released varied depending on the micelle formulation. The type of spacer used impacted total drug release. ABZ micelles released more DOX than GLY micelles. Similarly, release rates of ABZ micelles were faster than those of GLY micelles, though these were not statistically different. The lack of a more complete drug release model led to large variability in release rates. Of the two methods (chain length versus drug binding linker) to control release rates, modifying drug binding linkers remained the most promising. Furthermore, *in vitro* studies revealed that micellar

treatments were equipotent to free DOX treatment as long as micelles were composed of block copolymers containing fewer than 35 hydrophobic repeating units.

Block copolymer synthesis was repeated with a fixed scaffold and targeted 15 hydrophobic repeating units, leveraging the benefits of increased drug loading capacity with high therapeutic efficacy. Block copolymers herein were still modified with drug binding linkers to control drug release.

4.2 Materials and Methods

4.2.1 Materials

L-aspartic acid β-benzyl ester, methanol, DMSO-*d6*, dry ethyl ether, anhydrous hexane, hydrochloric acid, anhydrous THF, triphosgene, NaOH, anhydrous hydrazine, benzene, dry DMF, anhydrous DMSO, DMSO, methyl 4-aminobenzoate, and HBTU were purchased from Sigma-Aldrich (USA). Glycine-OMe was purchased from Novabiochem (SUI). DOX was purchased from LC Laboratories (USA). PEG-NH_2 was purchased from NOF Corporation (Japan). Regenerated cellulose dialysis bags (6,000-8,000 MWCO), Sephadex LH-20 gels, and sterile filters (0.22 μm) were purchased from Fisher Scientific (USA).

4.2.2 Monomer and Block Copolymer Scaffold Synthesis

A PEG-p(BLA) scaffold was synthesized in two steps: monomer synthesis and ring-opening polymerization (Figure 11, yellow). BLA-NCA monomers were prepared first. L-aspartic acid β-benzyl-ester (21.0 g, 223 mmol) and triphosgene (12.1 g, 40.8 mmol) were dissolved with dry THF in Schlenk and round bottom flasks, respectively. Dissolved triphosgene was added to L-aspartic acid β-benzyl-ester. The reaction was carried out with constant stirring at 45°C under N_2. The solution turned clear after one hour,

signifying a completed reaction. Anhydrous hexanes were then added to the reaction solution, which was subsequently stored overnight at -20°C for BLA-NCA monomer recrystallization. The supernatant was discarded, and BLA-NCA crystals were washed three times with anhydrous hexanes to ensure a pure product.

Amine-activated poly(ethylene glycol) (PEG-NH_2) was used as a macroinitiator for BLA-NCA ring-opening polymerization. Freeze-dried PEG-NH_2 (4.3 g, 0.36 mmol) and BLA-NCA monomers (2.14 g, 8.59 mmol) were dissolved in dry DMSO in separate flasks. BLA-NCA monomers were added to PEG, with the final reaction concentration reaching ~50 mg/mL. The reaction proceeded for two days with constant stirring at 45°C under N_2. The amount of BLA-NCA used in the reaction was calculated to produce 15 BLA repeating units, with a slight excess (10%). Final products were purified by repeated ether precipitation and collected after freeze-drying. ^{1}H-NMR confirmed successful synthesis (Figure 12).

4.2.3 Drug Binding Linker Insertion and DOX Conjugation

The PEG-p(BLA) scaffold was modified with one of two drug binding linkers: ABZ-HYD or GLY-HYD. PEG-p(BLA) was dissolved in 0.1 N NaOH (50-100 mg/mL) to remove the benzyl groups. Dissolved PEG-p(BLA) was transferred into a dialysis bag (6,000-8,000 MWCO) which was subsequently placed in a vessel containing deionized water (1 L). The outer solution was replaced with fresh deionized water at least eight times at time intervals exceeding one hour. Afterward, the outer solution was replaced with deionized water containing hydrochloric acid in equimolar proportions to NaOH. The outer solution was replaced twice more with deionized water, completing dialysis.

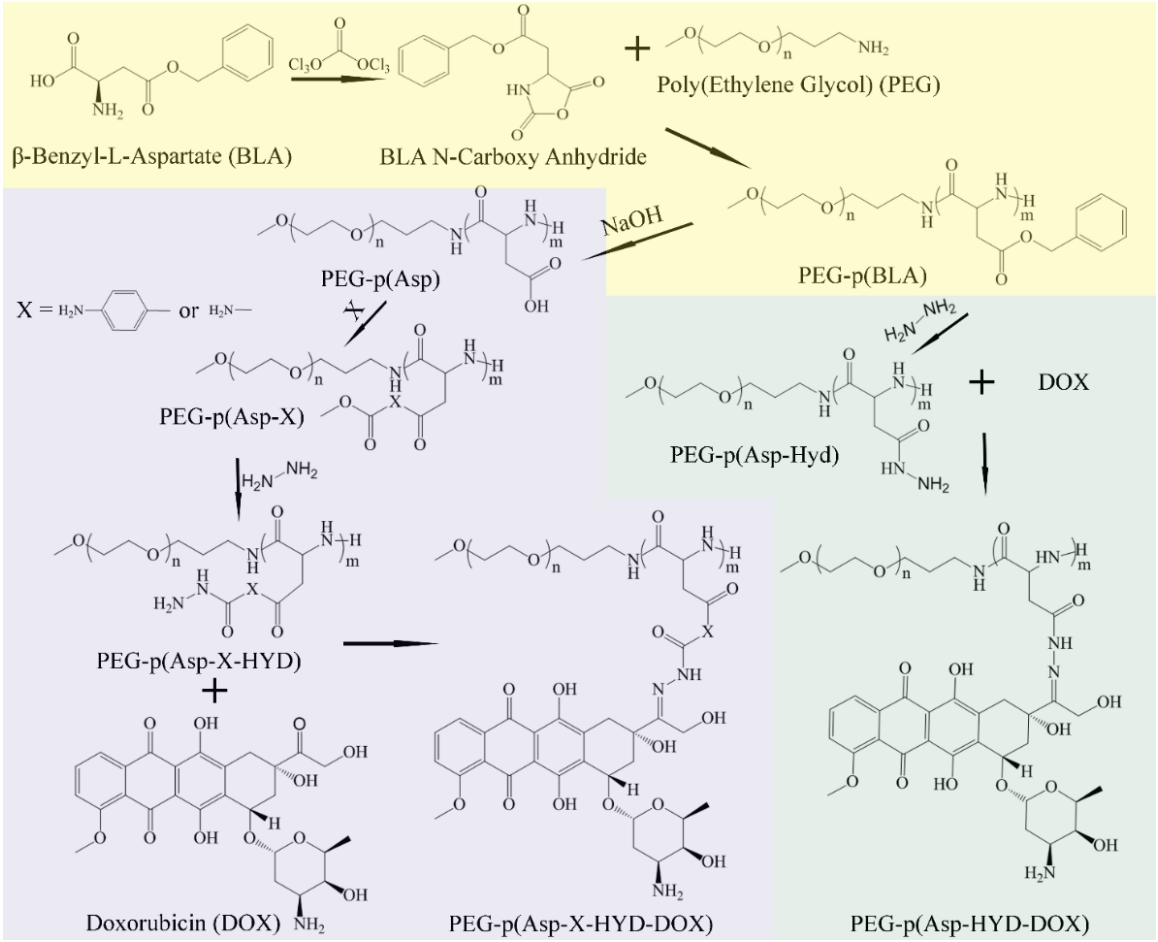

Figure 11. 12-16 Block Copolymer Synthesis Scheme

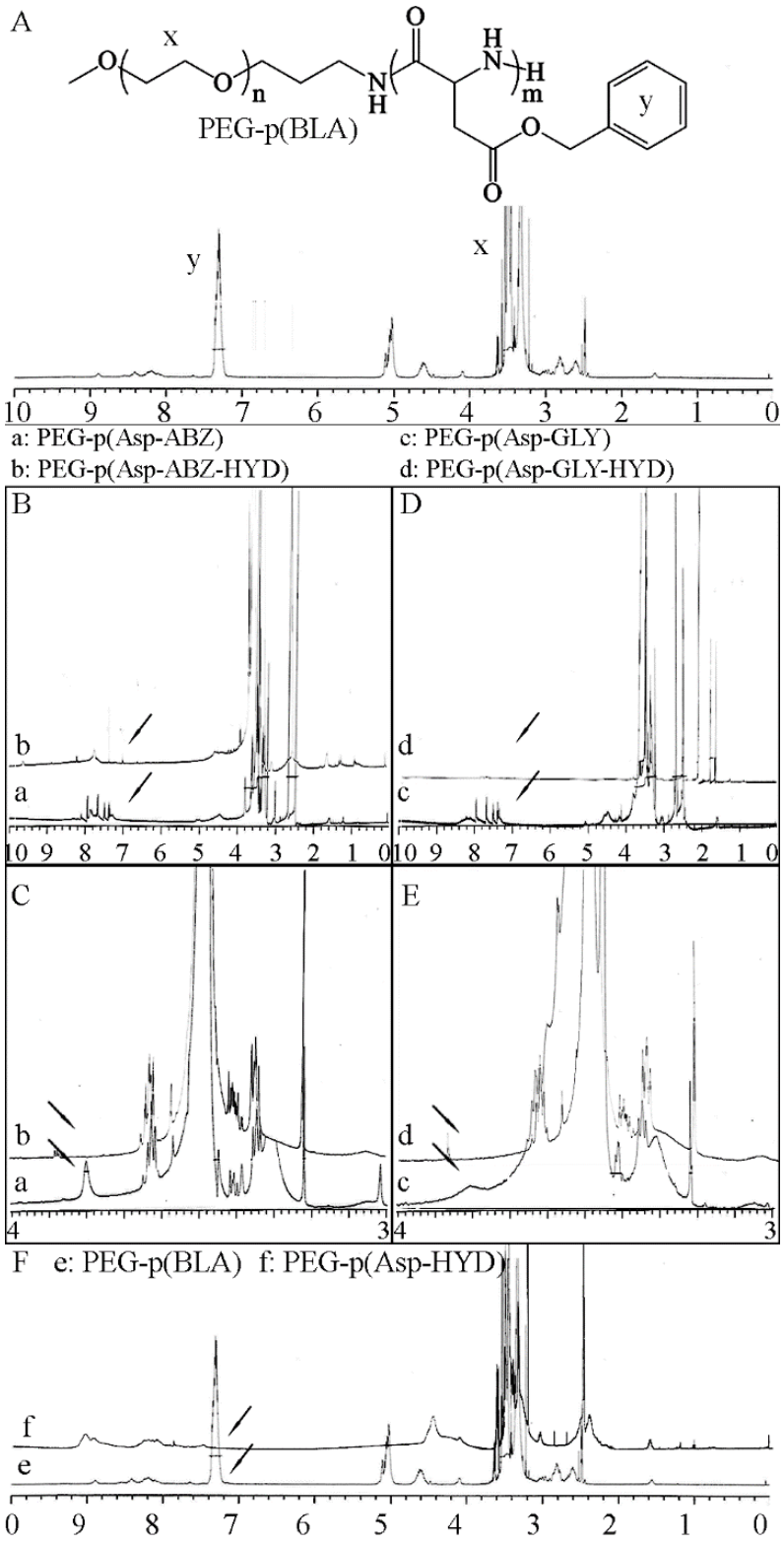

Figure 12. [1]H-NMR of Block Copolymer Scaffold (A) and Subsequent Block Copolymers Confirming Drug Binding Linker Insertion (B-F)

The solution within the dialysis membrane was collected and freeze-dried, yielding a fluffy, white PEG-p(Asp) polymer.

A coupling reaction was used to insert ABZ-OMe or GLY-OMe spacers into the PEG-p(Asp) backbone. Freeze-dried PEG-p(Asp) (1.0 g, 71.8 µmol) was dissolved in DMSO. Either ABZ-OMe (378 mg, 151 µmol) or GLY-OMe (301 mg, 125.6 µmol) was added to the PEG-p(Asp) solution. The amount of spacers used in the reaction reflected the number of aspartate binding sites on PEG-p(Asp). HBTU was used as the coupling agent. The reaction progressed overnight with constant stirring at 40°C. Pure PEG-p(Asp-ABZ-OMe) and PEG-p(Asp-GLY-OMe) block copolymers were collected after ether precipitation, dialysis, and freeze-drying. Successful reactions were confirmed with ^{1}H-NMR.

Methyl esters of block copolymers were replaced with hydrazide after an aminolysis reaction. Freeze-dried PEG-p(Asp-GLY-OMe) (938 mg, 62 µmol) was dissolved in dry DMF. Excess anhydrous hydrazine (650 mg, 20 mmol) with respect to Asp-GLY-OMe repeating units was added to the PEG-p(Asp-GLY-OMe) solution. The reaction proceeded for one hour with constant stirring at 40°C under N_2. PEG-p(Asp-ABZ-OMe) (860 mg, 54 mmol) was reacted with excess hydrazine (543 mg, 17 mmol) under identical conditions. The resulting material was collected after ether precipitation and freeze-drying. PEG-p(Asp-ABZ-HYD) and PEG-p(Asp-GLY-HYD) syntheses were confirmed with ^{1}H-NMR.

A third block copolymer [PEG-p(Asp-HYD)] was synthesized as a control. The hydrazide group was inserted into the block copolymer backbone, but a spacer was not used. PEG-p(Asp-HYD) synthesis was carried out in a one-pot reaction. PEG-p(BLA)

(849.5 mg, 56.42 µmol) was freeze-dried and dissolved in dry DMF. Anhydrous hydrazine (289.1 mg, 9034 µmol) was added to PEG-p(BLA). The reaction proceeded for one hour with constant stirring at 40°C under N_2. Block copolymers were collected after ether precipitation and freeze-drying. PEG-p(Asp-HYD) synthesis was confirmed with ^{1}H-NMR.

DOX was conjugated to each of the three block copolymers. DOX was reacted with PEG-p(Asp-GLY-HYD) (899 mg, 59 µmol), PEG-p(Asp-ABZ-HYD) (824 mg, 50 µmol), or PEG-p(Asp-HYD) (750 mg, 53 µmol) in DMSO for two days while gently shaking at 40°C. Physically-entrapped DOX was first removed by ether precipitation. For further purification, block copolymers were dissolved in methanol and eluted through a Sephadex LH-20 column. Final products were dissolved in deionized water and filtered using a 0.22 µm filter. A red powder was collected after freeze-drying. Final block copolymers were stored as solids at -20°C.

4.2.4 Polymer Micelle Preparation and Characterization

Irrespective of drug binding linker, block copolymers were simply dissolved in aqueous solution to prepare micelles. PEG-p(Asp-HYD-DOX), PEG-p(Asp-ABZ-HYD-DOX), and PEG-p(Asp-GLY-HYD-DOX) block copolymers formed HYD, ABZ, and GLY micelles, respectively.

Prepared micelles were thoroughly characterized. Particle size and ζ-potential were determined using a Zetasizer Nano-ZS (Malvern, UK) equipped with a He-Ne laser (4 mW, 633 nm) light source and 173° angle scattered light collection configuration. Block copolymers were dissolved in deionized water at 2.0 mg/mL concentrations for

both experiments. Three separate samples were prepared for both particle size and ζ-potential determination. Each sample was analyzed separately.

A SpectraMax M5 (Molecular Devices, USA) equipped with variable spectrum filters and SoftMax Pro Software was used to determine drug loading. A calibration curve based on free DOX in deionized water was prepared with standard samples ranging from 0.98 to 250 μM. Drug loading was determined based on the calibration curve. The DOX peak at 480 nm was used as the fingerprint peak for detection. Block copolymer absorbance spectra confirmed that the DOX conjugation did not alter the DOX spectra (Figure 13).

4.3 Results

4.3.1 Denotation

Block copolymer modifications are denoted by a corresponding abbreviation within the parenthesis of the hydrophobic block. For example, PEG-p(Asp-GLY-OMe) block copolymers describe PEG-p(Asp) modified with GLY-OMe. Final block copolymers are denoted by: PEG-p(Asp-HYD-DOX), PEG-p(Asp-ABZ-HYD-DOX), and PEG-p(Asp-GLY-HYD-DOX). The respective block copolymer micelles are HYD, ABZ, GLY or micelles.

4.3.2 Monomer and Block Copolymer Scaffold Synthesis

A PEG-p(BLA) scaffold composed of 12,000 MW PEG and 16 BLA repeating units was synthesized in a two-part reaction (Figure 11, yellow). Pure BLA-NCA monomers were prepared by adding triphosgene to L-aspartic acid β-benzyl-ester. Needle-like white crystals were collected after recrystallization in hexanes. The addition of BLA-NCA to amine-activated PEG yielded PEG-p(BLA) block copolymers. Ether precipitation

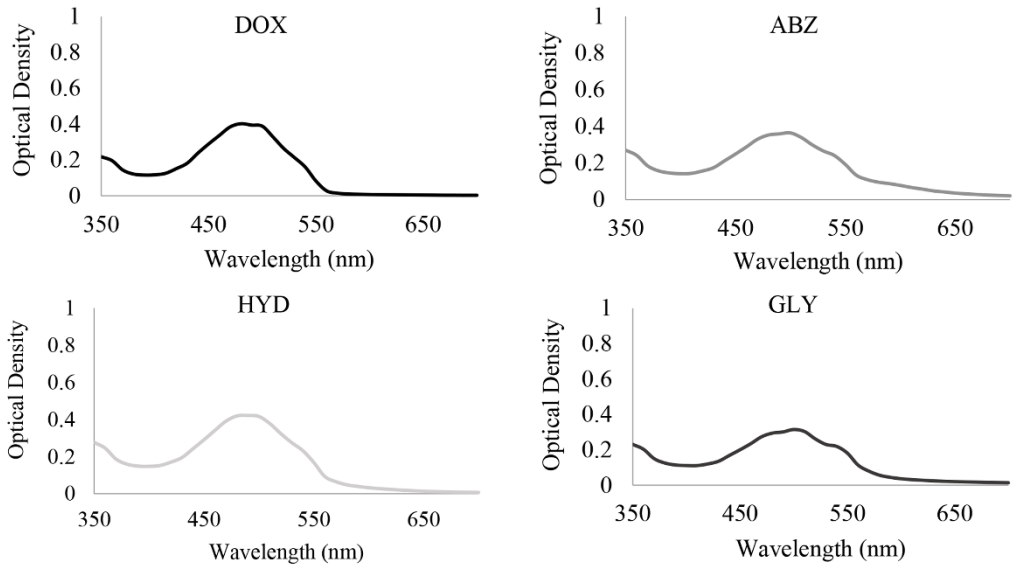

Figure 13. Absorbance Spectra of Free DOX and DOX Conjugated to Block Copolymers. Observed Absorptivity at 480 nm for DOX, HYD, ABZ, GLY was 3.30, 3.31, 3.33, 3.31, Respectively

removed monomers and homopolymers. ^{1}H-NMR confirmed successful synthesis. A prominent peak at 3.5 ppm was attributed to PEG (Figure 12A, letter x). Benzyl groups of BLA appeared as a peak at 7.3 ppm (Figure 12A, letter y). The number of BLA units was determined ratiometrically by integrating the areas of the two peaks. The PEG:BLA integration ratio was 1091:80, equating to 16 BLA repeating units.

4.3.3 Drug Binding Linker Insertion and DOX Conjugation

HYD, ABZ-HYD, and GLY-HYD drug binding linkers were inserted into the block copolymer scaffold. For ABZ-HYD and GLY-HYD insertion, PEG-p(BLA) was first deprotected, generating PEG-p(Asp) (Figure 11, green). Deprotection removed the benzyl ring from PEG-p(BLA) and produced a carboxylic acid moiety. ABZ-OMe or GLY-OMe spacers were then inserted into PEG-p(Asp) backbone through a coupling reaction using HBTU. Resulting block copolymers were further modified with hydrazide using an aminolysis reaction.

PEG-p(BLA) deprotection and drug binding linker insertion were both confirmed with ^{1}H-NMR. Successful conversion of PEG-p(BLA) to PEG-(Asp) resulted in the BLA peak disappearance at 7.3 ppm. ^{1}H-NMR spectra of both PEG-p(Asp-ABZ-OMe) and PEG-p(Asp-GLY-OMe) block copolymers showed this absence, confirming deprotection (Figure 12B and 12D, black arrows). Following deprotection, spacers containing methyl ester protecting groups were introduced into PEG-p(Asp) block copolymers. ^{1}H-NMR spectra of PEG-p(Asp-ABZ-OMe) and PEG-p(Asp-GLY-OMe) revealed methyl ester peaks at 3.8 ppm (Figure 12C and 12E, gray arrows). Additionally, the presence of the ABZ-OMe benzyl group led to the appearance of a peak at 7.8 ppm, signifying successful spacer insertion. Methyl esters were subsequently replaced with hydrazide groups,

resulting in PEG-p(Asp-ABZ-HYD) and PEG-p(Asp-GLY-HYD) block copolymers. After hydrazide insertion, ^{1}H-NMR spectra showed the disappearance of methyl ester peaks (Figure 12C and 12E). Furthermore, small, broad peaks related to hydrazide were observed at approximately 9.0 ppm (Figure 12B and 12D). ^{1}H-NMR spectra differences between before and after hydrazide insertion confirmed a successful reaction.

PEG-p(Asp-HYD) block copolymers were synthesized separately. A one-pot reaction was used by directly adding hydrazine to PEG-p(BLA) (Figure 11, purple). The reaction was confirmed with ^{1}H-NMR. The PEG-p(BLA) benzyl peak at 7.3 ppm completely disappeared (Figure 12F, black arrows). Additionally, a smaller broad peak at 9.0 ppm from hydrazide appeared after the reaction (Figure 12F).

DOX was covalently attached to PEG-p(Asp-HYD), PEG-p(Asp-ABZ-HYD), and PEG-p(Asp-GLY-HYD) block copolymers, forming PEG-p(Asp-HYD-DOX), PEG-p(Asp-ABZ-HYD-DOX), and PEG-p(Asp-GLY-HYD-DOX) block copolymers, respectively. Final block copolymers were purified thoroughly. Ether precipitation removed DMSO and the majority of physically-entrapped DOX, while a Sephadex LH-20 column eluted with methanol removed any remaining free DOX. For the last step of purification, block copolymers were dissolved in deionized water and filtered with a 0.22 μm filter. Immediately afterward, dissolved block copolymers were placed on dry ice. Block copolymers were lyophilized, and the resulting red powder was collected. Final block copolymer powders were stored at -20°C.

4.3.4 Polymer Micelle Preparation and Characterization

Irrespective of drug binding linker, block copolymers were simply dissolved in aqueous solution to prepare micelles. Micelles were characterized by determining particle size, ζ-

Table 5. 12-16 Micelle Characterization

Compound	Drug Loading (wt/wt%)	Particle Size (nm)	PDI	ζ-Potential (mV)
GLY	26 ± 1.1%	54 ± 12	0.27 ± 0.02	+ 0.5 ± 1.5
ABZ	17 ± 1.5%	58 ± 11	0.22 ± 0.01	- 4.0 ± 0.6
HYD	26 ± 1.6%	117 ± 37	0.20 ± 0.02	+ 13 ± 0.2

Data were obtained by triplicate measurements and are show as average ± standard deviation.

potential, polydispersity index, and drug loading (Table 5). DLS analysis indicated that all micelles were <125 nm in diameter. ABZ and GLY micelles were almost identical in diameter (58 and 54 nm, respectively). HYD micelles were larger, having a 117 nm diameter. The polydispersity index for each micelle was approximately 0.2. The micelle ζ-potential was also determined. ABZ and GLY micelles had a neutral surface charge, both with ζ-potentials within 5 mV of zero, while the ζ-potential of HYD micelles was slightly positive (+13 mV). Drug loading was determined spectrometrically. Results indicated that GLY and HYD micelles had nearly identical drug loading by weight/weight percent (26%). Drug loading of ABZ micelles was slightly less (17%).

4.4 Discussion

4.4.1 Block Copolymer Synthesis

Block copolymer synthesis was carried out in three major steps: scaffold synthesis, drug binding linker insertion, and DOX conjugation. A PEG-p(BLA) scaffold with 16 BLA units was successfully synthesized, as confirmed by ^{1}H-NMR. The synthesis process aimed to produce 15 BLA repeating units, controlled by the amount of BLA-NCA added to the reaction. A slight excess (10%) of BLA-NCA was used in the reaction to account for partially inactive BLA-NCA. This extra BLA-NCA yielded an additional repeating unit. One of three drug binding linkers was inserted into the PEG-p(BLA) scaffold: HYD, ABZ-HYD, or GLY-HYD. A three-step reaction process was used for ABZ-HYD and GLY-HYD insertion. PEG-p(BLA) was deprotected, replacing BLA with aspartate moieties. A coupling reaction was then used to insert spacers (ABZ-OMe or GLY-OMe), as direct spacer insertion into the PEG-p(BLA) scaffold proved unsuccessful. Once inserted, the methyl esters of spacers were replaced with hydrazide. ^{1}H-NMR confirmed

each step of the reaction. HYD drug binding linker insertion used a one-pot reaction, since hydrazide can readily replace PEG-p(BLA) benzyl groups. DOX was covalently attached to each block copolymer, resulting in PEG-p(Asp-HYD-DOX), PEG-p(Asp-ABZ-HYD-DOX), and PEG-p(Asp-GLY-HYD-DOX). Ether precipitation followed by Sephadex LH-20 column purification removed any physically-entrapped DOX.

4.4.2 Polymer Micelle Preparation and Characterization

PEG-p(Asp-HYD-DOX), PEG-p(Asp-ABZ-HYD-DOX), and PEG-p(Asp-GLY-HYD-DOX) block copolymers were used to prepare HYD, ABZ, and GLY micelles, respectively. Micellar properties including particle size, ζ-potential, and drug loading were determined. The insertion of drug binding linkers minimally affected micellar particle size or surface charge. ABZ and GLY micelles were approximately 50 nm in diameter, while HYD micelles were just over 100 nm in diameter. The discrepancy in size was attributed to the difference in block copolymer structure. In the absence of an ABZ or GLY spacer, block copolymers used to form HYD micelles were less hydrophobic. It was therefore proposed that the HYD micelle core was less compact and that HYD micelles were less thermodynamically stable.

The surface charge of micelles was determined, as it plays a key role *in vitro* and *in vivo*. Particles with ζ-potentials within 10 mV of zero are minimally taken up by the mononuclear phagocyte system (10). ABZ and GLY micelles had a relatively neutral ζ-potential. However, the ζ-potential of HYD micelles was slightly positive. The PEG shell of micelles was previously shown to shield charge, creating a neutral barrier (128). The slightly positive surface charge of HYD micelles further indicated that they may be

thermodynamically less stable. Overall, each micellar formulation was near the ζ-potential range where uptake by the mononuclear phagocyte system is reduced.

Drug loading was approximately 25% (weight/weight) for both HYD and GLY micelles, while drug loading of ABZ micelles was 17%. Lower drug loading with ABZ micelles was also observed in the initial synthesis. 12-35 ABZ micelles had lower drug loading than 12-35 GLY micelles. The additional presence of benzyl rings may have interfered with DOX conjugation. Even with lower drug loading, ABZ micelles contained a pharmaceutically relevant amount of DOX.

4.5 Conclusions

A block copolymer scaffold with 16 hydrophobic repeating units was synthesized. Block copolymers were modified with one of three drug binding linkers (HYD, ABZ-HYD, or GLY-HYD). DOX was successfully attached to block copolymers using a hydrazone bond. Drug loading was at least 15% (weight/weight) in all formulations. Block copolymers formed micelles with comparable characteristics. Furthermore, ABZ and GLY micelles were nearly identical in size and surface charge.

CHAPTER FIVE

5 DOXORUBICIN DRUG RELEASE FROM MICELLES: MODELING AND ANALYSIS

5.1 Introduction

Drug release rates *in vitro* and *in vivo* play key roles in drug efficacy (129). NDDS varying in drug release rates must be developed to illuminate these effects. Block copolymer micelles have been used as NDDS with success in preclinical and clinical trials. Through the use of a hydrazone bond, DOX can be chemically conjugated to block copolymers. Hydrazone bonds have been shown to be pH-sensitive, thereby minimizing DOX release in physiological conditions (130). Spacers prior to the hydrazone moiety have been shown to affect drug release.

In initial studies with 12-5, 12-15, and 12-35 block copolymers, the hydrazone bond was shown to be pH-sensitive. However, modeling results indicated that spacer insertion (ABZ or GLY) did not alter release rates. The initial studies used a model which combined multiple factors into a single apparent release rate. The oversimplification of drug release hindered in-depth analysis of DOX release rates. However, comparing the degree of DOX release over 48 hours yielded intriguing results. A change in total DOX release was observed as ABZ micelles released more DOX than GLY micelles. In order to better understand how drug release is affected by block copolymer composition, additional studies were required.

In this work, the block copolymer scaffold (12-16) was fixed, eliminating a variable which could affect drug release. Block copolymers modified with drug binding linkers (HYD, ABZ-HYD, or GLY-HYD) and conjugated DOX were used to prepare

respective polymer micelles. Though HYD, ABZ, and GLY micelles were characterized, drug release parameters had yet to be determined.

DOX release from prepared micelles involves multiple processes, such as DOX hydrolysis from the block copolymers and DOX partitioning within the micelle. Furthermore, dynamic dialysis creates an additional barrier for release, as the drug must diffuse through a membrane to reach a reservoir. Each of these parameters must be determined to understand which factors are key in drug release. Accordingly, multiple drug release studies at pH 5.0 and pH 7.4 were performed, and drug release parameters were determined using a comprehensive mathematical model. With a more complete understanding of drug release, not only will *in vitro* and *in vivo* analysis be more thorough, but future micelle preparation can also be guided by these results.

5.2 Materials and Methods

5.2.1 Materials

Slide-A-Lyzer® dialysis cassettes (10,000 MWCO), Sephadex LH-20 gels, potassium biphthalate sodium hydroxide buffer solution, potassium phosphate monobasic buffer solution, and 96-well plates were purchased from Fisher Scientific (USA). Amicon® Ultra centrifugal filters (10,000 MWCO) were purchased from Millipore (USA). DOX was purchased from LC Laboratories (USA).

5.2.2 Dynamic Dialysis

DOX release from micelles was observed in acidic and neutral conditions at 37°C. Potassium biphthalate sodium hydroxide buffer solution (pH 5.0, 0.01 M ionic strength) and potassium phosphate monobasic buffer solution (pH 7.4, 0.02 M ionic strength) were used for all drug release studies, unless otherwise specified. Temperature and pH of

buffer solutions were monitored throughout the study, verifying no drift from initial conditions.

All drug release experiments were performed using the same method, only altering buffer pH or block copolymer concentration. DOX release from micelles at three block copolymer concentrations was observed (0.1, 0.5, or 1.0 mg/mL). Block copolymers were weighed and dissolved in 10 mM buffer solutions (pH 5.0 or pH 7.4). Block copolymer solutions (3 mL) were subsequently transferred into dialysis cassettes (10,000 MWCO). Each individual drug release experiment was performed using three dialysis cassettes, totaling three samples. Dialysis cassettes were placed into a 5.0 L reservoir. One hundred microliters of solution were removed from dialysis cassettes at the following time points: 0, 0.5, 1, 3, 6, 24, 48, and 72 hours. Drug release experiments performed at 0.1 and 0.5 mg/mL block copolymer concentrations had the following additional sampling times: 1.5, 2.0, 4.5, and 9.0 hours. A total of six drug release studies were performed at two pHs (5.0 and 7.4) and at three block copolymer concentrations (0.1, 0.5, and 1.0 mg/mL).

Buffer concentration effects were observed with dynamic dialysis. HYD, ABZ, and GLY block copolymers (0.5 mg/mL) were dissolved in buffer solutions. As previously, block copolymer solutions were transferred into dialysis cassettes which were subsequently placed in either 5 or 20 mM buffer solutions (pH 5.0, 0.005 and 0.02 M ionic strength, respectively). Temperature was held constant at 37°C and pH was monitored throughout the experiment. At predetermined time points (0, 0.5, 1, 1.5, 3, 4.5, 6, 9, 24, 48, and 72 hours), 100 µL of solution were removed for analysis.

The rate of free DOX transport through dialysis cassettes was monitored at both pH 5.0 and pH 7.4. DOX was dissolved in buffer solution (0.12 mg/mL) and transferred to dialysis cassettes. The dialysis cassettes were subsequently placed in a 5.0 L vessel containing either pH 5.0 or pH 7.4 buffer solutions (10 mM). One hundred microliter samples were taken during the first five hours for analysis. In order to monitor DOX binding to the dialysis membrane, a follow-up experiment was performed using the same dialysis cassettes from the free DOX transport experiments. Previously-used dialysis cassettes were emptied and filled with free DOX solutions (0.12 mg/mL). Dialysis cassettes were then placed into buffer solutions (5.0 L). Samples were taken for the first five hours and analyzed.

An additional control experiment was performed to observe the effect of block copolymers on free DOX disappearance from the dialysis cassettes. When the drug release study at 0.5 mg/mL block copolymer concentration was completed, the block copolymer solution was removed from dialysis cassettes and then spiked with free DOX. The samples were thoroughly mixed and placed back into dialysis cassettes, which in turn were placed into 5.0 L buffer solutions. DOX disappearance was then observed over a 72 hour period. This was done for each micellar formulation.

5.2.3 Non-Sink Conditions Drug Release

A secondary drug release experiment was performed using a non-sink condition drug release method developed by Kyle Fugit from Dr. Anderson's laboratory (University of Kentucky, Pharmaceutical Sciences). Block copolymers were weighed and dissolved in buffer solution (pH 5.0 or 7.4) at a 0.5 mg/mL concentration. Block copolymer solutions (3 mL) were transferred into a scintillation vial, which was subsequently placed in an

incubator. The incubator maintained a constant temperature of 37°C while the scintillation vials were gently shaken. At specific intervals, 250 µL of solution were removed and diluted with methanol to 500 µL. The samples were ultrafiltered using an Amicon® Ultra 0.5 mL centrifugal filter (10,000 MWCO). Ultrafiltration containers were centrifuged at 14,000 revolutions per minute (rpm) for 10 minutes. Afterwards, supernatants were collected and diluted to 500 µL. Ultrafiltration was repeated twice more. The final supernatant was collected and analyzed spectroscopically. Block copolymers (MW >13,000) were not expected to be removed during this process. Therefore, the supernatant was expected to contain only DOX conjugated to block copolymers or DOX partitioned into the micelle, as free DOX (580 MW) was not retained by the filter. Drug release was repeated twice, totaling three experiments.

Free DOX removal using ultrafiltration was validated two ways. Free DOX was dissolved in a 50% methanol:water mixture and ultrafiltered. After three ultrafiltration cycles, spectrometric analysis determined that no DOX was present in the concentrate. An additional confirmation was performed using two identical block copolymer solutions. One sample was spiked with free DOX and vortexed vigorously. Both samples underwent three ultrafiltration cycles. At the end of three cycles, there was no statistical difference between the DOX concentrations in the two samples, confirming free DOX removal.

Recovery percentages of block copolymers were calculated for HYD, ABZ, and GLY micelles to confirm reproducibility. Block copolymers were dissolved in buffer solution and immediately ultrafiltered according to protocol. Micellar DOX

concentrations were determined before and after ultrafiltration. The percent recovered was calculated and reported. This experiment was performed in triplicate.

5.3 Results

5.3.1 Drug Release (1.0 mg/mL) by Dynamic Dialysis

Drug release studies were performed under sink conditions at physiological pH (7.4) and intralysosomal pH (5.0) at a 1.0 mg/mL concentration for each micelle composition (HYD, ABZ, and GLY). DOX release from micelles was observed over 72 hours. Multiple samples were taken during that time and drug release results were plotted as percent drug remaining versus time. Drug release profiles indicated a two phase release of DOX, with an initial quick release followed by a slower, prolonged release. As a preliminary analysis, micellar drug release was fitted to a simple biphasic model consisting of two separate first order release processes (Figure 14). The model fit the drug release profile well, suggesting that DOX release from micelles occurs at two separate rates. A more thorough model was later employed.

Irrespective of micelle composition, more DOX was released at pH 5.0 than at pH 7.4. After 72 hours, DOX release from HYD micelles was 77% at pH 5.0 and 52% at pH 7.4. At this same time point, ABZ micelles released 52% and 35% of DOX at pH 5.0 and pH 7.4, respectively. Similarly, GLY micelles exhibited 45% and 28% DOX release at pH 5.0 and pH 7.4, respectively. It was apparent that total drug release followed a pattern of HYD micelles releasing the largest percentage of DOX followed by ABZ and GLY micelles, irrespective of pH. This trend (HYD>ABZ>GLY) persisted for the 24 and 48 hour time points.

For additional analysis, the AUC for drug concentration remaining between zero

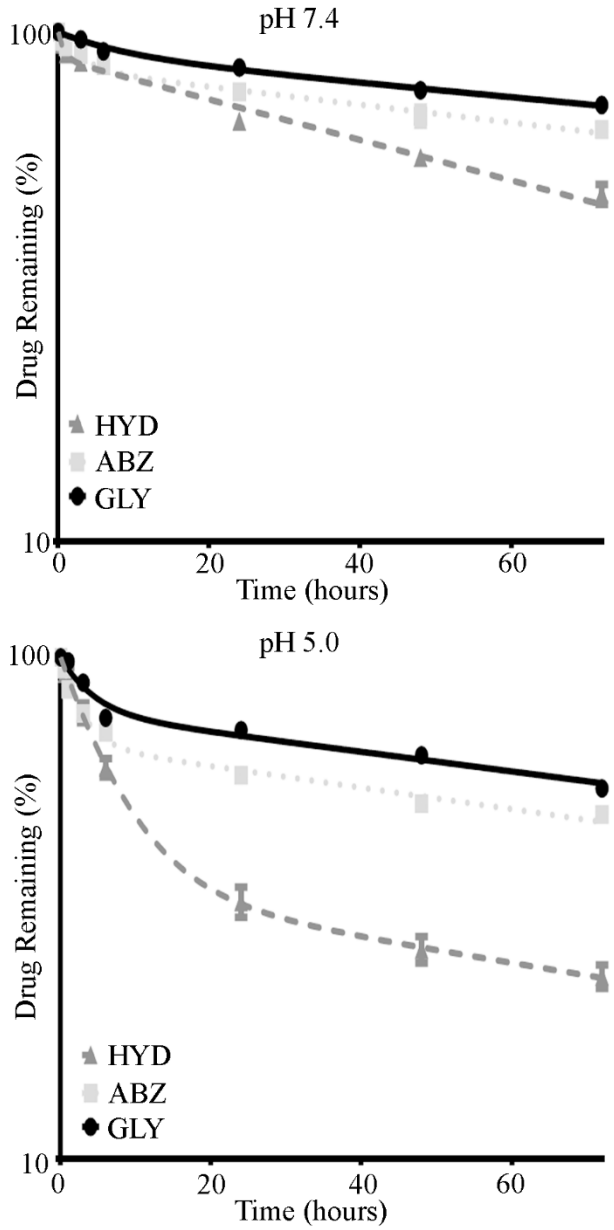

Figure 14. DOX Release from HYD, ABZ, and GLY Micelles at a 1.0 mg/mL Concentration by Dynamic Dialysis. Drug Release was Fitted to a Biphasic Model

and 72 hours was calculated. Comparing DOX release from the same micellar system in different conditions showed that the pH 5.0 AUC was lower than the pH 7.4 AUC in each case. The most drastic change was observed for HYD micelles, with a decrease of almost 50% in AUC from pH 7.4 to pH 5.0 (4650 versus 2600 hours*remaining %). AUCs of ABZ and GLY micelles also differed, but the differences were less substantial (5340 versus 4150 hours*remaining % and 5900 versus 4910 hours*remaining %, respectively). HYD micelles exhibited the lowest AUC in both pHs. The ABZ micelle AUC followed, while GLY micelles exhibited the highest AUC. Relative AUC was calculated using the following formula: AUC/AUC_{HYD}. Results clearly showed the large difference between HYD micelles and both ABZ and GLY micelles. At pH 5.0, the relative AUC of ABZ micelles was 1.60, while GLY micelles had a relative AUC of 1.89. At pH 7.4 differences were smaller but still present. The relative AUC of ABZ and GLY micelles was 1.14 and 1.27, respectively.

5.3.2 Dynamic Dialysis Drug Release (Additional Studies)

Additional drug release studies were performed at different block copolymer concentrations (0.1 and 0.5 mg/mL) (Figure 15). Decreasing the block copolymer concentrations from 1.0 to 0.5 mg/mL resulted in greater DOX release from all micellar systems irrespective of pH. For example, total DOX release from HYD micelles at pH 5.0 increased from 52% to 72%. Furthermore, total DOX release from micelles at the 0.5 mg/mL concentration followed the trend: HYD>ABZ>GLY. Drug release studies at 0.1 mg/mL in pH 7.4 buffer led to a further increase in total drug release for all micellar formulations. Conversely, no change in drug release profiles was observed in pH 5.0 when lowering block copolymer concentration to 0.1 mg/mL. Consistent with previous

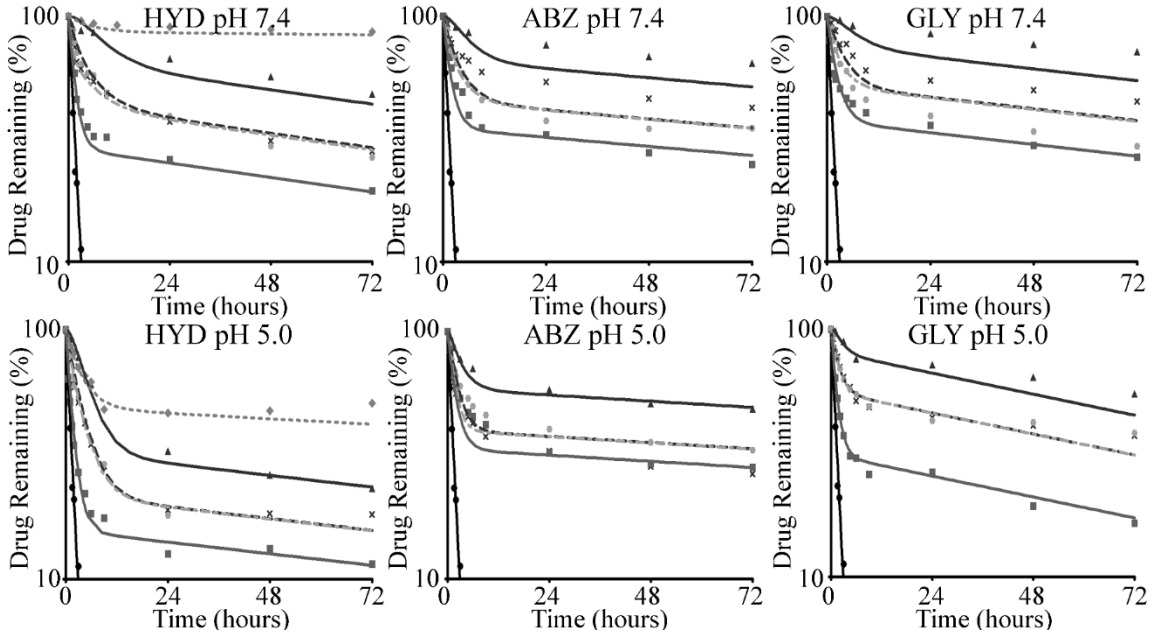

Figure 15. Simultaneous Fitting of Drug Release Data at pH 5.0 and 7.4. Diamonds Represent Non-Sink Drug Release. Triangles, Crosses, and Light Circles Represent Dynamic Dialysis Drug Release at 1.0, 0.5, and 0.1 mg/mL, Respectively. Squares Represent Spiked DOX Release. Dark Circles Represent Free DOX Release

Table 6. 72 hour Drug Release AUC Analysis (1.0 mg/mL Concentration)

Micelle	72 hour AUC (hours*remaining %)		Relative AUC (AUC/AUC_{HYD})	
	pH 5.0	pH 7.4	pH 5.0	pH 7.4
HYD	2600 ± 250	4650 ± 190	1.00 ± 0.13	1.00 ± 0.06
ABZ	4150 ± 70	5340 ± 230	1.60 ± 0.10	1.14 ± 0.06
GLY	4910 ± 50	5900 ± 100	1.89 ± 0.10	1.27 ± 0.04

Determined values are shown as means ± standard deviations.

results, total DOX release was greater at pH 5.0 than at pH 7.4.

Drug release studies were conducted at pH 5.0 at two different buffer concentrations: 5 and 20 mM (Figure 16). The different buffer concentrations did not affect drug release. Drug release profiles from 5 and 20 mM buffer concentrations overlapped. Additionally, previous works have shown that ionic strength does not affect drug release in similar systems (114).

The disappearance of free DOX (0.12 mg/mL) from dialysis cassettes was observed at both pH 5.0 and pH 7.4. As a small molecule, DOX readily diffused through the dialysis membrane. After five hours, negligible amounts of DOX remained in both pH conditions. An additional study was performed to observe potential binding to the dialysis membrane. The dialysis cassettes from the initial free DOX disappearance studies were reused. Cassettes were reloaded with free DOX (0.12 mg/mL), and the disappearance of free DOX was monitored again. Results were identical to the initial study, as the disappearance rate of DOX was identical in both experiments (data not shown).

The final dynamic dialysis drug release study was a spike experiment. Polymer solutions were spiked with free DOX, and DOX elimination from cassettes was observed. Prior to free DOX spike, 29% and 18% DOX remained in HYD micelles at pH 7.4 and pH 5.0, respectively. Spiking the HYD micellar solution with free DOX increased DOX concentration within the dialysis membrane. However, within six hours DOX returned to previous levels (31% and 17% remaining at pH 7.4 and 5.0, respectively). This signified that free DOX escaped the dialysis membrane while DOX associated with block copolymers remained. Furthermore, release from HYD micelles continued with the same

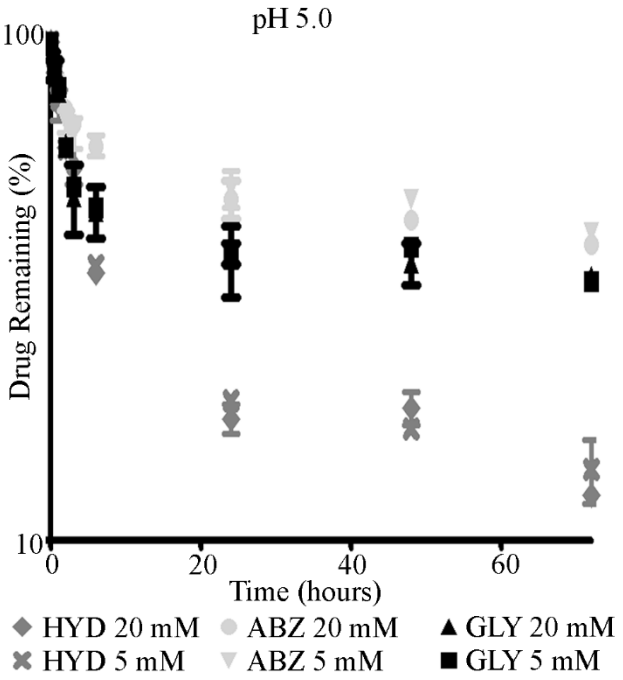

Figure 16. Drug Release from Micellar Systems at pH 5.0 in Different Buffer Conditions

overall trend. Similar results were observed with the free DOX spike experiments using ABZ and GLY micelles. Percent DOX remaining in ABZ micelles prior to free DOX spiking was 27% and 42% at pH 5.0 and pH 7.4, respectively. After six hours, the DOX levels returned to 42% at pH 7.4. For GLY micelles, initial percent DOX remaining was 37% and 45% at pH 5.0 and pH 7.4, respectively. Six hours afterward, percent DOX remaining returned to 31% at pH 5.0 and 44% at pH 7.4. Spike experiment results indicated that free DOX in the presence of block copolymer escapes quickly, mimicking the rate of free DOX escape.

5.3.3 Non-Sink Conditions Drug Release

DOX release from HYD, ABZ, and GLY micelles was first observed under non-sink conditions at pH 5.0 (0.5 mg/mL) (Figure 15). At predetermined time points, samples were taken and prepared for analysis. Each sample underwent ultrafiltration to separate free DOX from conjugated and partitioned DOX. DOX concentration in the concentrate was measured spectroscopically. Drug release studies were carried out up to one week. DOX release was not observed from GLY or ABZ micelles after the first 24 hours. At every point, DOX concentrations were statistically equivalent to the initial concentrations. Therefore, GLY drug release studies were discontinued. The drug release experiment with ABZ micelles was continued for an additional day, but even then there was no change in DOX concentration. Significant DOX release (15%) was observed from HYD micelles within the first hour. DOX release continued up to the nine hour mark, reaching 52%. After this point, DOX release remained unchanged throughout the remainder of the study.

Drug release experiments were only performed with HYD micelles at pH 7.4.

Drug release studies were planned for ABZ and GLY micelles at pH 7.4 but were not performed due to lack of DOX release at pH 5.0. After the first hour, no drug release was observed from HYD micelles. A slight decrease (5%) in DOX concentration was observed at the three hour mark. DOX release continued for the first 72 hours, reaching a maximum of 14%, and remaining constant beyond this point. Overall, more DOX was released at pH 5.0 (52%) than at pH 7.4 (15%).

5.3.4 Mathematical Model Description

A mathematical model was developed for data fitting and simulations in collaboration with Kyle Fugit. Kyle wrote the code for the model, producing drug release parameters. An initially proposed model considered three major factors: release of DOX from the micelle (k_1), DOX partitioning (K_p), and DOX transport through the dialysis membrane (k_d) (Figure 17). The remaining variables in the initial model were: conjugated DOX (C_1^m), free DOX partitioned in the micelle (C_U^m), free DOX in the aqueous phase (C_U^w), free DOX in the reservoir (C_R), and the percent of DOX initially conjugated to block copolymers (P_C). This initial model assumed DOX release from micelles (k_1) followed first order release. A secondary assumption was that all DOX molecules within the micelle behaved similarly. However, drug release studies clearly showed biphasic DOX release from micelles (Figures 14-16). In order to account for the two phases of release, the initially proposed model was modified by introducing two release rate constants (k_f, k_s) (Figure 18). Based on this scheme, a mathematical model was developed as described below.

Total DOX mass (M_T) present in dialysis cassettes can be divided into two main species: unconjugated DOX (M_U) and conjugated DOX (M_C):

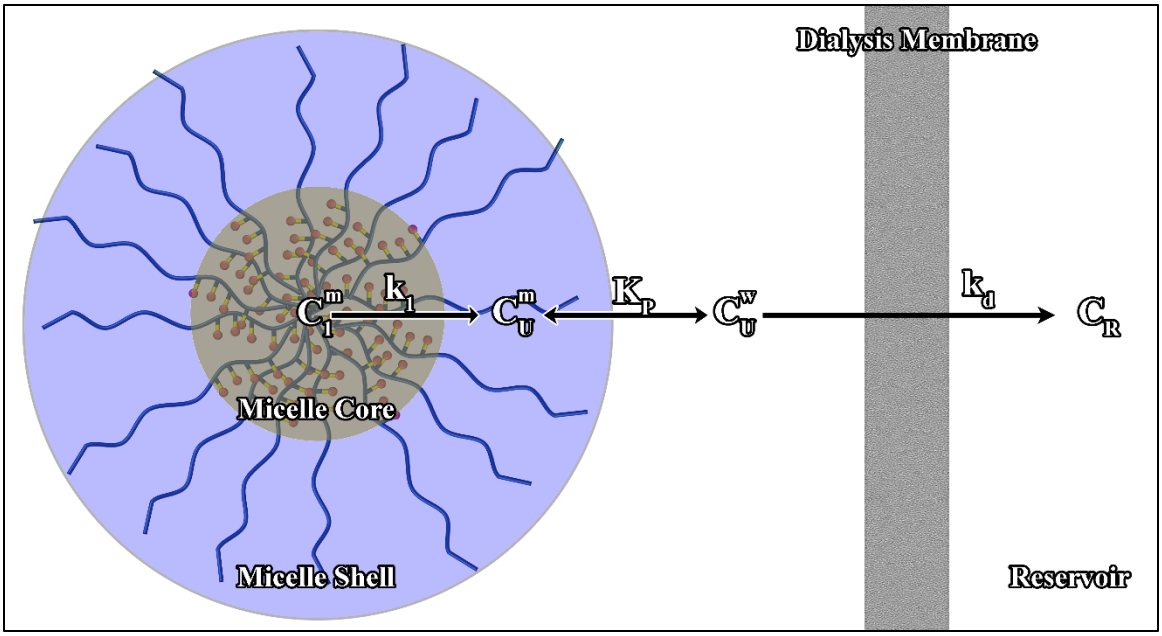

Figure 17. Initially Proposed Drug Release Mode of Covalently Attached DOX

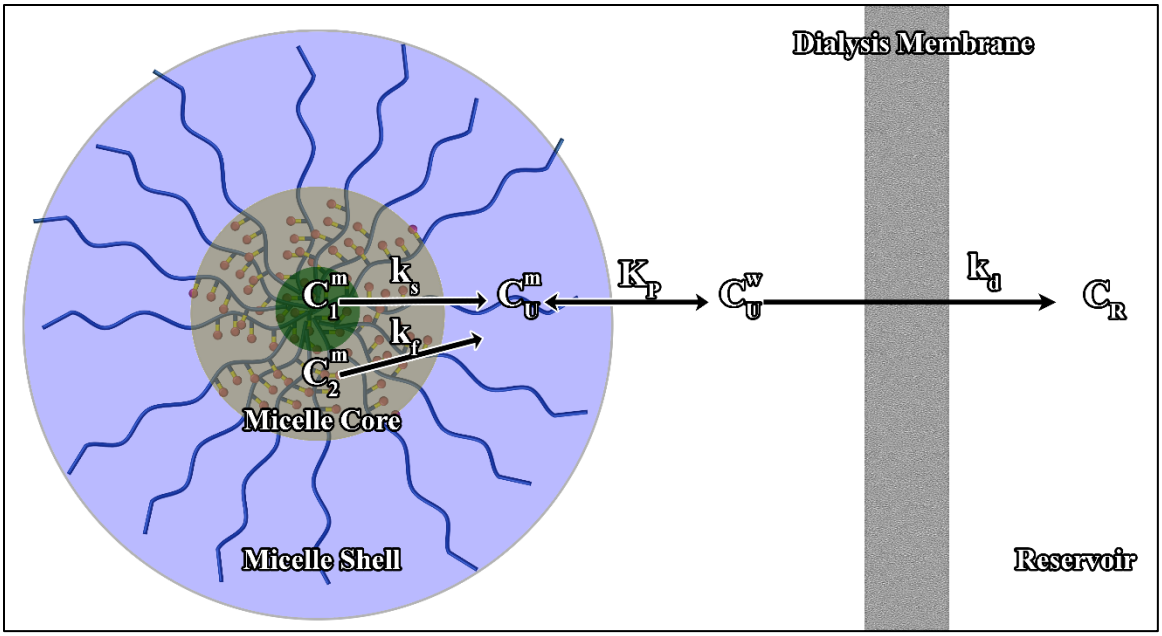

Figure 18. Final Drug Release Model of Covalently Attached DOX

$$M_T = M_U + M_C$$

Furthermore, unconjugated DOX can either be partitioned within the micelles (M_{Um}) or within the aqueous phase (M_{Uw}). The two populations of conjugated DOX (M_{Cf} & M_{Cs}) represent DOX undergoing fast and slow release.

$$M_U = M_{Uw} + M_{Um}$$

$$M_C = M_{Cf} + M_{Cs}$$

The total mass balance of DOX can then be rewritten as:

$$M_T = M_{Uw} + M_{Um} + M_{Cf} + M_{Cs}$$

The masses can then be converted into concentrations using volume ratios of the aqueous (w) and micellar (m) environments:

$$a = \frac{V^w}{V_T}; b = \frac{V^m}{V_T}$$

where V^w is the volume of the aqueous phase; V^m is the micellar volume; and V_T is the total volume. Volume fractions herein are calculated based on the mass. Combining the volume ratio with the mass balance yields the following equation:

$$C_T = aC_U^w + bC_U^m + bC_f^m + bC_s^m$$

As described above, micellar DOX release in dynamic dialysis experiments depends on DOX escape from micelles and DOX transport through the dialysis membrane. The differential equations below describe this process.

$$\frac{dC_f^m}{dt} = -k_f C_f^m$$

$$\frac{dC_s^m}{dt} = -k_s C_s^m$$

$$\frac{dC_U}{dt} = b\left(k_f C_f^m + k_s C_s^m\right) - k_d(C_U^w - C_R)$$

$$\frac{dC_R}{dt} = 0.018k_d(C_U^m - C_R)$$

Where $\frac{dC_f^m}{dt}$ and $\frac{dC_s^m}{dt}$ represent the change in concentration of covalently attached DOX; $\frac{dC_U}{dt}$ describes the change in free DOX concentration within the dialysis membrane; and $\frac{dC_R}{dt}$ describes the change in free DOX concentration within the reservoir. The volume ratio of the dialysis cassette to the reservoir is 0.018. The rates guiding drug release include DOX escape from micelles (k_f & k_s), and DOX transport through the dialysis membrane (k_d). Furthermore, DOX can partition within the micelle or the aqueous phase (K_p).

$$K_p = \frac{C_U^m}{C_U^w}$$

Using this information, C_U^w can be rewritten in terms of total unconjugated DOX:

$$C_U^w = \frac{C_U}{a + bK_p}$$

This term can then be substituted in the differential equations:

$$\frac{dC_U}{dt} = b\left(k_f C_f^m + k_s C_s^m\right) - k_d\left(\frac{C_U}{a + bK_p} - C_R\right)$$

$$\frac{dC_R}{dt} = k_d f_R\left(\frac{C_U}{a + bK_p} - C_R\right)$$

It is important to note that at time zero DOX can be present either in the conjugated (C_f^m, C_s^m) or free form (C_U). Percent conjugated DOX (P_c) is used to distinguish between the two forms of DOX. Additionally, F_{kf} describes the fraction of DOX undergoing fast release. These terms are incorporated into the model as initial conditions:

$$C_f^m(0) = \frac{P_c}{100}\frac{F_{kf}}{b}C_{T,0}$$

$$C_s^m(0) = \frac{P_c}{100}\frac{(1-F_{kf})}{b}C_{T,0}$$

$$C_U(0) = \left(1 - \frac{P_c}{100}\right)C_{T,0}$$

$$C_R(0) = 0$$

The same model with minor adjustments is used to describe drug release under non-sink conditions. The equation describing total drug concentration is altered due to the analysis method. For non-sink drug release studies, free DOX is separated from conjugated DOX and DOX partitioned within the micelle. After separation, only conjugated and partitioned DOX concentrations are measured; therefore, the total measured DOX concentration becomes:

$$C_T = b(C_f^m + C_s^m + C_U^m)$$

Using the partition coefficient, total concentration can be rewritten in terms of total unconjugated DOX.

$$C_U^m = \frac{K_p C_U}{a + bK_p}$$

$$C_T = b(C_f^m + C_s^m + \frac{K_p C_U}{a + bK_p})$$

Differential equations related to micellar DOX concentrations remain the same, but $\frac{dC_R}{dt}$ may be disregarded as there is no reservoir present. DOX transport through the dialysis membrane does not occur in non-sink conditions. Therefore, the change in unconjugated DOX concentration over time can be simplified. Differential equations for non-sink drug release are shown below.

$$\frac{dC_f^m}{dt} = -k_f C_f^m$$

$$\frac{dC_s^m}{dt} = -k_s C_s^m$$

$$\frac{dC_U}{dt} = b\left(k_f C_f^m + k_s C_s^m\right)$$

In dynamic dialysis the model required the term P_c to account for any unconjugated DOX. Initial conditions in non-sink drug release are changed due to removal of free DOX by ultrafiltration.

$$C_f^m(0) = \frac{F_{kf}}{b} C_{T,0}$$

$$C_s^m(0) = \frac{(1-F_{kf})}{b} C_{T,0}$$

$$C_U(0) = 0$$

Using this mathematical model, drug release data from each individual micelle were fitted simultaneously.

5.3.5 Mathematical Modeling Results

Drug release studies were performed at pH 5.0 and pH 7.4. At least eight separate drug release experiments were performed for each micelle formulation under varying conditions. Additionally, each individual drug release experiment was repeated three times. Drug release from ABZ and GLY micelles was observed at three different block copolymer concentrations (0.1 mg/mL, 0.5 mg/mL, and 1.0 mg/mL). An additional experiment was performed for observing the release of free DOX in the presence of block copolymers. The same experiments were performed using HYD micelles with an additional experiment under non-sink conditions. Free DOX transport studies were incorporated into the model to more accurately determine the rate of free DOX escape from dialysis cassettes.

Utilizing the models described in the previous section, drug release studies were fitted to determine the following drug release parameters: $k_f, k_s, k_d, K_p, F_{kf}, P_c$ (Table 7). The fitting determined k_d using the spiked experiment. Intriguingly, depending on the micellar concentration, percent of initially conjugated DOX (P_c) varied. Modeling results indicated that DOX was completely conjugated in drug release studies performed at 1.0 mg/mL concentrations, while 35-50% unconjugated DOX was present in studies performed at lower concentrations. Block copolymers used in all drug release experiments were identical in every aspect. As described in the previous methods section, all block copolymers were synthesized and subsequently stored in conical tubes as solids at -20°C. Samples were removed and used as needed for experiments. The sole difference between block copolymers used for drug release at lower concentrations and drug release at 1.0 mg/mL was the time frame over which the experiments were performed. The drug release study at the 1.0 mg/mL concentration was completed approximately 14 months prior to other experiments.

Due to differences in percent DOX conjugated, it was proposed that the hydrazone bond underwent hydrolysis during storage releasing DOX from block copolymer. This hypothesis was tested in three ways: modeling, ultrafiltration, and Sephadex LH-20 purification (Table 8). All three methods determined the percent DOX conjugated 14 months after initial storage. Modeling drug release at 0.1 and 0.5 mg/mL block copolymer concentrations determined that between 35% and 50% of the DOX was unconjugated. The presence of unconjugated DOX was equated to degradation of the hydrazone bond. A secondary method of degradation analysis used the centrifugal ultrafiltration validation study; typically greater than 90% recovery is expected after

Table 7. Modeled Drug Release Parameters

Micelle	pH	k_f (hr^{-1})	k_s (hr^{-1})x10^{-2}	k_d (hr^{-1})	K_px10^3	F_{kf}	P_c (1.0)	P_c (0.1,0.5)
HYD	7.4	0.24 ± 0.1	0.55 ± 0.1	1.0 ± 0.6	30 ± 5.9	0.35 ± 0.04	100	59
ABZ		0.27 ± 0.2	0.36 ± 0.5	0.91 ± 0.1	11 ± 8.3	0.24 ± 0.27	100	59
GLY		0.10 ± 0.1	0.42 ± 0.1	1.0 ± 0.6	46 ± 44	0.18 ± 0.08	100	59
HYD	5.0	0.27 ± 0.0	0.39 ± 0.4	0.93 ± 0.1	8.6 ± 1.2	0.66 ± 0.01	100	64
ABZ		0.10 ± 0.1	0.31 ± 0.5	0.72 ± 0.0	0	0.27 ± 0.18	80	50
GLY		0.52 ± 0.4	0.80 ± 0.4	0.74 ± 0.1	0	0.15 ± 0.03	100	66

Data reported as fitted value ± standard error.

Table 8. Percent of Conjugated DOX Determined by Different Methods

Method	HYD	ABZ	GLY
Ultrafiltration	62 ± 4	65 ± 2	65 ± 3
Modeling	66 ± 1	50 ± 5	64 ± 3
Sephadex LH-20	67 ± 2	68 ± 1	69 ± 2

Data reported as fitted or determined value ± standard error.

ultrafiltration purification. In the case of block copolymers, the recovery percentage was between 62% and 65%. The poor degree of recovery, in close agreement with modeling results, was attributed to presence of free DOX. A third confirmation was performed using Sephadex LH-20 purification. Fifteen month old material was purified, removing any free DOX formed during storage. Drug loading was measured before (B_{DL}) and after purification (A_{DL}). The difference in drug loading was used to calculate the percent conjugated DOX ($A_{DL}/B_{DL} * 100$). According to this experiment, between 31% and 33% of conjugated DOX was lost to hydrazone degradation, depending on the micelle formulation. These values matched the percent unconjugated as determined by modeling. The three separate methods were in agreement, all pointing to hydrazone bond degradation after prolonged storage.

Using the information regarding degradation, the model was run again, but this time the percent DOX conjugated was set as determined by Sephadex LH-20 purification (Table 8). At a 1.0 mg/mL concentration, the percent conjugated was set at 100% for all micelles, while at 0.1 and 0.5 mg/mL concentrations the percent conjugated was set to 67%, 68%, and 69% for HYD, ABZ, and GLY micelles, respectively. By eliminating a parameter, the model was able to more precisely describe drug release (Table 9).

The initial fast DOX release rate constant (k_f) at pH 7.4 was comparable from one micelle to the next, as k_f of HYD, ABZ, and GLY micelles was 0.24, 0.27, and 0.30 $hour^{-1}$, respectively. The slow release rate constant (k_s) was substantially slower than the fast release rate constant. In this case, the half-life was more than 80 hours, irrespective of micelle formulation. The DOX fraction undergoing fast release (F_{kf}) was also similar in all micelles. These results were consistent with drug release studies performed with

Table 9. Drug Release Parameter Determined Through Mathematical Modeling

Micelle	pH	k_f (hr^{-1})	k_s (hr^{-1})	k_d (hr^{-1})	K_p	F_{kf}
HYD	7.4	0.24 ± 0.12	0.0055 ± 0.001	0.81 ± 0.03	3000 ± 590	0.38 ± 0.06
ABZ		0.27 ± 0.20	0.0036 ± 0.001	0.79 ± 0.03	1100 ± 830	0.34 ± 0.06
GLY		0.30 ± 0.11	0.0046 ± 0.001	0.80 ± 0.03	2200 ± 1000	0.25 ± 0.04
HYD	5.0	0.29 ± 0.05	0.0045 ± 0.001	0.80 ± 0.03	620 ± 170	0.68 ± 0.03
ABZ		1.15 ± 0.97	0.0059 ± 0.002	0.78 ± 0.03	0	0.36 ± 0.05
GLY		0.64 ± 0.5	0.0082 ± 0.001	0.77 ± 0.02	0	0.20 ± 0.05

Data reported as fitted value ± standard error.

12-5, 12-15, and 12-35 micelles. Spacers seemed to have little to no effect in neutral conditions.

Micellar drug release parameters determined at pH 5.0 were compared to those at pH 7.4. Focusing on ABZ and GLY micelles first, it was evident that the fraction of DOX undergoing fast release was equivalent across both conditions. At pH 5.0, F_{kf} for ABZ micelles was 0.36, and at pH 7.4 it was 0.34. For GLY micelles F_{kf} was slightly lower. Furthermore, determined initial fast release rate constants at pH 5.0 and pH 7.4 were also similar. However, the fast release rate constant (k_f) had a very wide standard deviation, so quantitative analysis could not be performed. The ability to precisely determine k_f was lost due to degradation during storage. The sole differences between drug release at pH 5.0 and pH 7.4 were the slow release rate constant (k_s) and the partition coefficient (K_p). For both ABZ and GLY micelles, k_s was consistently, and statistically greater in acidic conditions. Furthermore, K_p was larger at pH 7.4 than at pH 5.0.

For HYD micelles, k_f was not statistically different from one pH condition to the next. However, F_{kf} differed greatly; at pH 5.0 and pH 7.4, F_{kf} was 0.68 and 0.38, respectively. This nearly twofold difference was not observed for the other micelles. Unlike ABZ and GLY, there was no difference in k_s between pH 5.0 and pH 7.4. A larger partition coefficient was observed again at pH 7.4.

Comparing release rate differences between micelles at pH 5.0 yielded inconclusive results. Though k_f for HYD was 0.29 hour^{-1}, this was not statistically different than any other k_f. The secondary phase for DOX release was very slow, irrespective of block copolymer. The primary difference between the determined drug

release parameters was in F_{kf}. HYD F_{kf} was 0.68, while ABZ and GLY micelles had a 0.36 and 0.20 F_{kf}, respectively.

5.4 Discussion

Block copolymers based on 12-16 PEG-p(BLA) with HYD, ABZ-HYD, or GLY-HYD drug binding linkers were synthesized. DOX was covalently attached to block copolymers with a hydrazone linker. Each block copolymer was used to prepare a respective micelle (HYD, ABZ, or GLY). Micellar physicochemical properties were determined previously, while experiments herein were used to observe effects of drug binding linker on drug release.

The first set of drug release studies was performed in pH 5.0 and pH 7.4 buffers at a 1.0 mg/mL block copolymer concentration. At each time point past the three hour mark, more DOX was released at pH 5.0 than at pH 7.4, regardless of drug binding linker. AUC analysis reaffirmed this notion, as pH 7.4 AUC was always greater than pH 5.0 AUC, signifying less drug release at pH 7.4. The combination of these results indicated that there was a pH effect on drug release, with more DOX released in acidic conditions. Comparing pH 5.0 DOX release at specific time points revealed the differences between HYD, ABZ, and GLY micelles. HYD micelles released the most DOX from the third hour onward, followed by ABZ micelles. Specifically, ABZ micelles released more DOX than GLY micelles at the following time points: 1.0, 3.0, 24, and 48 hours. AUC analysis reinforced these results, as the AUC for drug remaining was lowest for HYD micelles, followed by ABZ micelles, and then GLY micelles. It appeared that the introduction of spacers led to lower overall drug release. Furthermore, the GLY modification resulted in the lowest overall drug release over 72 hours.

An important takeaway from the drug release study at 1.0 mg/mL concentration was not only that drug release was pH-dependent and drug binding linkers affected total drug release, but also that drug release was biphasic. Biphasic drug release has been observed in multiple systems, but a consensus has not been reached on the cause of the two phases (13, 76, 131-133). The exact reason behind the biphasic release herein has not been confirmed, but multiple hypotheses are presented, the first of which is that the hydrolysis of DOX from block copolymers occurs at different rates depending on the location of DOX in the micelle core. DOX closest to the core/shell interface can be hydrolyzed more readily due to facile penetration of hydronium ions. The deeper DOX is in the core of the micelle, the more difficult it is for hydrolysis to occur. Overall, this leads to spatial variation in rates of hydrolysis. DOX closest to the core/shell interface would be hydrolyzed the fastest and each DOX molecule further in the core would have a gradually slower hydrolysis rate. Another hypothesis is that differences in core heterogeneity in terms of hydrophobic and polar environments could account for the two hydrolysis rates. Alternatively, the fast rate of release could represent DOX hydrolysis from single block copolymers, while the slow release rate could represent DOX hydrolysis from a micellar system. This last hypothesis seems unlikely, as drug release studies performed in dialysis cassettes maintained high block copolymer concentrations, especially in drug release studies performed at 1.0 mg/mL concentrations. At these high concentrations, block copolymers are expected to exist primarily as micelles. Though the exact reason behind biphasic drug release was not confirmed, the mathematical model employed took into account two differential release rates.

A thorough mathematical model of drug release from micelles had yet to be developed. Previously, apparent release rates were calculated using zero and first order release models, leaving open a number of possibilities as to what affected drug release. The apparent release rate combined DOX hydrolysis, DOX partitioning, and DOX diffusion into a single rate. Furthermore, only the pH effect was observed, without taking into account effects of block copolymer and buffer concentrations. For this reason, multiple release studies were performed with 12-16 micelles and a more detailed mathematical model was developed to elucidate factors impacting drug release.

A key factor in drug release is DOX partitioning into the micelle. The degree of partitioning can greatly change DOX release and must thus be taken into account (134, 135). Following the release study at 1.0 mg/mL, drug release studies at two lower block copolymer concentrations were performed and analyzed to probe the effect of drug partitioning. As block copolymer concentration decreases, DOX partitioning decreases. When two drug release studies performed at two different block copolymer concentrations have overlapping drug release profiles, partitioning is assumed to be minimized (136). This phenomenon was observed at pH 5.0, as drug release profiles from HYD, ABZ, and GLY micelles at 0.1 and 0.5 mg/mL block copolymer concentrations overlapped in all three cases. However, at pH 7.4 drug release profiles did not overlap completely, signifying that partitioning was still having an impact on the rate of release. The model showed this, as DOX partitioning was a factor at pH 7.4 for all micelles. Partitioning was minimized at pH 5.0, and in the case of ABZ and GLY micelles modeling determined that partitioning effects were insignificant. Across all micelle formulations, DOX partitioning in acidic conditions was significantly lower than in

neutral conditions. This was assumed to be because DOX is in its protonated state at pH 5.0, but at pH 7.4 is a mixture of protonated and neutral species.

Drug release studies were also performed with free DOX since the dialysis membrane acts as a barrier to drug diffusion and can impact release rates if not taken into account (137, 138). Irrespective of pH or micelle formulation the rate constants for DOX disappearance from dialysis cassette was approximately 0.80 $hour^{-1}$. Two additional studies were performed to confirm that DOX binding to the dialysis membrane was not a factor. The first study monitored DOX release from a pre-used dialysis cassette. The rate of DOX disappearance determined from this study matched previous studies. An additional study monitored DOX release in the presence of block copolymers. Again, the presence of polymers essentially had no effect on free DOX disappearance from the dialysis cassette. It was therefore surmised that DOX binding to the dialysis membrane played little to no role in these drug release studies. It is important to note that drug release studies were performed at relatively high DOX concentrations and monitored until <5% DOX remained in dialysis cassettes. In terms of modeling, DOX binding to the dialysis membrane was not relevant at these high concentrations. This did not exclude the possibility of DOX binding; it only validated that the rate of free DOX escape at high concentrations was not impacted by binding to the membrane.

Drug release data from each micellar system were fitted to the mathematical model described previously (Figure 15). Fitted curves matched experimental data. However, determined drug release parameters had large variability minimizing the ability to distinguish effects of different formulations and pH conditions. The fast release rate constant (k_f) was not statistically different in any formulation, regardless of pH. The drug

release at a 1.0 mg/mL block copolymer concentration was influenced by partitioning and could not alone produce the fast release rate constant. Remaining drug release studies were performed after hydrolysis of the hydrazone bond during storage. The fast release rate constant was masked by free DOX escape due to this loss. Determined slow release rate constants (k_s) yielded similar issues. Statistically, the release rates were not different from each other. The sole exception was the GLY formulation k_s, which was marginally higher than the HYD formulation k_s, but even with this difference both micelles exhibited a half-life greater than 80 hours. The DOX fraction undergoing fast release (F_{kf}) was also determined by modeling. At pH 7.4, F_{kf} was similar (~0.30) when comparing release from HYD, ABZ, and GLY micelles, but at pH 5.0 F_{kf} differed depending on formulation. HYD micelles had the largest F_{kf} (0.68). The thermodynamic stability of HYD micelles could explain this difference. HYD micelle particle size suggested stability issues as well. ABZ and GLY micelles were roughly 50 nm in size with a narrow size distribution, while HYD micelles were 100 nm in diameter with a much wider size distribution. The larger, more variable size was possibly due to a more porous micelle. This was observed in pH 7.4, as HYD micelles again had a high F_{kf} (0.38). Not only was the HYD F_{kf} large in both pH conditions, but it was significantly higher than the ABZ and GLY F_{kf} at pH 5.0. This difference may be due to pH-dependent swelling of micelles, but this avenue was not further explored. More experiments are required for a more complete understanding of HYD micellar stability. In the case of ABZ and GLY micelles, the F_{kf} remained unchanged irrespective of pH condition.

To summarize, drug release from HYD, ABZ, and GLY micelles was observed and modeled. Analysis of total drug release indicated a pH-dependence. Furthermore, comparing total release at individual time points (i.e. 3 hours) revealed the same trend. More DOX was consistently released in acidic conditions, regardless of micelle type. AUC analysis was in agreement, showing that over the time course of the experiments, more DOX was released at pH 5.0. Intriguingly, differences in total release were also observed between HYD, ABZ, and GLY micelles at pH 5.0, suggesting that linkers played a role in drug release.

Hydrazone bond degradation under the specified storage conditions was unprecedented. Multiple possible modes of degradation were proposed. First, the hydrazide linkage could have been hydrolyzed during the freeze-drying process prior to storage. This was unlikely for a number of reasons. Before any analysis was performed, all material was freeze-dried, including the material used for drug release studies at a 1.0 mg/mL block copolymer concentration. According to modeling, the percent of DOX conjugated to block copolymers in this study was 100% (Table 7). If hydrolysis occurred during freeze-drying, the percent DOX conjugated would have shown a ~30% loss. Furthermore, mice treated with block copolymer in Chapter 7 showed no adverse toxicity, even when exposed to micelles at high DOX-equivalent concentrations. This again would not be possible if degradation occurred during freeze-drying. Another possibility was degradation during storage at -20°C. Storage under inert conditions was overlooked, thus block copolymers were exposed to the atmosphere prior to being placed in -20°C. In the presence of air, moisture uptake may have caused hydrolysis of the hydrazone bond. This was surmised to be the most likely scenario but additional studies

are required to elucidate degradation. If the hydrazone bond was hydrolyzed as a solid and linear degradation occurred, roughly 2% of free DOX formation would occur in 30 days. The experimental schedule is reported to better understand how degradation may have impacted each individual experiment (Table 10). Micellar characterization was not affected by the degradation, as experiments were performed directly after synthesis. While degradation was taken into account in the modeling, the need to include extra parameters to account for degradation probably contributed to the large uncertainty in some parameter values. The remaining possible effects of degradation are discussed in each of the following chapters.

5.5 Conclusions

DOX release from HYD, ABZ, and GLY micelles was analyzed in both acidic and neutral conditions. Irrespective of drug release conditions and formulation, micelles exhibited biphasic DOX release. A drug release model accounting for biphasic release was developed and parameters were estimated through mathematical modeling. Overall, modeling results were inconclusive with regard to spacer effects, as determined parameters were largely statistically equivalent. However, analyzing DOX release at selected time intervals revealed a pH-sensitive response, with more DOX released at pH 5.0 than at pH 7.4. AUC analysis confirmed this phenomenon. Furthermore, total DOX release at pH 5.0 varied depending on micellar formulation (HYD>ABZ>GLY). Though modeling led to inconclusive results, spacer insertion produced different drug release profiles. On a separate note, the hydrazone bond connecting DOX to block copolymers was found to degrade under current storage conditions. This degradation was a concern and is addressed in each subsequent chapter.

Table 10. Estimated Free DOX Formation Due to Hydrazone Hydrolysis During Storage

Experimental Description	Months After Synthesis	% Hydrolyzed
12-16 Scaffold Synthesis	0	0
12-16 Drug Loading	0	0
12-16 Characterization	0	0
Dynamic Dialysis (1.0 mg/mL)	0	0
IC50 A549 (72 hours)	1	2
Cellular Internalization A549 (FL)	1	2
Biodistribution Studies	3	6
Antitumor Study (HT29)	4	8
IC50 HT29 (72 hours)	6	12
Cellular Internalization HT29 (FL)	6	12
Antitumor Study (A549)	6	12
IC50 Reduced Block Copolymers	8	16
IC50 A549 and HT29 (48 hours)	9	18
Cellular Internalization (Microscopy)	11	22
Drug Release (Non-Sink Conditions)	13	26
Dynamic Dialysis (0.1/0.5 mg/mL)	14	28
Sephadex LH-20 Confirmation	16	32

CHAPTER SIX

6 EFFECTS OF TUNABLE DRUG RELEASE: *IN VITRO* ANALYSIS

6.1 Introduction

Biocompatible block copolymer micelles were used to delineate effects of differential drug release *in vitro* (Figure 19). Micelles were prepared from block copolymers with covalently attached DOX. Though DOX conjugation was the same in the three block copolymers synthesized, each had a different drug binding linker: HYD, ABZ-HYD, or GLY-HYD. Depending on the linker used, a different drug release profile was observed. Over a 72 hour time period, total DOX released from micelles followed a trend of HYD>ABZ>GLY. Additionally, the amount of drug released at specific time points differed depending on micellar formulation. The micelles herein provided three differential drug release profiles, with free DOX representing instantaneous exposure. The effects of differential drug release *in vitro* were assessed based on this understanding. This study was therefore expected to provide critical information on the potential benefits of differential drug release.

The efficacy of micellar treatments was compared to free DOX treatment in an *in vitro* cell culture system using human colon (HT29) and lung (A549) cancer cell lines. By dosing cells with DOX-equivalent concentrations, effects of differential drug release were elucidated. Additionally, the internalization of DOX from micelles (either free DOX or conjugated DOX) was observed and compared to free DOX. Further *in vitro* analyses were performed with block copolymers incapable of releasing DOX. Internalization and cytotoxicity studies provided insight into internalization of block copolymers and block copolymer biocompatibility, respectively.

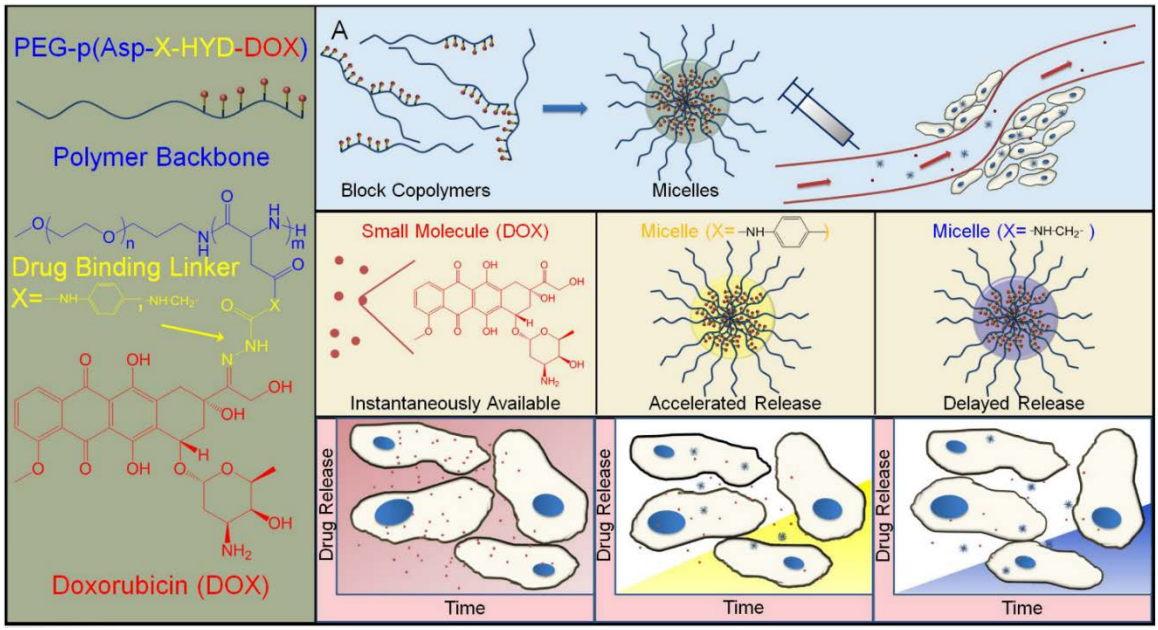

Figure 19. In Vitro *Effect of Differential Drug Release*

6.2 Materials and Methods

6.2.1 Materials

DMSO, DMF, dry ethyl ether, methanol, Hoechst dye, and sodium borohydride were purchased from Sigma-Aldrich (USA). DOX was purchased from LC Laboratories (USA). Phosphate buffer saline, Sephadex LH-20 gels, and other cell culture supplies (e.g. 96-well culture plates, pipettes, and flasks) were purchased from Fisher Scientific (USA). Kaighn's modification of Ham's F-12 medium (F12-K), McCoy's 5A medium, fetal bovine serum (FBS), trypsin-EDTA (0.25% trypsin and 2.21 mM EDTA), and the A549 cell line were purchased from ATCC (USA).

6.2.2 Free DOX and Micellar Treatment Cytotoxicity

The cytotoxicity of block copolymer micelles was observed in the A549 and HT29 cancer cell lines. HT29 cells were cultured regularly in McCoy's 5A media containing 10% FBS. Cell culturing conditions were maintained at 37°C in a humidified atmosphere with 5% CO_2. Culturing conditions for A549 cells were identical, save for the use of F-12K media instead of McCoy's 5A. Cells (5,000 cells/well) undergoing exponential growth were pre-incubated for 24 hours in 96-well plates. At this point, cell-culture media was removed and replaced with drug containing media. Cells were treated with increasing concentrations of free DOX (10^{-5} to 100 μM) or micellar DOX-equivalent concentrations. After 48 hours of exposure, cell viability was determined using a Resazurin assay. The cytotoxicity experiment was repeated a minimum of three times. IC50 was calculated using Prism. A secondary study was done under identical conditions, but cells were exposed to treatment for 72 hours instead of 48 hours.

6.2.3 DOX Intracellular Uptake

The uptake of DOX from either micelles or free DOX treatment was observed in both HT29 and A549 cells using two methods: microplate fluorescent analysis and microscopy. Cell culturing conditions were unchanged from cytotoxicity experimental conditions. Intracellular uptake experiments were carried out identically in both cell lines.

Internalization studies with a microplate reader were performed using 96-well plates. Ten thousand cells were pre-incubated for 24 hours in cell culture media, which was removed and replaced with drug-containing media. Cells were treated with 100 μM DOX-equivalent concentrations. At predetermined time points, media was removed and cells were washed with PBS. After the final PBS wash, cells were lysed with 100 μL of DMSO. DOX fluorescence was measured spectrometrically with an excitation at 490 nm and emission at 590 nm. This procedure was performed at the following time intervals: 0.5, 1, 3, 6, 24, 48, and 72 hours.

Fluorescent microscopy was the secondary method used to analyze DOX uptake. Twenty thousand cells were placed into chamber slides with cell culture media. After 24 hours, media was removed and replaced with drug containing media. Cells were treated with free DOX or micelle formulations at a 100 μM DOX-equivalent dose. Additionally, a separate experiment was performed in which cells were treated with PBS alone. At specific time points (0.5, 1, 3, 6, 24, 48, and 72 hours), chamber slides were removed from the incubator, and cells were washed with PBS three times. After the final wash, PBS containing Hoechst dye was added to each chamber. Ten minutes later, PBS containing dye was removed to prepare chamber slides for imaging. Images were taken

through the bright field channel, the GFP channel, and the DAPI channel. Microscope settings were fixed. Overlaid images were analyzed using ImageJ (139).

6.2.4 Hydrazone Bond Reduction

The hydrazone bonds connecting DOX to block copolymers were reduced, rendering block copolymers incapable of releasing DOX. PEG-p(Asp-HYD-DOX) (43.26 mg), PEG-p(Asp-ABZ-HYD-DOX) (41.35 mg), and PEG-p(Asp-GLY-HYD-DOX) (42.22 mg) were dissolved in DMF with excess sodium borohydride. The reaction proceeded overnight at room temperature. DMF was removed with ether precipitation, while sodium borohydride was removed through dialysis against deionized water. Block copolymers were collected after freeze-drying. Sephadex purification was used as an additional step to ensure product purity. Block copolymers were collected and stored at -20°C. Final block copolymers maintained a red color, closely resembling initial material. Additional drug release studies were not performed due to sample shortage. Block copolymers with reduced hydrazone bonds are referred to as HYD-Red, ABZ-Red, and GLY-Red.

6.2.5 Cytotoxicity and Intracellular Uptake of Reduced Block Copolymers

The cytotoxicity and cellular internalization of block copolymers with reduced hydrazone bonds was observed in A549 and HT29 cells. Cell culturing conditions were described previously. For cytotoxicity studies, 5,000 cells were pre-incubated in 96-well plates for 24 hours. Cells were subsequently treated with increasing concentrations of HYD-Red, ABZ-Red, and GLY-Red block copolymers (2.5×10^{-5} to 2.5×10^{2} μg/mL). Cell viability was determined using a Resazurin assay after 72 hours, and results were analyzed using Prism. Intracellular uptake of HYD-Red, ABZ-Red, and GLY-Red block copolymers was

observed after 0.5, 3, 24, and 72 hour exposure using the microscopy method. Experiments were carried as previously stated.

6.3 Results

6.3.1 Free DOX and Micellar Treatment Cytotoxicity

Cytotoxicity of block copolymers was determined in HT29 and A549 cells after 48 and 72 hour exposure to treatment. The IC50 of each micellar formulation was compared to free DOX (Figures 20 and 21, Table 11). Determining the cytotoxicity over two different time periods gave insights regarding the effects of differential release rates.

The 48 hour treatment cycle produced similar results in both cell lines. In HT29 cells, the IC50 of micelle treatments was comparable to IC50 with free DOX treatment. In this case IC50 values from HYD, ABZ, and GLY micellar treatments were 0.58, 0.37, and 0.42 μM respectively. Free DOX treatment resulted in a 0.18 μM IC50. This same trend was observed in the A549 cell line. Treatment with HYD, ABZ, and GLY micelles yielded IC50s of 7.49, 2.99, and 3.38 μM, respectively. Under the same conditions, the IC50 of free DOX was 5.77 μM. The free DOX IC50 was not statistically different than the IC50 after micellar treatments. The 7.24 HYD μM IC50 after micellar treatment was considered reliable even though the curve was elevated. The raised curve was a sign of an issue with the control for that particular experiment, while remaining measurements appeared to be unaffected. Additionally, highest and lowest cell viability after specific treatments were used in calculating IC50. Since the entire HYD curve was elevated, the IC50 determination was not impacted.

When exposure time was increased to 72 hours, studies with HT29 cells yielded similar results. The IC50 of free DOX remained 0.18 μM. When cells were exposed to

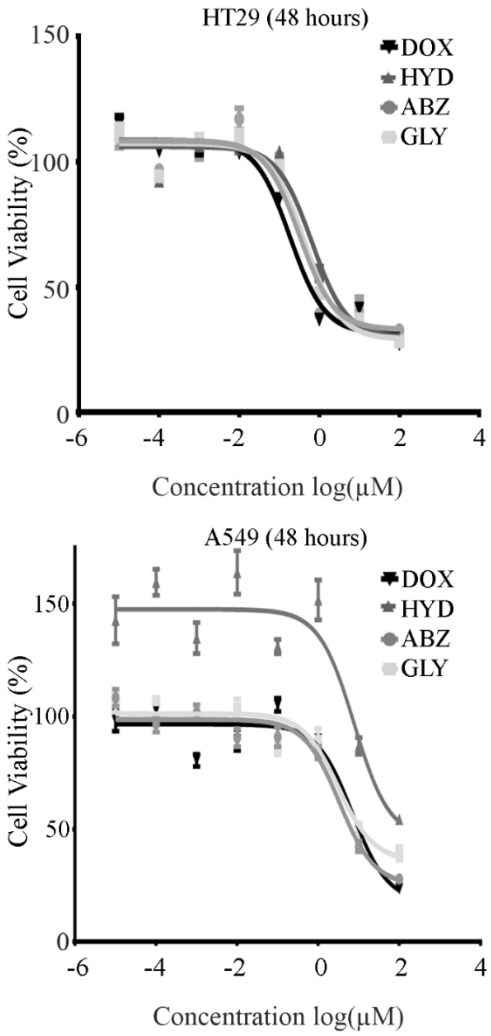

Figure 20. IC50 Determination after 48 hour Treatment Exposure

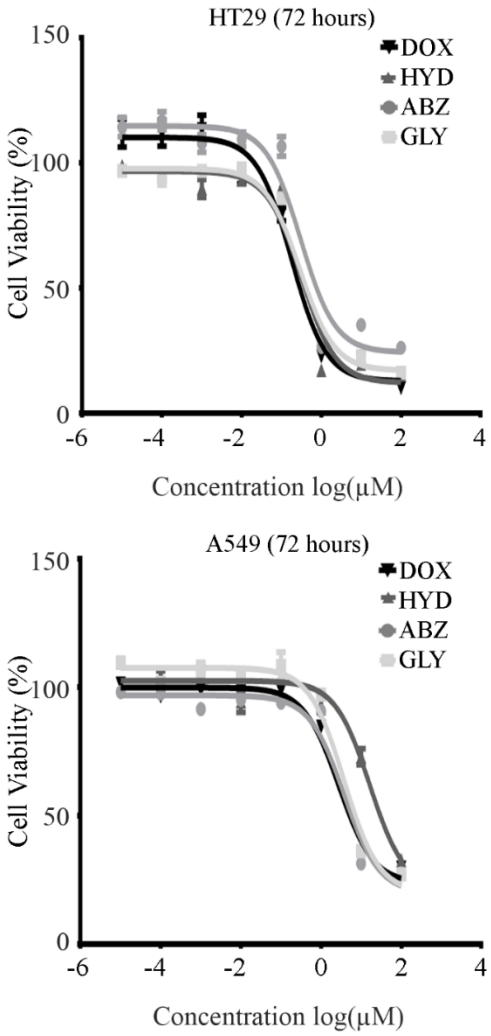

Figure 21. IC50 Determination after 72 hour Treatment Exposure

Table 11. Treatment Cytotoxicity in HT29 and A549 Cells with Varying Exposure Times

Cell Line	Time (hours)	Cytotoxicity	DOX	HYD	ABZ	GLY
HT29	48	log (IC50)	-0.75 ± 0.19	-0.30 ± 0.37	-0.44 ± 0.10	-0.39 ± 0.09
		IC50 (μM)	0.18	0.50	0.36	0.41
	72	log (IC50)	-0.74 ± 0.17	-0.50 ± 0.07	-0.31 ± 0.28	-0.27 ± 0.10
		IC50 (μM)	0.18	0.32	0.48	0.53
A549	48	log (IC50)	0.78 ± 0.05	0.86 ± 0.01	0.58 ± 0.22	0.52 ± 0.35
		IC50 (μM)	5.89	7.24	3.80	3.31
	72	log (IC50)	0.43 ± 0.10	1.23 ± 0.25	0.60 ± 0.14	0.57 ± 0.11
		IC50 (μM)	2.95	16.9***	3.98	3.71

IC50 values are described in two ways: as log (IC50 concentration) ± the standard deviation; and as the corresponding IC50 concentration in μM. Statistical significance is indicated by *** ($p < 0.001$).

HYD, ABZ, and GLY micelles, the IC50 decreased to approximately 0.30 µM. Though the free DOX IC50 was lower than the IC50 from micellar formulations, there was no statistical difference between the two. In A549 cells, ABZ and GLY micellar treatments had similar IC50s to free DOX treatment. The only outlier was the HYD formulation, which resulted in a higher IC50.

6.3.2 DOX Intracellular Uptake

The intracellular uptake of free DOX and DOX from micellar treatment was observed in A549 and HT29 cells over a 72 hour period. DOX internalization from micelles was related to the presence of either free DOX or conjugated DOX. Because it was not possible to distinguish the two, DOX internalization studies of micellar treatments refer to free and conjugated DOX in combination.

Two methods were used to monitor DOX internalization: microplate fluorescent analysis and microscopy. Microplate fluorescent analysis consisted of exposing cells to treatment for a predetermined amount of time and lysing cells with DMSO. The resulting fluorescent signal was measured, accounting for the DOX entrapped in cells. The fluorescent signal was converted to % dose. With this method, very similar trends were seen between A549 and HT29 cells (Figure 22). Free DOX was internalized quickly and to a greater extent in both cell lines. DOX from HYD micelles was also internalized relatively quickly, though less-so than free DOX. Compared to DOX from ABZ and GLY micelles, DOX from HYD micelles was taken up by cells to a greater extent at each time point in both cell lines. Intriguingly, DOX from GLY micelles was internalized slightly more than DOX from ABZ micelles even though GLY micelles exhibited lower drug release in previous experiments. This was especially evident in A549 cells. Overall,

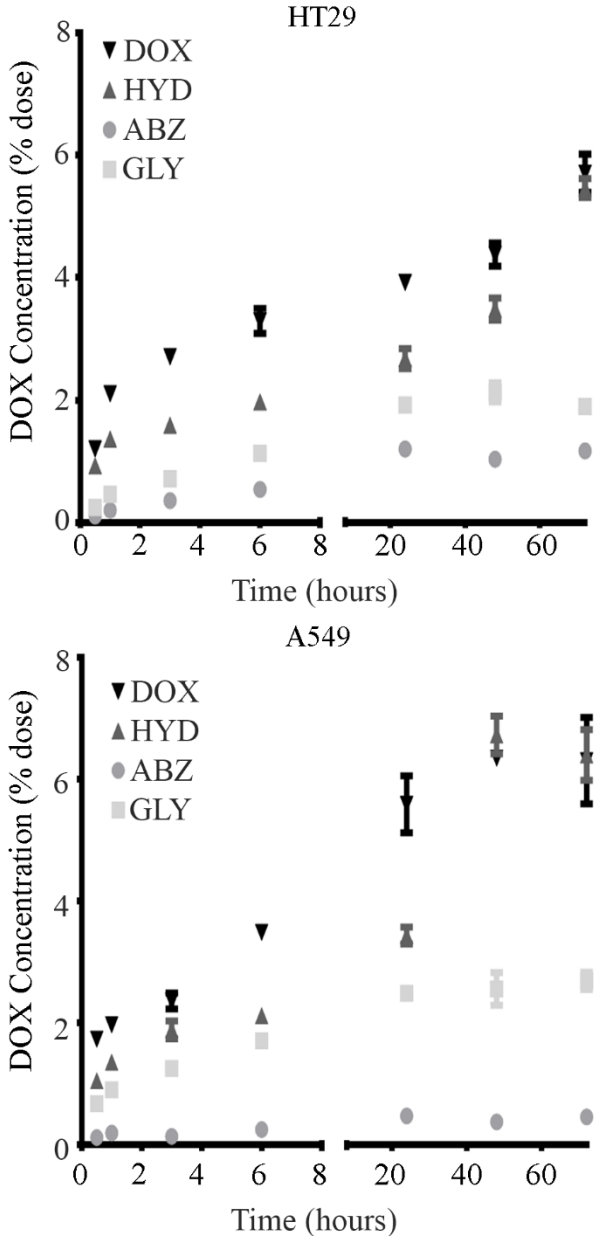

Figure 22. HT29 and A549 Cellular Internalization Using Microplate Fluorescence Analysis

the uptake study showed that DOX was internalized to some degree, irrespective of micelle type.

As a secondary confirmation of intracellular uptake, a microscopy method was used. Experimental conditions were the same as with microplate fluorescent analysis, with the exception of data collection. Cells were cultured in chamber slides and treated either with free DOX or with micelles containing a DOX-equivalent concentration. At predetermined time points (0.08, 0.5, 1.0, 3.0, 6.0, 24, 48, and 72 hours), cells were washed with PBS, stained, and imaged. The 48 and 72 hour time points were similar to the 24 hour images and were therefore not shown. Three images were taken with a fluorescent microscope. A bright field image was taken to observe cell outlines, including the cell membranes. A DAPI filter was used to observe stained nuclei (blue), and a GFP filter was used to observe DOX fluorescence (red). The three images were overlaid for qualitative analysis (Figures 23 and 24). As a control, cells were also treated with PBS. In both cell lines, there was no fluorescent signal observed from PBS treatment in images taken with the GFP channel. This supported the notion that fluorescence in the GFP channel was related to DOX alone.

At as early as 30 minutes, signs of free DOX uptake were seen in HT29 cells. This uptake from free DOX treatment continued to increase steadily through the first 24 hours, with cells turning almost completely red by that point. For micellar treatments, signs of DOX uptake did not appear until the one hour time point. At the subsequent time points, DOX signal increased. DOX uptake from HYD micelles was greatest, followed by GLY and then ABZ micelles. The same trend was seen with A549 cells. Free DOX was internalized most quickly, while DOX internalization from micelles followed the

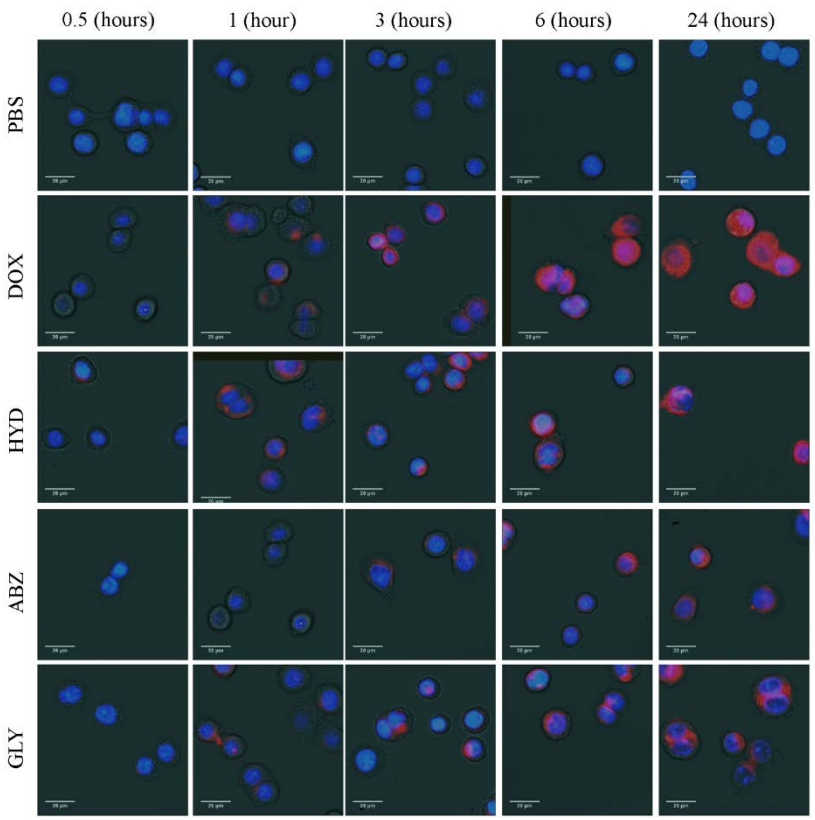

Figure 23. Cellular Uptake of DOX after Micellar or Free DOX Treatment in HT29 Cells. Scale Bars are 20 µm

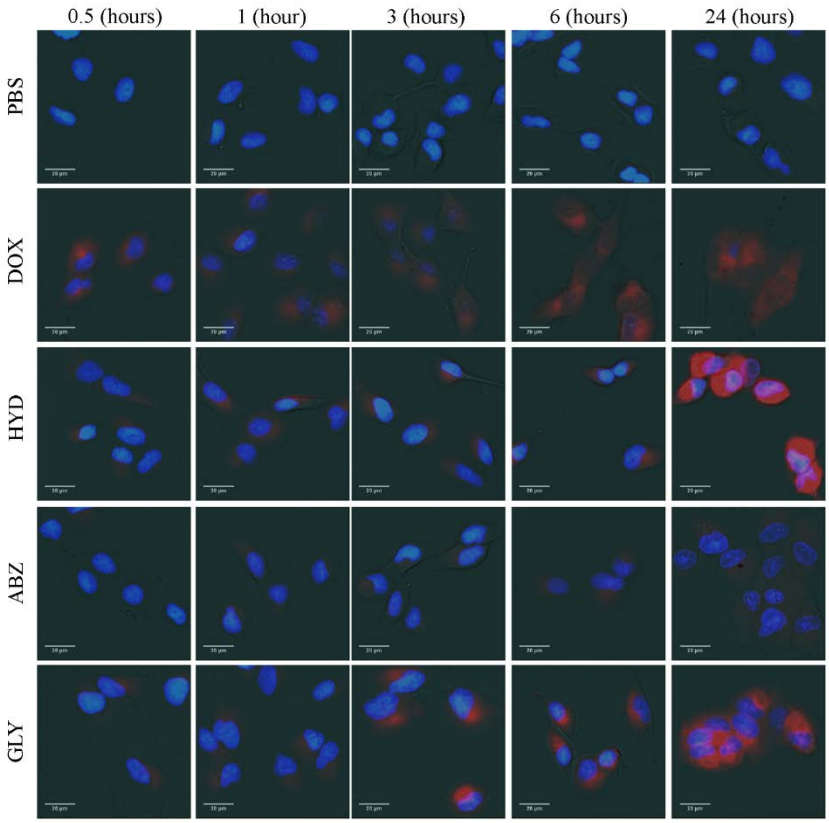

Figure 24. Cellular Uptake of DOX after Micellar or Free DOX Treatment in A549 Cells. Scale Bars are 20 µm

same order (HYD>GLY>ABZ).

DOX fluorescence was analyzed quantitatively using ImageJ (Figure 25). For each time point, the fluorescent intensity per cell from the GFP channel was measured. Since uptake trends were similar in both cell lines, analysis was performed simultaneously. PBS treatment did not produce a fluorescent signal in the GFP channel at any time point. Treatment with free DOX resulted in the quickest internalization to the greatest extent through the first 24 hours. At the 72 hour time point, the peak uptake of free DOX was reached. Interestingly, the difference between 24 and 72 hour exposure was minimal. HYD micelle treatment followed a similar trend as the signal from DOX increased through the first 24 hours at which point the uptake appeared to stagnate. DOX signal was the smallest from ABZ and GLY micelles over the time period of the study.

For both methods, AUC analysis was performed over the 72 hours of the internalization study (Table 12). AUC confirmed that DOX internalization followed the trend of DOX>HYD>GLY>ABZ. Relative AUC (AUC/AUC_{DOX}) was also calculated. Comparing relative AUC determined from both methods showed that results were comparable. Relative AUC of GLY treatment was almost identical; 0.43 versus 0.45 in HT29 cells and 0.43 versus 0.48 in A549 cells. Similar relative AUC values were also observed for HYD and ABZ treatments in the HT29 cell line. Overall the two methods show the same general trends in cellular internalization.

6.3.3 Hydrazone Bond Reduction

Hydrazone bonds of block copolymers were reduced to prevent the release of DOX. After undergoing reduction, block copolymers were purified to ensure no free DOX was remained. Ether precipitation was the first line of purification, followed by dialysis.

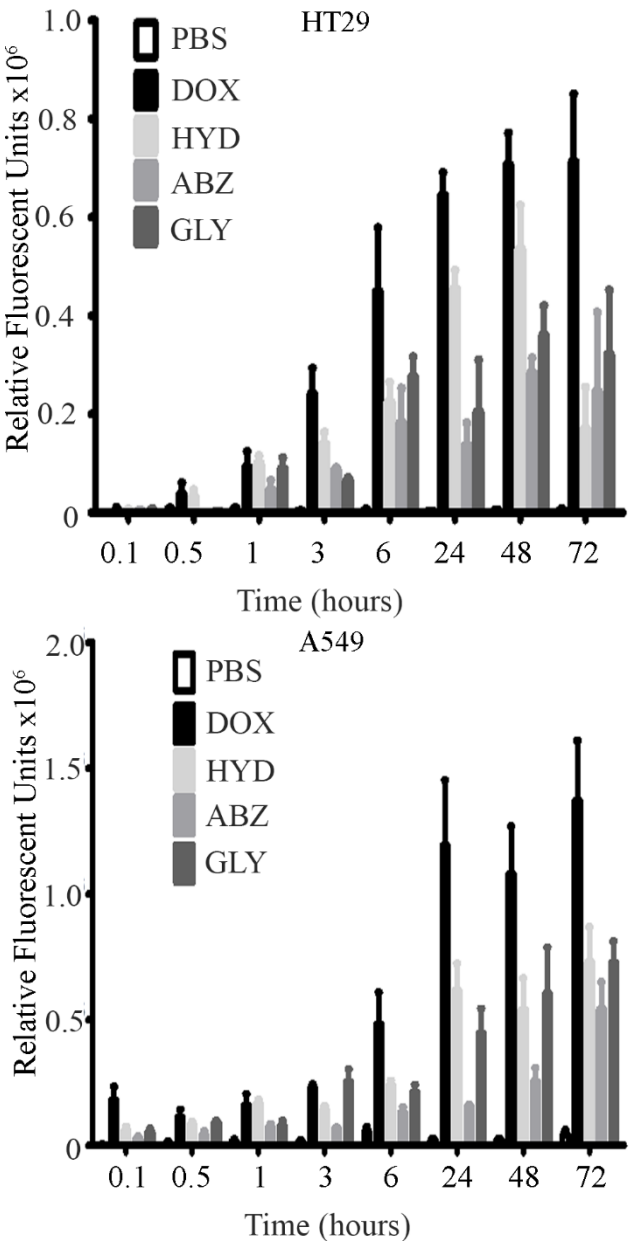

Figure 25. Quantitative Cellular Internalization Analysis

Table 12. Cellular Internalization Analysis Using Fluorescent and Microscopy Methods

		72 hours AUC ([‡]X*hours)				
	Method	PBS	DOX	HYD	ABZ	GLY
HT29	Microplate	-	300 ± 10	232 ± 17	71 ± 4	129 ± 16
A549	Microplate	-	391 ± 25	339 ± 22	28 ± 3	169 ± 20
HT29	Microscopy	0.03 ± 0.01	4.45 ± 0.6	2.73 ± 0.4	1.49 ± 0.2	2.00 ± 0.7
A549	Microscopy	0.21 ± 0.06	7.33 ± 1.2	3.77 ± 0.7	1.75 ± 0.4	3.55 ± 0.6
		Relative AUC (AUC/AUC_{DOX})				
	Method	PBS	DOX	HYD	ABZ	GLY
HT29	Microplate	-	1.00 ± 0.05	0.77 ± 0.05	0.24 ± 0.06	0.43 ± 0.13
A549	Microplate	-	1.00 ± 0.09	0.87 ± 0.09	0.07 ± 0.11	0.43 ± 0.13
HT29	Microscopy	-	1.00 ± 0.21	0.61 ± 0.21	0.33 ±0.21	0.45 ± 0.41
A549	Microscopy	-	1.00 ± 0.21	0.51 ± 0.21	0.24 ± 0.31	0.48 ± 0.21

[‡]X units are in % of initial dose for the fluorescent detection method, and in relative fluorescent units x 10^7 for the microscopy method. Determined values are expressed as mean ± standard deviation.

Sodium borohydride was not soluble in ether, but soluble in water. Dialysis against deionized water removed sodium borohydride. For the last purification step, block copolymers were eluted through a Sephadex LH-20 column. The presence of conjugated DOX was evident as all block copolymers retained a red color. Additionally, there was a strong signal from microscopy imaging of reduced block copolymers in the GFP channel which confirms DOX presence. However, DOX drug loading was undetermined after reduction. Reduced polymers are referred to by the drug binding linker, followed by the abbreviation Red (i.e. HYD-Red).

6.3.4 Cytotoxicity and Intracellular Uptake of Reduced Block Copolymers

The cytotoxicity of reduced block copolymers was observed in both HT29 and A549 cell lines (Figure 26). Cells were treated with a 250 µg/mL maximum concentration of reduced block copolymers (gray bars). This dose was the approximate equivalent of 100 µM DOX-equivalent treatment (black bars). Comparing the two treatments, it was clearly evident that reduced block copolymers were significantly less toxic. In fact, HT29 cellular viability remained almost identical to the control after reduced block copolymer exposure. Similar results were seen in A549 cells. The sole exception was treatment at the highest dose. There appeared to be polymer toxicity at the 250 µg/mL dose.

In addition to cytotoxicity studies, the cellular internalization of reduced block copolymers was observed (Figures 27 and 28). After 30 minutes, uptake of block copolymers was minimal. In HT29 cells, slight uptake of ABZ and GLY block copolymers was observed at the three hour time point. A large increase in the internalization of ABZ and GLY block copolymers was observed after 24 hour exposure. This increase continued through the 72 hour time point. For A549 cells, uptake from

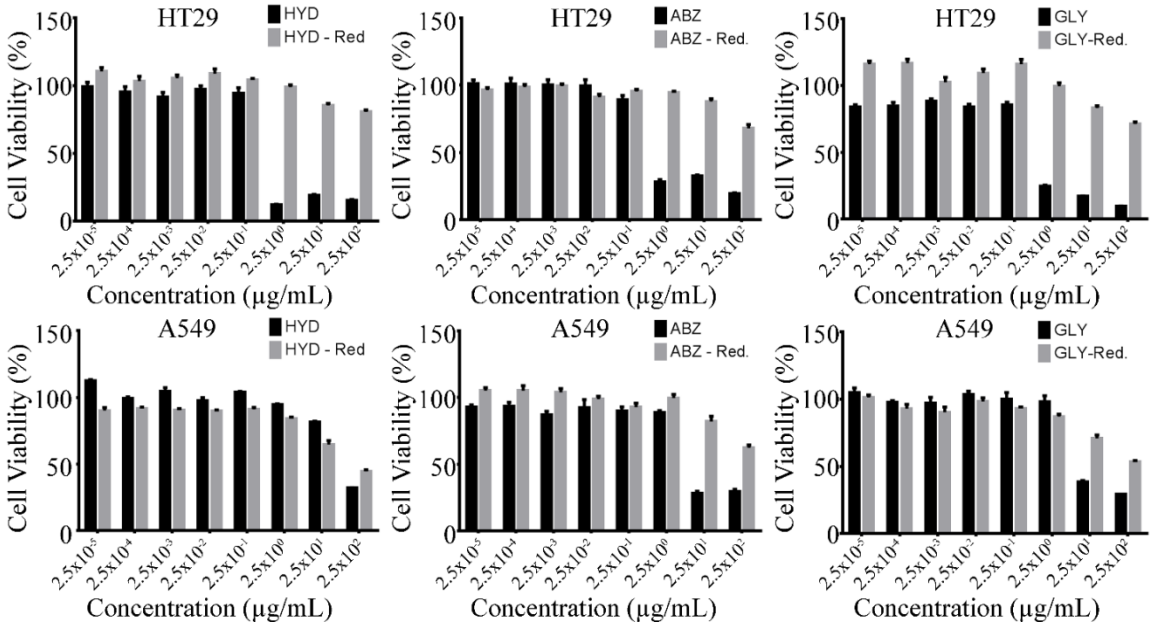

Figure 26. Cytotoxicity of Block Copolymer Micelles with a Reduced Hydrazone Bond

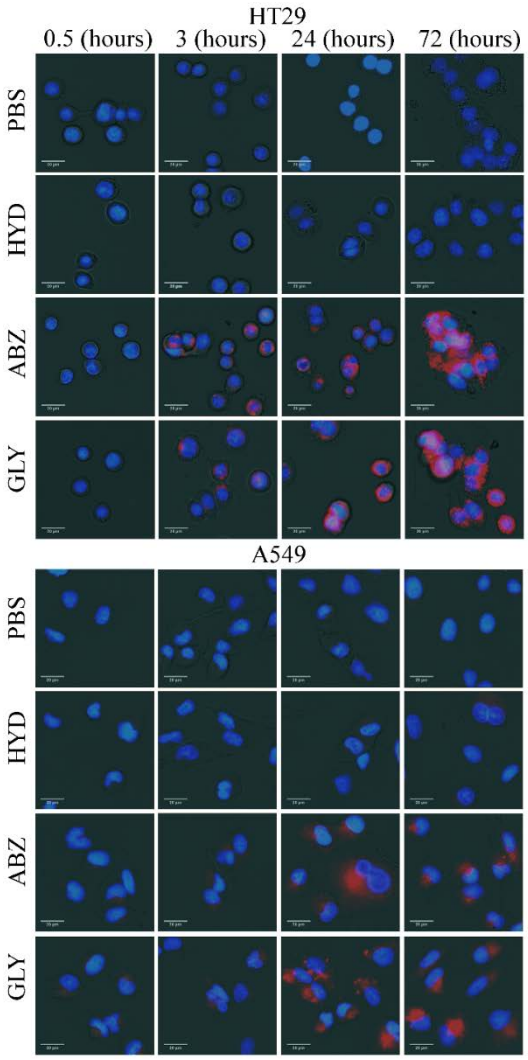

Figure 27. Cellular Uptake of Reduced Micelles in A549 and HT29 Cells. Scale Bars are 20 µm

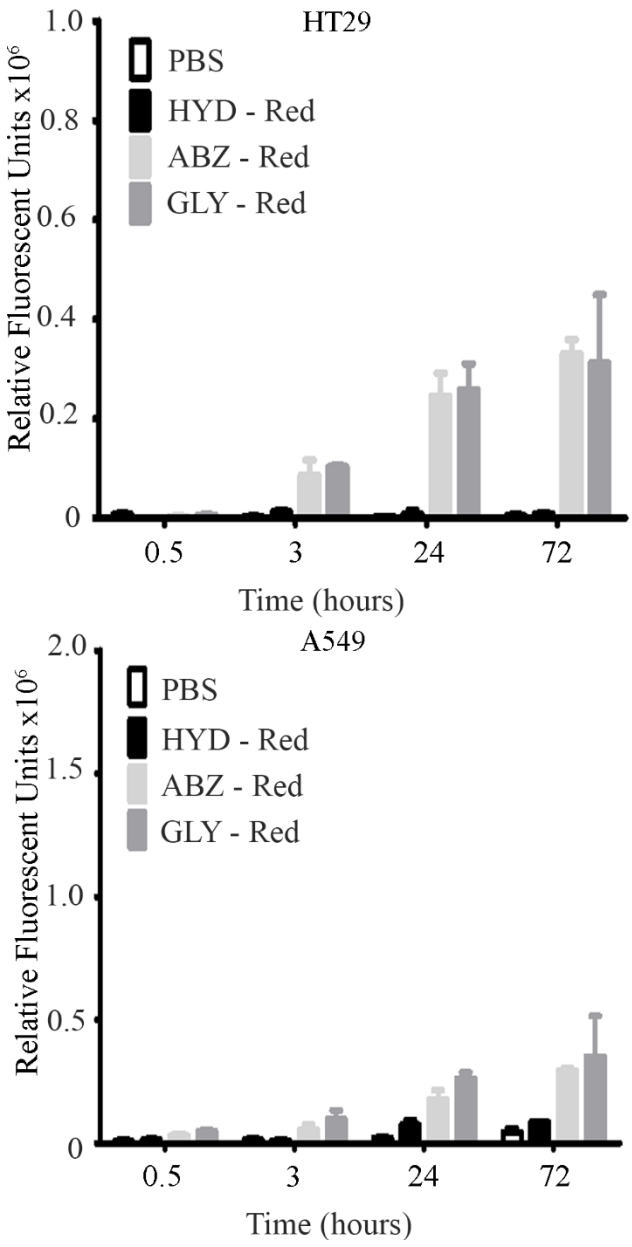

Figure 28.Quantification of Cellular Internalization of Reduced Micelles Using Microscopy

ABZ and GLY block copolymers was not evident until the 24 hour mark. Afterwards, uptake continued to increase until the 72 hour time point. Intriguingly, HYD block copolymers were not internalized to a great extent in either cell line. The overall lower uptake of block copolymers pointed to successful hydrazone reduction, as internalization after free DOX treatment was much greater.

6.4 Discussion

Multiple *in vitro* studies were performed to analyze efficacy of micellar treatments and also to determine DOX internalization. Prior to discussing specific results, it is important to note when the experiments were performed. Hydrazone bond hydrolysis during storage was observed and this degradation could have played a role in experiments. Cytotoxicity and internalization studies with A549 cells were done immediately after block copolymer synthesis. These experiments were not expected to be influenced by solid state hydrolysis. Experiments with HT29 cells were performed within six months of block copolymer synthesis. A maximum of 12% free DOX formation was expected after six months. Therefore, results from HT29 experiments were expected to be minimally affected. Experiments with reduced block copolymers were unaffected by degradation, as these micelles were purified prior to use. The last experiments performed were the 48 hour cytotoxicity studies and all cellular uptake studies using the microscopy method. By the time these experiments were performed up to 22% free DOX was predicted to be formed. Though experiments were performed with partially free DOX, the trends never changed. The overall message is unaffec7ted by hydrazone hydrolysis during storage.

6.4.1 In Vitro *Analysis of Block Copolymers with Reduced Hydrazone Bonds*

Three micelles were prepared for testing *in vitro*: HYD, ABZ, and GLY micelles. Each of these micelles was composed of block copolymer with covalently attached DOX. It was previously shown that PEG-poly(aspartate) block copolymers were non-toxic, but block copolymers with attached DOX have yet to be analyzed (78). It was hypothesized that the only active pharmaceutical ingredient present in micellar formulations was DOX released from block copolymers. To test this hypothesis the bond between block copolymers and DOX was reduced (Figure 29).

The hydrazone bond connecting DOX to block copolymers is pH-sensitive. This bond is cleaved in the presence of hydronium ions. As the hydrazone bond undergoes hydrolysis, DOX is released. By reducing this imine bond to an amine, pH-sensitive release is prevented. Successful reduction of the hydrazone bond produced HYD-Red, ABZ-Red, and GLY-Red block copolymers. The cytotoxicity and cellular internalization of these block copolymers was tested *in vitro*. Results gave insight not only to the biocompatibility of the block copolymers, but also to the uptake of block copolymers.

A pitfall of this study was that the drug loading after hydrazone reduction was not determined. The degree of conjugated DOX could thus change after reduction. Internalization of reduced block copolymers may have been impacted as the amount of conjugated DOX could vary from one block copolymer to the next. However, all block copolymers retained a red color and exhibited fluorescence *in vitro*, signifying DOX presence. Drug loading before and after hydrazone reduction was assumed to be similar.

HT29 cells treated with reduced block copolymers showed minimal toxicity. In comparison to treatment with non-reduced formulations there was essentially no

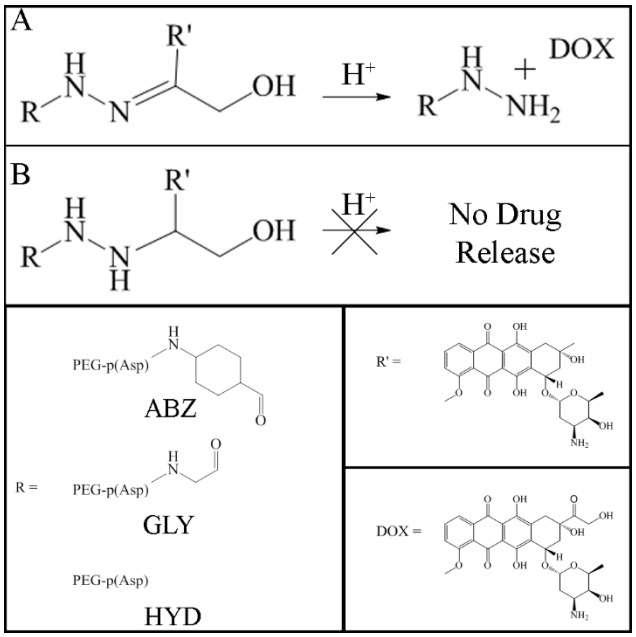

Figure 29. Reduction of Hydrazone Bond

cytotoxic effect. Even at the highest dose, cell viability approached 100% with all reduced block copolymer treatments. It was therefore deduced that for micellar treatment to have an effect, DOX must first be cleaved from the block copolymers. Studies with A549 cells produced similar results. After treating cells with reduced block copolymers, no toxicity was observed up to 2.5 mg/mL. Even at the highest dose, a significantly smaller effect was observed after reduced block copolymer treatment. There was a slight discrepancy with HYD-Red block copolymers at the highest dose, as this treatment resulted in minor toxicity. However, this toxic effect was not expected to be relevant *in vivo*. Concentrations this high were not expected at the tumor site. Overall, reduced block copolymers exhibited minimal toxicity. It was surmised that the active pharmaceutical ingredient in micellar treatments was released DOX.

In addition to cytotoxicity studies, the internalization of reduced block copolymers was observed. It was postulated that the main method of intracellular delivery of DOX after micellar treatment occurs through endocytosis, as described in previous works (18, 140). Therefore it was important to understand the internalization of micelles. In this experiment, cells were treated with block copolymers containing irreversibly attached DOX. These block copolymers readily formed micelles, but internalization studies could not distinguish the difference between a single block copolymer and block copolymers as parts of a micellar system. It was still expected that the primary species internalized were micelles.

After half an hour, internalization of reduced block copolymers was minimal, but within three hours a fluorescent signal was observed in both HT29 and A549 cells. Block copolymer internalization continually increased after the three hour mark, with the peak

internalization observed at 72 hours. Intriguingly, uptake of HYD-Red block copolymers was significantly lower than ABZ-Red and GLY-Red block copolymers in both cell lines. Decreased uptake of HYD-Red block copolymers could have been hindered by micellar stability issues. Higher particle size and positive surface charge may have also affected HYD-Red block copolymer internalization. As previously shown, spacer insertion led to block copolymers which formed micelles with a narrow size distribution and a neutral surface charge. Consequently, it was observed that ABZ-Red and GLY-Red block copolymers were internalized to a greater extent. These results indicated that micellar characteristics can affect intracellular uptake. Even though the internalization of HYD-Red block copolymers was low, all reduced block copolymers were taken up by cells; thereby creating the opportunity to deliver drugs intracellularly.

6.4.2 Free DOX and Micellar Treatment Cytotoxicity

Efficacy of micellar treatments was determined in A549 and HT29 cell lines to elucidate the effect of drug release *in vitro*. It was earlier shown that DOX irreversibly conjugated to block copolymers generates minimal response, whereas DOX released from block copolymers produces a strong therapeutic effect. DOX cleavage and release from block copolymers can occur extracellularly or intracellularly. DOX released extracellullarly can be taken up as a small molecule. During treatment, block copolymers are assumed to exist as micelles. Micelle can be internalized through endocytosis. During this process, intracelllular DOX release was believed to occur. *In vitro*, both modes of DOX release were expected to occur concurrently.

Intracellular DOX release was expected to play a greater role than extracellular release due to the lower pH associated with endocytosis. A pH-dependent release of DOX

was observed in drug release studies with all micelles. After 72 hours, only ~30% of DOX was released from both ABZ and GLY micelles whereas up to 55% of DOX was released at pH 5.0. An even greater difference in total drug release was observed with HYD micelles. During the time frame of cytotoxicity experiments, drug release studies showed that HYD micelles released the largest amount of DOX, followed by ABZ micelles. GLY micelles released the least amount of DOX in this same time frame. With three distinct release profiles, cells were exposed to different degrees of free DOX after micellar treatment. Treatment with free DOX was another reference point, as treated cells were directly exposed to a large amount of free DOX.

Cells were treated at DOX-equivalent doses for either 48 or 72 hours. Drug release studies showed that this time frame was not long enough to complete DOX release from micelles. After 48 hours, at least 19%, 30%, and 42% of DOX remained in HYD, ABZ, and GLY micelles respectively. After 72 hours, a maximum of 82% of DOX was released from HYD micelles. ABZ and GLY micelles released at most 72% and 63% of DOX in the same time frame.

After 72 hour exposure, micellar treatments were equipotent to DOX treatment in HT29 cells. With A549 cells, IC50s of micellar treatments were slightly elevated, while only HYD micelles produced a statistically different IC50. The elevated IC50 of HYD treatment was unexpected as drug release studies revealed HYD micelles released DOX to the greatest extent compared to ABZ and GLY micelles. The initial larger DOX release from HYD micelles appeared not to have a beneficial effect. The uptake of the polymer itself may have played a role in the efficacy of HYD micelle treatment. Even though the amount of free DOX available to cells differed, similar efficacy was observed

after ABZ and GLY treatment. This was consistent with results from 12-5 and 12-15 micelles. This phenomenon has also been observed in literature as micellar systems were proven as effective as free drugs (141, 142). But the efficacy from micellar treatment was system dependent, as other works showed micellar treatments produced lower efficacy then free drugs (143, 144).

A second set of experiments was performed with shorter exposure time (48 hours). Changing the exposure time could alter the cytotoxicity due to micellar treatment, since total drug release changed with time. However, results were consistent with the 72 hour exposure experiments. The 48 hour treatment showed no statistical difference between cells treated with micelles and free DOX. Though the IC50 from HYD micelle treatment was slightly elevated, it was not significantly different. Treatment with HYD micelles resulted in higher IC50s. The internalization of HYD micelles was thought to play a role, as uptake of HYD-Red block copolymers was low.

By comparing treatment efficacy, the effects of drug release were observed. Reduced block copolymer experiments proved that block copolymers by themselves were essentially not toxic. Surprisingly, micellar treatments were equipotent to free DOX in almost all cases. All micelles delivered drugs at a slow rate but showed equipotency. Overall results indicated that controlling rate of release can be as important as the dose delivered.

6.4.3 DOX Intracellular Uptake

The uptake of DOX after treatment with HYD, ABZ, GLY micelles or free DOX was observed in both HT29 and A549 cells. Two methods were used: microplate fluorescent analysis and microscopy. The difference between the two methods was the analysis

process. Treatment and cell culturing conditions were the same for both methods; thus straightforward comparisons of the two methods were possible. For the microplate fluorescent method, DOX content in cells was measured spectroscopically. Conversely, the microscopy method looked at the cellular internalization using a fluorescent microscope. Images produced from microscopy were analyzed using ImageJ. The two separate methods were in agreement, showing similar internalization trends.

With the fluorescence detection method, quick free DOX uptake was observed in both A549 and HT29 cells. By the half hour mark both cell lines had taken up a significant amount of DOX. After this initial fast uptake, high intracellular DOX levels were maintained over the remainder of the experiment. Extracellular DOX binding could explain high levels of early internalization, but this was probably not the case. Repeated PBS washing was performed to remove any extracellular bound DOX. Additionally, no extracellular DOX appeared in images from microscopy where the same PBS wash was used.

At early time points, DOX from micellar treatment was present in small amounts. This was unsurprising as micelles were expected be internalized through endocytosis, whereas free DOX could readily be uptaken by cells. Uptake of reduced block copolymer was also low in this same time frame. In both HT29 and A549 cells, the uptake of DOX from micellar treatment gradually increased through the first six hours. Though DOX from micelles was internalized at a slower rate than free DOX, uptake levels from micelles was maintained through 72 hours.

The overall trends were the same using the microscopy method. In addition to the quantitative value of microscopy studies, the location of DOX can be assessed. Free

DOX not only entered the cell quickly, but it appeared to collect near the nucleus. After six hours, the stain of the nuclease was overtaken by the DOX fluorescent signal. This continued in later time points. Micelle treatment yielded similar results, but at slower rates. DOX fluorescence closed in on the nucleus as the experiment progressed. This suggests that both micelle and free DOX treatments affect the nucleus. These results were unsurprising, as a primary mechanism of action of DOX is DNA intercalation.

Regarding degradation of the hydrazone bond during storage, experiments performed with microplate fluorescent analysis should not be affected. However, microscopy experiments were performed at a later date and up to 22% free DOX may have been present. Even though this could have occurred, results from the microscopy method mirrored fluorescent results, maintaining the same trend.

6.5 Conclusions

The efficacy and internalization of three micellar formulations were tested in two cell lines: A549 and HT29. Micellar formulations maintained DOX activity *in vitro*, while the block copolymers themselves exhibited minimal toxicity. This was key in demonstrating that DOX can be released in its original form and maintain its activity. Additionally, results indicated that free DOX was the sole active ingredient in micellar treatment.

Preparing block copolymers with irreversibly attached DOX showed that cells are able to internalize block copolymers. Cytotoxicity results indicated that treatment with ABZ and GLY micelles was equipotent to DOX. Both formulations released DOX at a slow rate, revealing the impact of release rates. Moreover, cell internalization studies confirmed that micelles deliver DOX to cells. With this information, treatment methods

could be optimized. By preparing formulations which deliver drugs continuously, the overall dose could be reduced while maintaining the same level of efficacy.

CHAPTER SEVEN

7 *IN VIVO* EFFICACY OF BLOCK COPOLYMER MICELLES

7.1 Introduction

Three block copolymers were synthesized previously, each with a unique drug binding linker (HYD, ABZ-HYD, or GLY-HYD). Micelles prepared from these block copolymers produced three distinct DOX release profiles. Over 72 hours, HYD micelles released the largest amount of DOX, followed by ABZ micelles and then GLY micelles. Additionally, drug release modeling revealed that DOX release was biphasic from all micelles. Importantly, it was observed that after an initial fast DOX release, a secondary slow DOX release phase occurred. This was consistent across all three formulations. Furthermore, these micelles shared similar characteristics. Beyond drug release profiles, ABZ and GLY micelles were nearly identical. By maintaining these overall characteristics, micelles were expected to behave similarly *in vivo*, allowing for drug release effects to be explored.

In this work, the effects of tunable drug release are studied primarily in two ways: biodistribution and antitumor activity. First, the biodistribution of micelles is established. Previous works show that block copolymer micelles have low critical micelle concentrations, and therefore remain intact after IV administration. Furthermore, NDDSs within a specified size range minimize non-specific accumulation of cytotoxic agents, thereby lowering toxicity (145, 146). Micelles herein are expected to exhibit similar properties. The degree of tumoral accumulation of micelles also plays a key role and must therefore be identified. The secondary method of observing effects of modulated drug release is through antitumor studies. Micelle treatments are compared to free DOX

treatment to confirm the rationale of using the NDDSs developed herein. An additional comparison between micelles is also performed, comparing the three different drug release profiles to one another, providing guidance for future treatment regimens.

7.2 Materials and Methods

7.2.1 Materials

D-luciferin was purchased from Sigma-Aldrich (USA). DOX was purchased from LC Laboratories (USA). Sterile filters (0.22 μm), plastic blood collection tubes, and other cell culture supplies (e.g. 96-well culture plates, pipettes, and flasks) were purchased from Fisher Scientific (USA). Kaighn's modification of Ham's F-12 medium (F12-K), McCoy's 5A medium, fetal bovine serum (FBS), trypsin-EDTA (0.25% trypsin and 2.21 mM EDTA), and the A549 cell line were purchased from ATCC (USA).

7.2.2 Biodistribution Studies

Six-week old female SCID mice were purchased from Taconic (USA) and acclimated for one week. Mice were randomly divided into four groups of sixteen, each group representing a treatment (DOX, HYD, ABZ, or GLY). For each treatment, mice were further split into groups of four, as tissue was collected at four time points: 0.5, 3, 24, and 48 hours. Mice were injected with 3 x 10^6 A549 cells subcutaneously in the right flank. When tumor volume reached 100 mm^3, mice were injected intravenously (IV) through the tail vein with 10 mg/kg DOX-equivalent solutions. Prior to treatment, micelles were sterilized through filtration using a 0.22 μM filter.

After each treatment, blood (>100 μL) was withdrawn from mice through cardiac puncture at two time points. Blood samples were placed in blood collection tubes. Serum was collected after centrifugation at 10,000 rpm. For analysis, serum (20 μL) was added

to DMSO (80 µL) resulting in an 80% DMSO solution. Sample DOX concentration was determined using fluorescent spectroscopy (excitation 485 nm, emission 603 nm). A calibration curve was prepared as described in previous sections. Pharmacokinetic parameters were determined using Phoenix WinNonlin Software (Version 6.2.1, Pharsight). Mice were euthanized immediately after the second blood withdrawal. Major organs (heart, liver, lungs, kidneys, and spleen) and tumors were excised and stored at -20°C. Tissue was weighed in preparation for analysis. An 80% DMSO solution was added to tissue samples, which were subsequently homogenized and centrifuged at 14,000 rpm. The supernatant was collected, and DOX concentration present in tissue was determined with fluorescent spectroscopy (excitation 485 nm, emission 603 nm). It is important to note that DOX concentrations measured in biodistribution studies represent the combined total of free DOX and conjugated DOX as their fluorescent signals could not be separated. In summary, blood samples were collected at: 0.03, 0.5, 1, 3, 6, 24, and 48 hours and tissue samples were collected at 0.5, 3, 24, and 48 hours.

7.2.3 Antitumor Activity

Two antitumor studies were performed. In the first antitumor study, tumor-bearing mice were treated with a single, high DOX dose. In the second antitumor study, tumor-bearing mice were dosed twice at considerably smaller DOX doses. Mouse body weight, tumor length (L) and width (W) were monitored in both studies. Tumor measurements were used to calculate volume using the formula:

$$V = \frac{\pi}{6} L W^2$$

The length of the tumor was considered the larger of the two measurements.

For the first study, six-week old SCID mice were purchased from Taconic (USA).

After one week of acclimation, murine xenograft tumor models were prepared by injecting 3 x 10^6 A549 cells into the back of mice. When tumor volume reached 100 mm^3, mice (n=4) were injected via the tail vein with of one of five treatments: PBS, DOX, HYD, GLY or ABZ. The treatments represented a negative control (PBS), and four treatments at 50 mg/kg DOX-equivalent concentrations. To prepare the samples for injection, DOX was dissolved in PBS with a small amount of DMSO at a 10 mg/mL concentration. HYD, ABZ, and GLY block copolymers were dissolved in PBS at a 10 mg/mL DOX-equivalent concentration. Tumor size and mouse body weight were measured every two days until day 10, and every four days thereafter.

The same protocol with minor adjustments was used in the second antitumor study. Six-week old SCID mice were obtained from Taconic (USA). Mice were acclimated for one week, after which time they were injected with 3 x 10^6 HT29 cells. When tumors reached 100 mm^3, mice (n=6) were injected via the tail vein with one of five treatments: PBS, DOX, HYD, GLY or ABZ. After four days, mice were dosed again. Both doses were at 10 mg/kg DOX-equivalent concentrations. Pilot studies showed that these animal models tolerated this treatment well. Tumor size and mouse body weight were measured every two days until day 10, and at least once per week thereafter. For sample preparation, DOX was dissolved in PBS (2 mg/mL) with minimal DMSO. Similarly, block copolymers were dissolved in PBS to achieve a 2 mg/mL DOX-equivalent concentration.

7.2.4 In Vivo *and* Ex Vivo *Imaging*

At the end of the A549 antitumor study, mice were imaged *in vivo*, and mouse tissue was imaged *ex vivo*. On day 28, one mouse was chosen at random from each group (PBS,

ABZ, or GLY) for tumor imaging. Mice were anesthetized and injected in the peritoneal cavity with a 100 µL D-luciferin solution (15 mg/mL). Non-invasive mouse images were taken 10 minutes post-injection using an *in vivo* imaging system (IVIS) (Advanced Molecular Vision, Xenogen IVIS, USA). Afterward, mice were euthanized for *ex vivo* imaging. Heart, liver, lungs, kidneys, spleen, and tumor tissue were collected. Fluorescent (excitation 500 nm, emission 600 nm) images were taken with IVIS to observe DOX presence. Furthermore, tumor tissue analyzed following the previous protocol.

All animal experiments were conducted in accordance with the Institutional Animal Care and Use Committee (IACUC) guidelines.

7.3 Results

7.3.1 Biodistribution Studies

Mice were treated with a 10 mg/kg DOX equivalent dose. DOX biodistribution from different treatments (DOX, HYD, ABZ, or GLY) was observed over 48 hours (Figure 30).

Tumor, liver, kidney, spleen, heart, and lung tissue was collected at 0.5, 3, 24, and 48 hours. DOX content was measured spectrometrically using a microplate reader method as established by Cao et. al (147). Free DOX treatment revealed that DOX was distributed to peripheral tissue very quickly, and without specificity. Within half an hour free DOX treatment yielded a 49 µg/g DOX concentration in the heart, and DOX concentrations of 120, 140, 28, and 58 µg/g in the kidneys, lungs, spleen, and liver, respectively. Intriguingly, tumor DOX concentration was only 1.9 µg/g. After 30 minutes, all micellar treatments resulted in significantly lower DOX accumulation in the liver, kidneys, heart, and lungs. Furthermore, DOX accumulation in the spleen post-ABZ

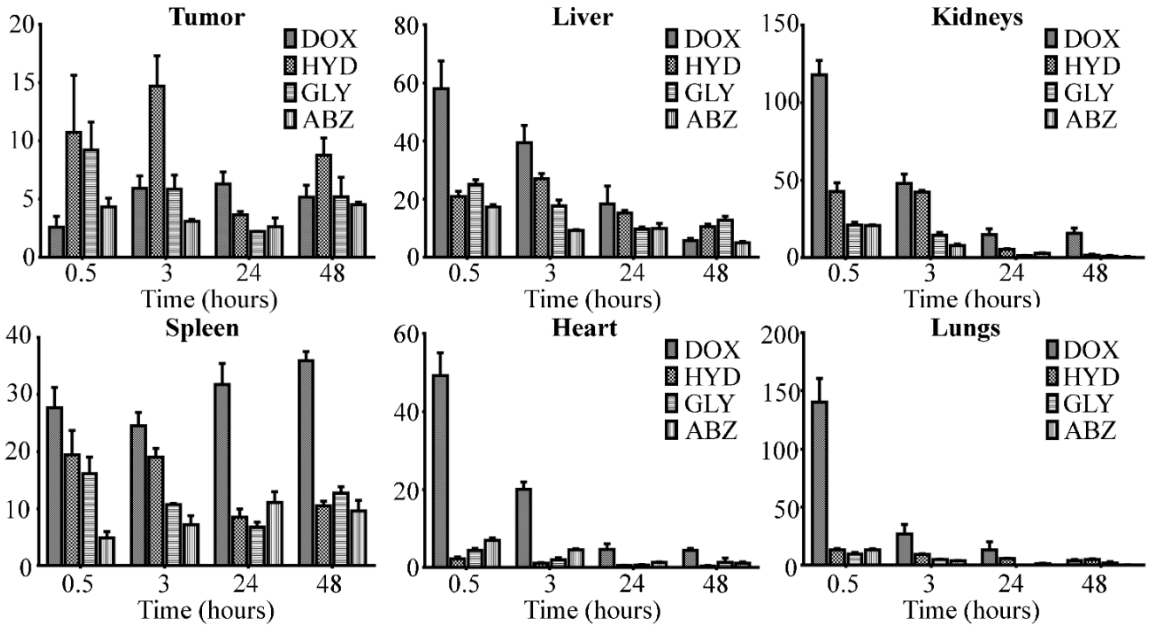

Figure 30. DOX Distribution after HYD, ABZ, GLY, or Free DOX Treatment in Tumor, Liver, Kidneys, Spleen, Heart, and Lung Tissue. Y-Axis Represents DOX Concentration [(µg DOX)/(g Tissue)]

and GLY treatment was significantly lower than after free DOX treatment. However, HYD and free DOX treatments resulted in equivalent DOX accumulation in the spleen. For the remainder of the study, DOX concentration decreased in the liver, kidneys, lung, and heart after treatment with free DOX. However, spleen and tumor DOX concentrations remained relatively unchanged through the 48 hour time point.

Comparable trends were observed with all micellar treatments. The overall decline in DOX concentration was observed in kidney, liver, and lung tissue. Specifically, DOX concentration in the lungs continuously decreased. Liver and kidney DOX concentrations dropped significantly in the first 24 hours, followed by a minor decrease. DOX levels in the spleen remained at nearly the same level over the course of the experiment. In sharp contrast to the free DOX treatment, heart DOX concentrations post-micellar treatments were miniscule across all time points. A significant amount of DOX in tumor tissue was observed after 48 hours with all micellar treatments.

AUC calculations were performed to further evaluate DOX distribution (Figure 31, Table 13). DOX accumulation in the spleen, kidneys, and lungs was significantly less from the micellar formulations than the free drug ($p < 0.01$). Additionally, AUC in the heart was 430 (µg DOX/g tissue)*hours from free DOX, while AUC after HYD, ABZ, and GLY dosing was 30, 100, and 40 (µg DOX/g tissue)*hours, respectively. Tumor and liver tissue AUC did not vary greatly, irrespective of treatment. Intriguingly, no statistical difference was observed among treatments regarding tumor tissue AUC. Comparing micellar treatments alone revealed no discernible difference of AUCs in liver, spleen, kidney, heart, and lung tissue.

In addition to AUC determination, AUC ratio ($AUC_{micelle}/AUC_{DOX}$) was

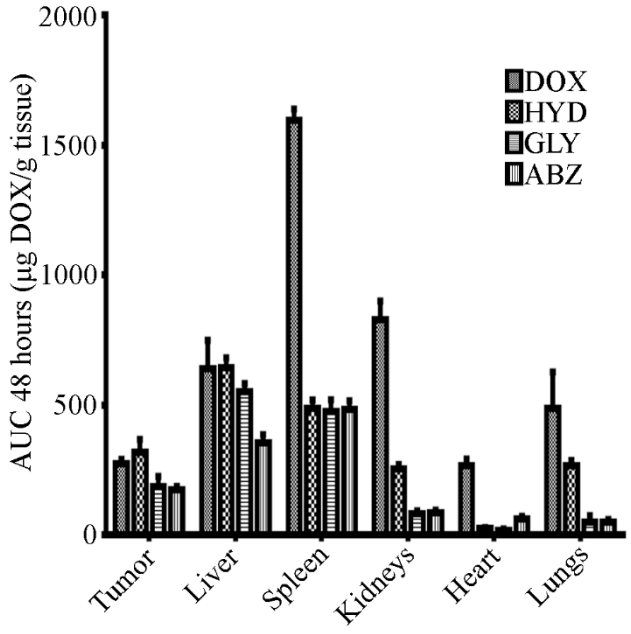

Figure 31. 48 Hour Biodistribution AUC Determination

Table 13. Analysis of Biodistribution Studies Through AUC Analysis

	AUC [(μg DOX/g tissue)*hours]			
	DOX	HYD	ABZ	GLY
Tumor	280 ± 40	320 ± 140	160 ± 30	210 ± 25
Liver	990 ± 150	810 ± 60	410 ± 80	630 ± 79
Spleen	1150 ± 140	570 ± 80	460 ± 70	490 ± 100
Kidney	1170 ± 180	670 ± 50	160 ± 50	240± 50
Heart	430 ± 60	30 ± 7	100 ± 20	40 ± 10
Lungs	790 ± 200	310 ± 30	80 ± 20	130 ± 20
	AUC Ratio ($AUC_{micelle}/AUC_{DOX}$)			
	DOX	HYD	ABZ	GLY
Tumor	1.0 ± 0.2	1.2 ± 0.5	0.6 ± 0.2	0.8 ± 0.2
Liver	1.0 ± 0.2	0.8 ± 0.2	0.4 ± 0.2	0.6 ± 0.2
Spleen	1.0 ± 0.1	0.4 ± 0.2	0.3 ± 0.2	0.3 ± 0.2
Kidney	1.0 ± 0.2	0.6 ± 0.2	0.1 ± 0.3	0.2 ± 0.3
Heart	1.0 ± 0.2	0.1 ± 0.3	0.2 ± 0.3	0.1 ± 0.3
Lungs	1.0 ± 0.3	0.4 ± 0.3	0.1 ± 0.3	0.2 ± 0.3

Determined values are shown as mean ± standard deviation.

calculated. An AUC ratio >1 corresponds to increased DOX accumulation relative to free DOX treatment, while AUC ratios <1 are equated to lower DOX accumulation.

All AUC ratios were less than one for spleen, kidney, heart, liver, and lung tissue. Though the HYD micelle treatment yielded a 1.2 tumor AUC ratio, this was statistically equivalent to other treatments.

With each treatment, DOX concentration in the serum was determined. Free DOX was quickly eliminated, with DOX levels reaching 0.5 µg/mL within three hours. Intriguingly, DOX from HYD treatment was also quickly eliminated. DOX concentration in the serum was only 1.2 µg/mL after three hours. In contrast, DOX levels after ABZ and GLY treatments were 28.9 and 19.0 µg/mL over the same time frame. Even after 48 hours, DOX concentrations after ABZ and GLY treatments were significant (0.8 and 1.2 µg/mL, respectively).

Pharmacokinetic parameters were estimated (Figure 32, Table 14). Data from all treatments produced a biphasic profile and were thus fitted with a two compartment model. AUC, AUC ratio, clearance, volume of distribution (V_{ss}), initial fast half-life ($t_{1/2f}$), and slower secondary half-life ($t_{1/2s}$) were determined based on this model. Estimated clearance confirmed quick DOX elimination after free DOX and HYD treatments, as modeling revealed a clearance of 7.5 and 4.9 ml/hour, respectively. On the other hand, DOX clearance after ABZ and GLY treatments was 0.4 and 0.6 ml/hour, respectively. Similarly, determined $t_{1/2f}$ and $t_{1/2s}$ after free DOX and HYD treatment were much faster than $t_{1/2f}$ and $t_{1/2s}$ determined after ABZ and GLY treatments. AUC ratios revealed an 18-fold difference between ABZ and free DOX treatments. The AUC ratios of GLY and HYD treatments were 12 and 1.5, respectively.

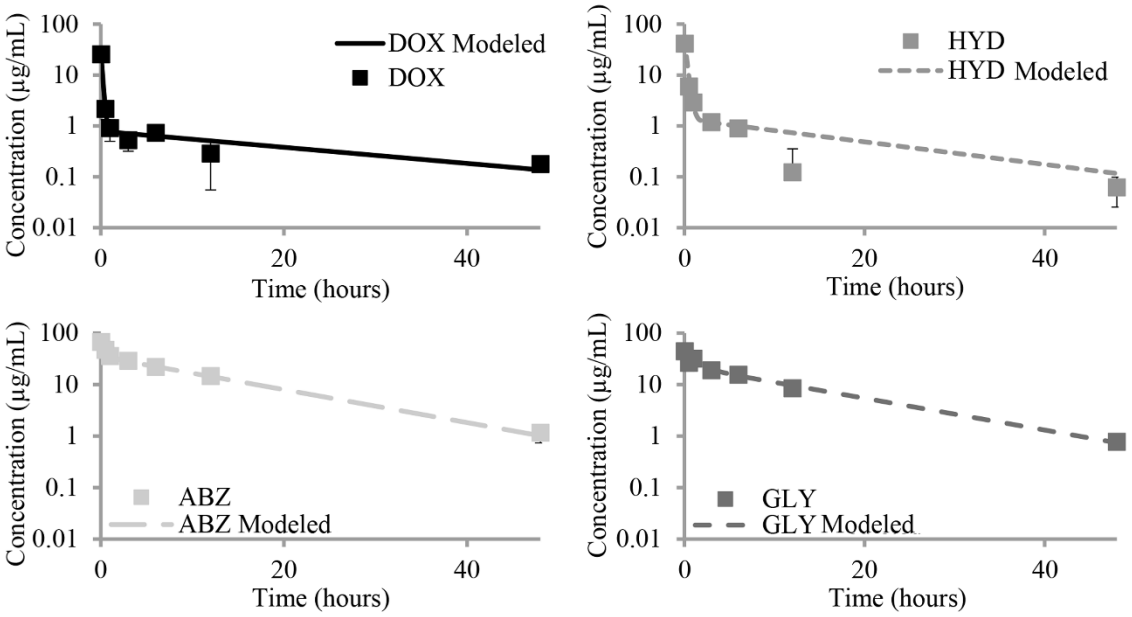

Figure 32. Pharmacokinetic Analysis of Micellar and Free DOX Treatments

Table 14. Pharmacokinetic Parameters of DOX and Micellar Treatments

Micelle	AUC (hrs*µg/mL)	AUC Ratio	Clearance (mL/hour)	$t_{1/2f}$ (hours)	$t_{1/2s}$ (hours)	V_{ss} (mL)	C_{Max} (µg/mL)
DOX	27 ± 11	1.0 ± 0.6	7.5 ± 3.1	0.11 ± 0.01	19 ± 12	166 ± 55	32 ± 2.3
HYD	40 ± 4.2	1.5 ± 0.4	4.9 ± 0.5	0.18 ± 0.03	14 ± 2.0	64 ± 12	54 ± 13
ABZ	487 ± 33	18 ± 0.4	0.35 ± 0.4	0.35 ± 0.09	9.4 ± 0.9	5.4 ± 0.30	68 ± 3.3
GLY	338 ± 18	12 ± 0.4	0.59 ± 0.0	0.86 ± 0.51	9.7 ± 0.5	7.8 ± 0.52	41 ± 4.3

Paramaters are shown ± the standard error.

7.3.2 Antitumor Activity

Antitumor efficacy of micellar treatments was compared to two controls: free DOX and PBS treatments. Two antitumor studies were performed. One monitored the effects of a single high DOX equivalent dose in mice with A549 xenografts. The secondary study observed the efficacy of treatments after two lower DOX equivalent doses in mice with HT29 xenografts.

For the high dose study, mice were injected on day zero with micellar solutions or free DOX at a 50 mg/kg DOX equivalent dose. Mice injected with free DOX did not survive due to high toxicity. Similarly, HYD micelle treatment was toxic and mice were euthanized shortly after dosing. PBS, ABZ, and GLY treated mice were weighed throughout the experiment to observe toxicity (Figure 33). Mice treated with PBS gained weight steadily. GLY treated mice not only did not lose weight, but actually steadily gained weight. A small degree of weight loss was observed with ABZ treated mice up to day six, but this loss was not statistically different than the initial weight ($p > 0.05$). After day six, mice treated with ABZ gained weight. Therapy with ABZ and GLY micelles showed promise, as tumor growth was retarded over a 28 day period (Figure 33). Relative tumor volume (V_x/V_0) was calculated, where V_x represents tumor volume on a specific day, and V_0 is the initial tumor volume. PBS treated mice experienced rapid tumor growth with tumor volume reaching 750 mm^3. ABZ treatment resulted in significant antitumor activity, as mice tumors reached a maximum of 2.5 relative tumor volume. Compared to the ABZ treated mice, GLY treated mice experienced an improved antitumor effect ($p < 0.05$). In terms of relative tumor volume, the maximum tumor size of mice treated with GLY was 1.3. This tumor volume was not significantly different than the initial tumor

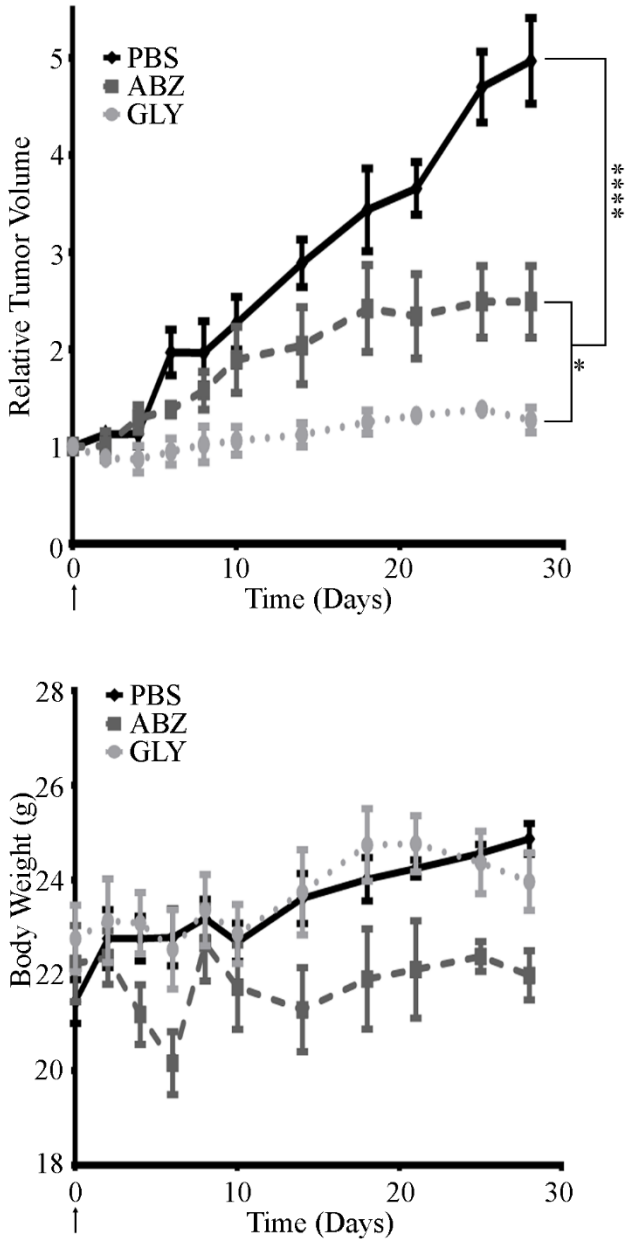

Figure 33. High Dose Antitumor Study with A549 Xenografts

volume ($p > 0.05$). Interestingly, tumor size initially decreased after GLY treatment. Overall, both GLY and ABZ treatments hindered tumor growth compared to the control ($p < 0.0001$).

Mice were dosed twice at 10 mg/kg DOX equivalent doses in the second antitumor study. An additional group of mice was treated with PBS as a control. Tumor volume and mouse body weight were monitored throughout the study (Figure 34). Six days after the initial injection, micelle treated mice experienced minimal tumor growth. However, tumors of both DOX and PBS treated mice doubled in volume. An additional week was required for tumors of ABZ and GLY treated mice to reach the same size. After 21 days, a trend in tumor volume was established [PBS>DOX>HYD> (ABZ and GLY)].

Mice were euthanized when tumors reached a relative tumor volume of 30. Under these guidelines, PBS treated mice were sacrificed first, followed by free DOX treated mice. Mice treated with free DOX survived only an additional week compared to PBS treated mice. Eleven days after the DOX group was euthanized, the HYD group reached the tumor volume cut-off. Mice treated with ABZ or GLY micelles survived 21 days longer than DOX treated mice, extending their lifespan by 40%. ABZ and GLY treated mice were sacrificed on day 74.

In addition to superior antitumor activity, mice treated with micelles did not exhibit weight loss over the course of study. In fact, HYD, ABZ, and GLY treated mice mimicked the weight change of the PBS group. On the other hand, DOX treated mice saw a sudden weight loss of almost three grams after the second dose. This weight loss equates to approximately 10% change in body weight. As the experiment progressed, the

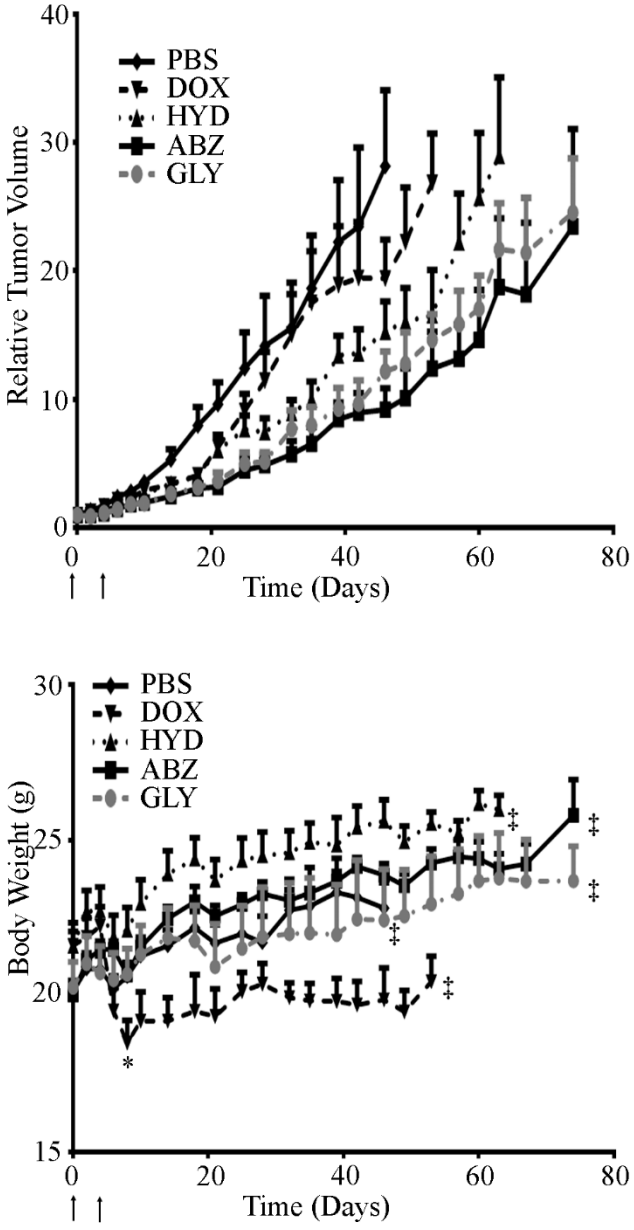

Figure 34. HT29 Xenograft Antitumor Study

DOX treated group slowly gained weight.

7.3.3 In Vivo *and* Ex Vivo *Imaging*

In vivo and *ex vivo* imaging was performed at the end of the high dose (50 mg/kg) antitumor study. For *in vivo* imaging, an IVIS instrument was used to explore the possibility of monitoring tumor growth through luminescence measurements. A549 cells used to establish xenografts were transfected with luciferase. For imaging, mice were injected in the peritoneal cavity with D-luciferin. The resulting tumor luminescence signal was observed (Figure 35). Tumors were subsequently excised and photographed for size comparison. Additionally, tumor length and width were measured with calipers to determine volume.

Results indicated that IVIS images were consistent with caliper measurements. The PBS treated mouse had the largest tumor (Figure 36A). The second and third largest tumors were from ABZ and GLY treated mice, respectively (Figures 36B and 36C, respectively). The luminescence region of interest (ROI) as derived from IVIS corresponded well with manual tumor size measurements. According to IVIS measurements, the tumor from the mouse treated with GLY was 2.7 times smaller than the ABZ treated one, while caliper measurements showed that the difference was twofold. Comparing ABZ to PBS treatment, the tumor volume difference was 2.7 greater according to IVIS and twofold according to caliper measurements.

Mice were euthanized and tissue was harvested for fluorescence *ex vivo* imaging. Tissue from mice treated with PBS showed no fluorescence (Figure 36). Similarly, there was no fluorescence signal present in the heart, lungs, liver, kidneys, or spleen in mice treated with ABZ or GLY. Intriguingly, a small signal was present from tumor tissue of

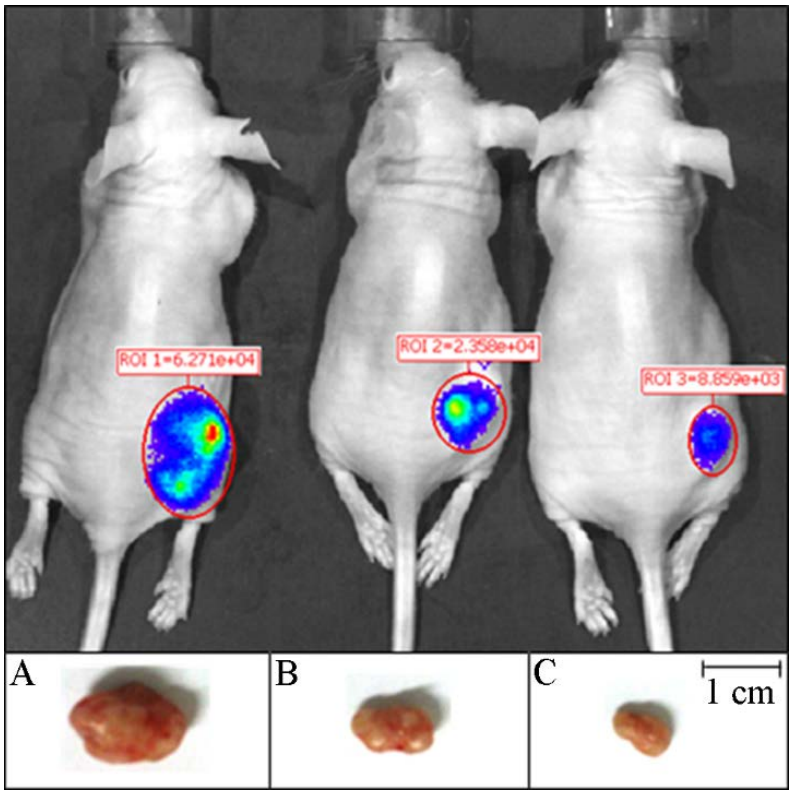

Figure 35. Determining Tumor Size Utilizing in Vivo *Imaging*

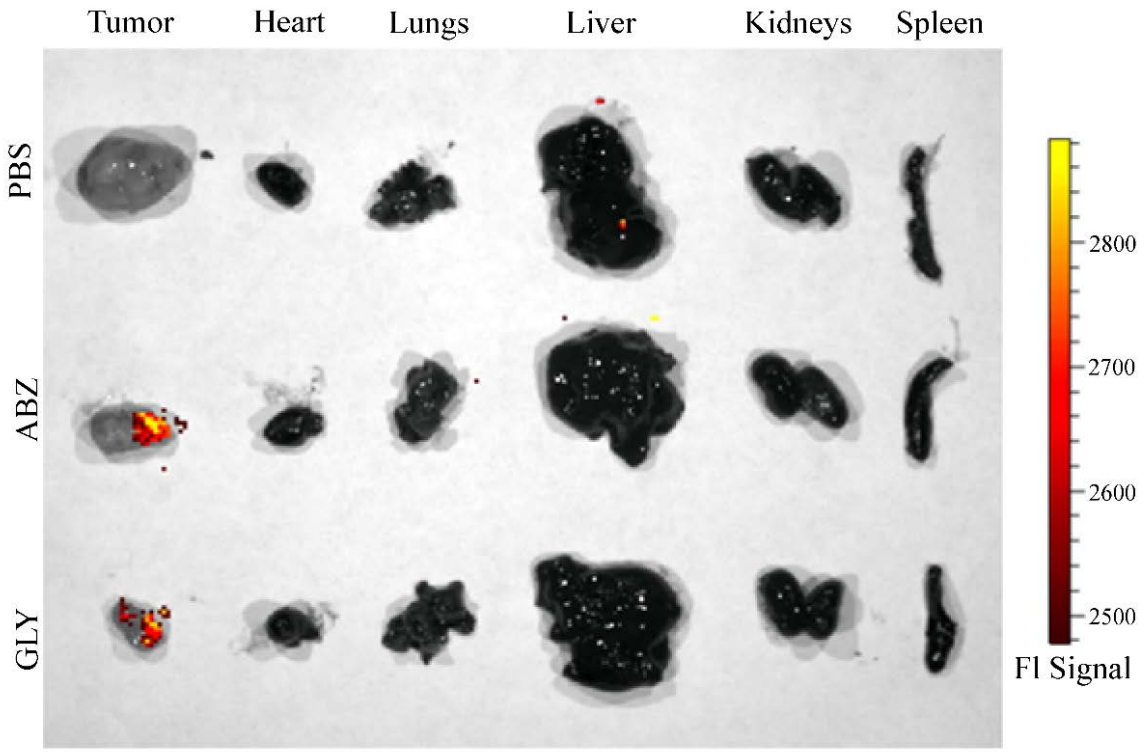

Figure 36. DOX Detection 28 Days after Initial Treatment

ABZ and GLY treated mice. In order to confirm the signal as the presence of DOX, the three tumors were analyzed as was done with the biodistribution study. Results from this method showed that tumor DOX concentration in the PBS treated mouse was zero; but a concentration of 2.5 μg/kg of DOX was observed in ABZ treated mouse. A slightly higher DOX concentration (3.4 μg/kg) was found in the GLY treated mouse tumor.

7.4 Discussion

Multiple *in vivo* studies were performed to determine DOX efficacy and biodistribution after treatments with free DOX or micellar formulations. It is important to note the time frame of these experiments due to possible hydrazone bond hydrolysis during storage. Biodistribution studies were performed within three months of block copolymer synthesis. The A549 antitumor study was performed less than four months after initial synthesis. In both cases, free DOX formation is expected to be less than 8%. Degradation should not affect overall results of these experiments. The antitumor studies with HT29 xenografts were performed five months after synthesis. For these experiments, up to 12% of DOX may have been cleaved from the polymer. This loss may have minimally impacted results.

7.4.1 Biodistribution Studies

Mice were treated with HYD, ABZ, GLY micelles, or free DOX at 10 mg/kg DOX equivalent doses to determine DOX biodistribution (Figures 30 and 31). A microplate reader method was used to determine DOX concentration. This analysis method was as effective as liquid chromatography-mass spectrometry (LC-MS) (147).

DOX concentrations present in tissue and serum were monitored over 48 hours. Free DOX was rapidly distributed throughout the body, as high DOX concentrations

were observed in all tissue within 30 minutes. Furthermore, AUC analysis confirmed high DOX distribution into peripheral tissue after free DOX treatment. Due to the larger particle size, micelles cannot readily diffuse through healthy vasculature to reach peripheral tissue (148, 149). In this study, micellar treatments greatly reduced non-specific delivery of DOX. Compared to free DOX treatment, only a fraction of DOX was found in the spleen, kidneys, and lungs after micellar treatments. Even in the liver, the total DOX concentration from ABZ and GLY micelles was less than that of free DOX. However, similar DOX concentrations were found in the liver after free DOX and HYD micelle treatments. It is important to note that cardiac toxicity is one of the main drawbacks of DOX in the clinic, and lowering DOX concentration in the heart may help lower this risk (150, 151). After micellar treatment, DOX concentration in the heart was less than 43% of that after free DOX treatment, suggesting that micellar treatment could reduce cardiac toxicity. Overall, micelles minimized DOX concentration in peripheral tissue.

DOX concentration from each treatment was also observed in tumor tissue. DOX from micellar treatment was initially present in tumors to a greater extent than that from free DOX treatment. Over the time frame of the experiment, DOX concentration in tissue varied depending on treatment with no trend arising. No significant difference in DOX tumor accumulation was observed, irrespective of treatment.

Pharmacokinetic parameters were estimated using a two compartment model (Figure 32). Each treatment followed a similar pattern of initial distribution in peripheral tissue, followed by an elimination phase. Free DOX was removed from the blood stream quickly. However, polymer micelle treatment showed a prolonged DOX circulation time.

This was believed to be due to the physicochemical properties of micelles. The micellar particle size may have prevented diffusion through healthy vasculature, as shown in similar studies (152). Additionally, the PEG shell could have shielded micelles from phagocytosis (153-155). Estimated pharmacokinetic parameters supported this notion. The quickest DOX clearance was observed after free DOX treatment. Furthermore, there was an order of magnitude difference in DOX clearance when comparing free DOX to GLY and ABZ treatments. Clearance after HYD treatment was slower than clearance of free DOX treatment, but this difference was smaller than the ABZ or GLY treatments. Drug release studies showed greater DOX release from HYD micelles then both ABZ and GLY micelles. The quicker DOX elimination could be explained by the greater DOX release. Furthermore, particle size analysis suggested a less compact HYD micelle core which could contribute to quicker elimination. Overall, DOX circulation time was greatly increased with micellar formulations.

7.4.2 Antitumor Activity

The antitumor effects of micellar treatment were observed in mice with either A549 or HT29 xenografts. Micelles developed herein had similar physicochemical properties. HYD, ABZ, and GLY micelles had a ζ-potential <+13; with a particle diameter <125 nm. In terms of total DOX release over 72 hours, micelles followed the pattern: HYD>ABZ>GLY. Two dosing schedules were tested: an elevated single dose, and a smaller dose over two injections.

For the single dose study, antitumor effects of each treatment were observed over 28 days. A single 50 mg/kg DOX equivalent injection was administered to mice. This further minimized extraneous factors in antitumor activity. Two controls were used in the

antitumor study: free DOX and PBS. A tumor growth base line was established by monitoring tumor growth of PBS treated mice. Mice were treated with free DOX to compare and contrast effects of micellar treatments. Unfortunately, free DOX treatment led to high toxicity and mice were euthanized the same day. It was suspected that quick DOX distribution in peripheral tissue caused adverse toxicity and eventual death. Mice treated with HYD micelles suffered a similar fate. Though they initially survived, adverse side effects were soon observed and mice were sacrificed. HYD micelles released the largest amount of DOX in pH 7.4, and it was believed that this fast release led to the high toxicity. Mice treated with GLY and ABZ micelles survived this high dose. Importantly, no adverse toxicity was observed in either GLY or ABZ treated mice. DOX release from both of these micelles was low at pH 7.4. Additionally, DOX from ABZ and GLY micelles was minimally distributed in peripheral tissue. The combination of lower DOX release and decreased distribution in peripheral tissue presumably led to the absence of observed toxicity.

The antitumor effects of micellar treatment supported *in vitro* results. Mice exposed to DOX released at slower rates showed enhanced antitumor activity. GLY and ABZ treated mice experienced significant antitumor activity. At the same time, tumors of PBS treated mice quintupled in volume. Tumors of ABZ treated mice only doubled in volume after 28 days, while tumors of GLY treated mice remained unchanged after 28 days. The primary difference between the two micelles was the drug release profiles, as ABZ micelles released more DOX than GLY micelles. However, the secondary slow release rate of DOX may have played a key role. As the study was performed over a 28 day period, this slow release would be most applicable. The secondary, slow release rate

of DOX from ABZ micelles was slightly slower than the DOX release rate from GLY micelles. The slow and prolonged release of DOX was assumed to contribute to the greater antitumor activity from micellar treatments, as tumors would be exposed to DOX for extended time period. Controlling the release rate can therefore be used to improve cancer chemotherapy treatments.

The secondary antitumor study compared the effectiveness of micellar treatment to free DOX in mice with HT29 xenografts. Mice survival was ensured by lowering the dose and spreading the treatment over two injections. Out of the mice treated with micelles, none had apparent adverse toxicity. Monitoring body weight confirmed this assessment. With the free DOX treatment, mouse body weight decreased after the second injection, suggesting toxicity. Nevertheless, mice survived all treatments allowing comparisons between micelles and free DOX treatments to be made.

Mice treated with PBS fared the worst as they reached the tumor size limit quickest and were thus euthanized. The immediate impact of free DOX treatment was observed within the first week of the second injection. At this point relative tumor size started to differentiate from PBS treated mice. However, the antitumor effect did not last long, as only a week later tumor growth increased drastically. It appeared that the therapeutic effect from free DOX treatment was short lived. On the other hand, micellar treatments showed a much longer lasting effect. Through the first 18 days, HYD, ABZ, and GLY treatments were similar to free DOX treatment. Thereafter micellar treatments continued tumor growth suppression whereas free DOX treatment began to fail. After 35 days micelle treated mice had a maximum relative tumor size of eight, while DOX treated mice had tumors 16 times the initial volume. Releasing DOX at slow, prolonged

rates, micelles improved on the antitumor effect of free DOX. Intriguingly, both ABZ and GLY micelles performed substantially better than HYD micelles. Tumors of mice treated with either GLY or ABZ micelles took almost 20% longer to reach the relative tumor volume of their HYD treated counterparts.

The combination of the larger percent of DOX undergoing fast release, with the quick elimination of HYD micelles *in vivo* probably contributed to the lower efficacy. Another factor minimizing efficacy of HYD treatment could be attributed to the large release of DOX in pH 7.4 with the HYD micelles. Overall, the results of this antitumor study are consistent with the high dose antitumor study. Micelles releasing DOX at slow rates improved tumor growth suppression the most.

7.4.3 In Vivo *and* Ex Vivo *Imaging*

Two sets of imaging studies were performed: whole body and tissue analysis. Studies were independent of one another. The first set out to observe the capability of using bioluminescence as a way to monitor tumor growth. The second was performed to monitor DOX in tissue.

Tumor xenografts were established using A549 cells for antitumor studies. These A549 cells were transfected with a luciferase gene. Cells expressing luciferase are bioluminescent and their bioluminescence can be detected after exposure to D-luciferin (156). At the end of the single dose antitumor study, whole body images of mice were taken. Mice were dosed with D-luciferin through an intraperitoneal injection. IVIS images were then taken to detect cancerous tissue (Figure 35). Measured bioluminescent signal was translated to relative tumor volume. The relative tumor volume from IVIS imaging and caliper measurements were then compared. The two methods showed good

correlation, as results from IVIS were consistent with caliper measurements. It was concluded that IVIS imaging was a good alternative to caliper measurements.

IVIS was used to fluorescently (excitation 500 nm, emission 600 nm) observe DOX presence in tissue. The DOX peak absorbance is at 485 nm, however measurements using 500 nm as the excitation can still detect DOX. There was no DOX detected in the heart, lungs, liver, kidneys, or spleen. This was unsurprising as *ex vivo* imaging was performed 28 days post treatment. Intriguingly, minute amounts of DOX were observed in tumor tissue of ABZ and GLY treated mice. DOX was not detected in the tumor of the PBS treated mouse.

An additional experiment was performed to confirm DOX presence in tumors. Tissue was analyzed in the same fashion as the biodistribution studies. Results showed the presence of small amounts of DOX in tumor tissue from ABZ and GLY treated mice. The tumor of the PBS treated mouse confirmed no DOX presence. These results were consistent with IVIS imaging. It appeared that DOX from micellar treatment remained present in tumor tissue for a prolonged period. Previous works have shown that due to poor lymphatic drainage, micelles can remain in the tumor tissue for an extended time. By remaining in the tumors, micelles can deliver DOX over extended time periods and possibly improve antitumor activity.

7.5 Conclusions

Block copolymer with three drug binding linkers (HYD, ABZ-HYD, or GLY-HYD) and covalently attached DOX were prepared for *in vivo* studies. Block copolymers formed micelles (HYD, ABZ, or GLY, respectively) which released DOX with distinct patterns as shown by drug release studies. Differences in drug release were most prominently

observed when analyzing total drug release. The effects of differential drug release were observed *in vivo* through biodistribution and antitumor studies.

Biodistribution studies compared and contrasted DOX treatment as a free drug and within a micellar system. Free DOX treatment resulted in quick DOX elimination and high accumulation in peripheral tissue. Conversely, the uptake of DOX after micelle treatment was minimized in the spleen, kidneys, heart, and lungs. This stark contrast could explain the miniscule toxicity observed with micellar treatments.

Two subsequent repetitions of the antitumor study yielded similar results. In both antitumor studies, treatments with micelles proved beneficial. At high doses, micelles suppressed tumor growth, while at lower doses micelles significantly retarded tumor growth. Specifically, mice treated with GLY at a high dose experienced complete tumor growth suppression. Maintaining this trend, lower doses of both ABZ and GLY micelles hindered tumor growth most effectively. It is important to note that micelles had a similar slow DOX release phase. By continuously exposing tumor tissue to DOX, micellar treatments were able to hinder tumor growth regardless of xenograft model. These studies showed that delivering DOX at slower rates for an extended period can enhance antitumor efficacy, rendering it apparent that modulating release is a key factor in efficacy.

CHAPTER EIGHT

8 CONCLUSIONS AND FUTURE DIRECTIONS

Despite the fact that it may play a key role in the improvement of chemotherapeutic efficacy, the effects of differential drug release have not yet been fully examined. To further explore the subject, a modifiable polymeric micelle NDDS based on PED-p(BLA) block copolymers was developed and detailed herein.

Multiple PEG-p(BLA) scaffolds with a varying number of BLA repeating units were synthesized and modified. Drug binding linkers (HYD, ABZ-HYD, or GLY-HYD) were inserted to the scaffolds. DOX was then covalently attached through a hydrazone bond. Regardless of block copolymer synthesis, a therapeutically significant amount of DOX was conjugated onto block copolymers. Final block copolymers formed micelles with similar characteristics to each other. All particles were less than 125 nm in diameter. The micellar surface charge of ABZ and GLY was neutral, while HYD modified micelles had a slightly positive ζ-potential.

The drug release characteristics of micelles were analyzed in both acidic (intracellular) and neutral (physiological) conditions through multiple drug release studies. Irrespective of drug release conditions and formulation, micelles exhibited biphasic DOX release. A mathematical model was developed to estimate drug release parameters, establishing a method to analyze DOX release from micellar systems. Modeling results proved inconclusive overall, as none of the determined parameters were statistically significant. However, drug release analysis at individual points showed that a pH effect was present; micelles released more DOX at pH 5.0 than at pH 7.4, a phenomenon further supported by AUC analysis.

Drug binding linker insertion led to differential drug release in pH 5.0 based on total drug released and AUC analysis. HYD micelles had the highest AUC of all the formulations, followed by ABZ and then GLY micelles. These results indicated that HYD micelles released the most DOX over a given time period. Though release rates determined through modeling yielded inconclusive results, it was evident that drug release profiles were dependent on micellar composition, and more specifically on the drug binding linker used.

The effect of modulated release was observed *in vitro* with three different release profiles (HYD>ABZ>GLY). Micellar formulation maintained DOX activity *in vitro,* while the NDDS itself exhibited minimal toxicity. Cellular uptake studies confirmed that both DOX and block copolymers were readily internalized. The cytotoxicity of micelles was analyzed and compared to that of free DOX across multiple cell lines. DOX delivered at a steady rate via micelles was equipotent to free DOX treatment underscoring the benefits of prolonged release versus a single bolus dose.

HYD, ABZ, and GLY micelles were analyzed *in vivo* to determine biodistribution and antitumor activity of DOX after micellar treatments. Micellar treatment minimized non-specific distribution of drugs in the body, reducing adverse toxicity. Even at very high DOX equivalent concentrations, ABZ and GLY micelles were not toxic. Perhaps most importantly, DOX concentration in the heart was drastically decreased with micellar treatments. Antitumor results further supported the finding that slow, prolonged release was more effective than a single large dose. ABZ and GLY micelles both hindered tumor growth in HT29 and A549 tumor xenograft models. It is evident that modulating release rate is a key factor in antitumor efficacy.

This research outlines a modifiable drug delivery platform which allows the effects of differential drug release to be observed, opening multiple avenues for future research. The modification of block copolymers with differential drug binding linkers has provided three drug release profiles for analysis. Though this is highly informative, it represents a narrow window in terms of drug release profiles. Further insight could be gained by synthesizing additional block copolymers to complete the drug release spectrum. By testing these formulations across multiple cell lines, a tailored treatment could then be developed.

Beyond the scope of drug release, the hydrazone bond was determined to be unstable when stored long-term. It will be important to identify the factors contributing to this breakdown. Defining optimal storage conditions is critical if this NDDS is expected to reach clinical trials. This does not apply exclusively to the polymeric micelle system developed herein, as hydrazone linkages are used extensively.

REFERENCES

1. R. Siegel, D. Naishadham, and A. Jemal. Cancer statistics, 2012. CA: A Cancer Journal for Clinicians. 62:10-29 (2012).

2. K. Kataoka, A. Harada, and Y. Nagasaki. Block copolymer micelles for drug delivery: design, characterization and biological significance. Advanced Drug Delivery Reviews. 47:113-131 (2001).

3. S.S. Desale, S.M. Cohen, Y. Zhao, A.V. Kabanov, and T.K. Bronich. Biodegradable hybrid polymer micelles for combination drug therapy in ovarian cancer. Journal of Controlled Release. 171:339-348 (2013).

4. G. Gregoriadis. Engineering liposomes for drug delivery: progress and problems. Trends in Biotechnology. 13:527-537 (1995).

5. D.C. Drummond, C.O. Noble, Z. Guo, K. Hong, J.W. Park, and D.B. Kirpotin. Development of a highly active nanoliposomal irinotecan using a novel intraliposomal stabilization strategy. Cancer Research. 66:3271-3277 (2006).

6. H.J. Lee and Y. Bae. Cross-linked nanoassemblies from poly(ethylene glycol)-poly(aspartate) block copolymers as stable supramolecular templates for particulate drug delivery. Biomacromolecules. 12:2686-2696 (2011).

7. A.W. Bosman, H.M. Janssen, and E.W. Meijer. About dendrimers: structure, physical properties, and applications. Chemical Reviews. 99:1665-1688 (1999).

8. F. Aqil, R. Munagala, J. Jeyabalan, and M.V. Vadhanam. Bioavailability of phytochemicals and its enhancement by drug delivery systems. Cancer Letters. 334:133-141 (2013).

9. A. Lavasanifar, J. Samuel, and G.S. Kwon. Poly(ethylene oxide)-block-poly(L-amino acid) micelles for drug delivery. Advanced Drug Delivery Reviews. 54:169-190 (2002).

10. S.D. Li and L. Huang. Pharmacokinetics and biodistribution of nanoparticles. Molecular Pharmacology. 5:496-504 (2008).

11. H.C. Shin, A.W. Alani, D.A. Rao, N.C. Rockich, and G.S. Kwon. Multi-drug loaded polymeric micelles for simultaneous delivery of poorly soluble anticancer drugs. Journal of Controlled Release. 140:294-300 (2009).

12. Y. Bae, N. Nishiyama, and K. Kataoka. In vivo antitumor activity of the folate-conjugated pH-sensitive polymeric micelle selectively releasing Adriamycin in the intracellular acidic compartments. Bioconjugate Chemistry. 18:1131-1139 (2007).

13. X. Guo, C. Shi, J. Wang, S. Di, and S. Zhou. pH-triggered intracellular release from actively targeting polymer micelles. Biomaterials. 34:4544-4554 (2013).

14. V.P. Torchilin. PEG-based micelles as carriers of contrast agents for different imaging modalities. Advanced Drug Delivery Reviews. 54:235-252 (2002).

15. Y. Bae, W.D. Jang, N. Nishiyama, S. Fukushima, and K. Kataoka. Multifunctional polymeric micelles with folate-mediated cancer cell targeting and pH-triggered drug releasing properties for active intracellular drug delivery. Molecular BioSystems. 1:242-250 (2005).

16. C. Oerlemans, W. Bult, M. Bos, G. Storm, J.F. Nijsen, and W.E. Hennink. Polymeric micelles in anticancer therapy: targeting, imaging and triggered release. Pharmaceutical Research. 27:2569-2589 (2010).

17. Y. Lee, S. Fukushima, Y. Bae, S. Hiki, T. Ishii, and K. Kataoka. A protein nanocarrier from charge-conversion polymer in response to endosomal pH. Journal of the American Chemical Society. 129:5362 (2007).

18. K. Sakai-Kato, K. Ishikura, Y. Oshima, M. Tada, T. Suzuki, A. Ishii-Watabe, T. Yamaguchi, N. Nishiyama, K. Kataoka, T. Kawanishi, and H. Okuda. Evaluation of intracellular trafficking and clearance from HeLa cells of Doxorubicin-bound block copolymers. International Journal of Pharmaceutics. 423:401-409 (2012).

19. C.Y. Zhang, Y.Q. Yang, T.X. Huang, B. Zhao, X.D. Guo, J.F. Wang, and L.J. Zhang. Self-assembled pH-responsive MPEG-b-(PLA-co-PAE) block copolymer micelles for anticancer drug delivery. Biomaterials. 33:6273-6283 (2012).

20. E.S. Lee, K. Na, and Y.H. Bae. Polymeric micelle for tumor pH and folate-mediated targeting. Journal of Controlled Release. 91:103-113 (2003).

21. A. Ponta and Y. Bae. PEG-poly(amino acid) block copolymer micelles for tunable drug release. Pharmaceutical Research. 27:2330-2342 (2010).

22. S. Ganta, H. Devalapally, A. Shahiwala, and M.M. Amiji. A review of stimuli-responsive nanocarriers for drug and gene delivery. Journal of Controlled Release. 126:187-204 (2008).

23. C.Y. Chen, T.H. Kim, W.C. Wu, C.M. Huang, H. Wei, C.W. Mount, Y.Q. Tian, S.H. Jang, S.H. Pun, and A.K.Y. Jen. pH-dependent, thermosensitive polymeric nanocarriers for drug delivery to solid tumors. Biomaterials. 34:4501-4509 (2013).

24. G. Saito, J.A. Swanson, and K.D. Lee. Drug delivery strategy utilizing conjugation via reversible disulfide linkages: role and site of cellular reducing activities. Advanced Drug Delivery Reviews. 55:199-215 (2003).

25. G. Jin and Y. Bae. Reductant-dependent none-partial-complete degradation of block copolymer disulfide crosslinked nanoassemblies. Journal of Applied Pharmaceutical Science. 3:1-6 (2013).

26. W. Chen, P. Zhong, F.H. Meng, R. Cheng, C. Deng, F.J. Jan, and Z.Y. Zhong. Redox and pH-responsive degradable micelles for dually activated intracellular anticancer drug release. Journal of Controlled Release. 169:171-179 (2013).

27. K.T. Oh, H.Q. Yin, E.S. Lee, and Y.H. Bae. Polymeric nanovehicles for anticancer drugs with triggering release mechanisms. Journal of Materials Chemistry. 17:3987-4001 (2007).

28. A. Rahman, D. Carmichael, M. Harris, and J.K. Roh. Comparative pharmacokinetics of free Doxorubicin and Doxorubicin entrapped in cardiolipin liposomes. Cancer Research. 46:2295-2299 (1986).

29. M. Gou, H. Shi, G. Guo, K. Men, J. Zhang, L. Zheng, Z. Li, F. Luo, Z. Qian, X. Zhao, and Y. Wei. Improving anticancer activity and reducing systemic toxicity of Doxorubicin by self-assembled polymeric micelles. Nanotechnology. 22:095102 (2011).

30. R.S. Kerbel, G. Klement, K.I. Pritchard, and B. Kamen. Continuous low-dose anti-angiogenic/metronomic chemotherapy: from the research laboratory into the oncology clinic. Annals of Oncology. 13:12-15 (2002).

31. A. Grattoni, H.F. Shen, D. Fine, A. Ziemys, J.S. Gill, L. Hudson, S. Hosali, R. Goodall, X.W. Liu, and M. Ferrari. Nanochannel technology for constant delivery of chemotherapeutics: beyond metronomic administration. Pharmaceutical Research. 28:292-300 (2011).

32. N.P. Shah, C. Kasap, C. Weier, M. Balbas, J.M. Nicoll, E. Bleickardt, C. Nicaise, and C.L. Sawyers. Transient potent BCR-ABL inhibition is sufficient to commit chronic myeloid leukemia cells irreversibly to apoptosis. Cancer Cell. 14:485-493 (2008).

33. W.J. Hrushesky. Circadian timing of cancer chemotherapy. Science. 228:73-75 (1985).

34. N. Nishiyama and K. Kataoka. Nanostructured devices based on block copolymer assemblies for drug delivery: Designing structures for enhanced drug function. Polymer Therapeutics II: Polymers as Drugs, Conjugates and Gene Delivery Systems. 193:67-101 (2006).

35. K.R. West and S. Otto. Reversible covalent chemistry in drug delivery. Current Drug Discovery Technologies 2:123-160 (2005).

36. B.Y. Hernandez, M.D. Green, K.D. Cassel, A.M. Pobutsky, V. Vu, and L.R. Wilkens. Preview of Hawaii Cancer Facts and Figures 2010. Hawaii Medical Journal. 69:223-224 (2010).

37. R. Siegel, C. DeSantis, K. Virgo, K. Stein, A. Mariotto, T. Smith, D. Cooper, T. Gansler, C. Lerro, S. Fedewa, C. Lin, C. Leach, R.S. Cannady, H. Cho, S. Scoppa, M. Hachey, R. Kirch, A. Jemal, and E. Ward. Cancer treatment and survivorship statistics, 2012. CA: A Cancer Journal for Clinicians. 62:220-241 (2012).

38. J.H. Atkins and L.J. Gershell. Selective anticancer drugs. Nature Reviews Drug Discovery. 1:491-492 (2002).

39. B.A. Chabner and T.G. Roberts. Timeline - Chemotherapy and the war on cancer. Nature Reviews Cancer. 5:65-72 (2005).

40. C.D. Scripture and W.D. Figg. Drug interactions in cancer therapy. Nature Reviews Cancer. 6:546-558 (2006).

41. D. Hanahan and R.A. Weinberg. The Hallmarks of cancer. Cell. 100:57-70 (2000).

42. D. Hanahan and R.A. Weinberg. Hallmarks of cancer: the next generation. Cell. 144:646-674 (2011).

43. Y. Bae and K. Kataoka. Intelligent polymeric micelles from functional poly(ethylene glycol)-poly(amino acid) block copolymers. Advanced Drug Delivery Reviews. 61:768-784 (2009).

44. R. Duncan. The dawning era of polymer therapeutics. Nature Reviews Drug Discovery. 2:347-360 (2003).

45. R. Duncan. Polymer conjugates as anticancer nanomedicines. Nature Reviews Cancer. 6:688-701 (2006).

46. P. Cao and Y. Bae. Polymer nanoparticulate drug delivery and combination cancer therapy. Future Oncology. 8:1471-1480 (2012).

47. V.P. Torchilin. Micellar nanocarriers: Pharmaceutical perspectives. Pharmaceutical Research. 24:1-16 (2007).

48. V.P. Torchilin, V.G. Omelyanenko, M.I. Papisov, A.A. Bogdanov, Jr., V.S. Trubetskoy, J.N. Herron, and C.A. Gentry. Poly(ethylene glycol) on the liposome surface: on the mechanism of polymer-coated liposome longevity. Biochimica et Biophysica Acta (BBA) - Biomembranes. 1195:11-20 (1994).

49. A. Gabizon, H. Shmeeda, and Y. Barenholz. Pharmacokinetics of pegylated liposomal Doxorubicin: review of animal and human studies. Clinical Pharmacokinetics. 42:419-436 (2003).

50. N. Bertrand and J.C. Leroux. The journey of a drug-carrier in the body: An anatomo-physiological perspective. Journal of Controlled Release. 161:152-163 (2012).

51. R.K. Jain, L.L. Munn, and D. Fukumura. Dissecting tumour pathophysiology using intravital microscopy. Nature Reviews Cancer. 2:266-276 (2002).

52. S.K. Hobbs, W.L. Monsky, F. Yuan, W.G. Roberts, L. Griffith, V.P. Torchilin, and R.K. Jain. Regulation of transport pathways in tumor vessels: Role of tumor type and microenvironment. Proceedings of the National Academy of Sciences. 95:4607-4612 (1998).

53. V.P. Torchilin. Passive and active drug targeting: drug delivery to tumors as an example. Handbook of Experimental Pharmacology:3-53 (2010).

54. Y. Lu and R.I. Mahato. Pharmaceutical perspectives of cancer therapeutics, Springer, Dordrecht; New York. Arlington, Va., 2009.

55. T.M. Allen and P.R. Cullis. Drug delivery systems: entering the mainstream. Science. 303:1818-1822 (2004).

56. H. Maeda. The enhanced permeability and retention (EPR) effect in tumor vasculature: the key role of tumor-selective macromolecular drug targeting. Advances in Enzyme Regulation. 41:189-207 (2001).

57. H. Maeda and Y. Matsumura. Tumoritropic and lymphotropic principles of macromolecular drugs. Critical Review in Therapeutic Drug Carrier Systems 6:193-210 (1989).

58. Y.H. Bae. Drug targeting and tumor heterogeneity. Journal of Controlled Release. 133:2-3 (2009).

59. R. Benelli, S. Monteghirfo, C. Balbi, P. Barboro, and N. Ferrari. Novel antivascular efficacy of metronomic docetaxel therapy in prostate cancer: hnRNP K as a player. International Journal of Cancer. 124:2989-2996 (2009).

60. L.D. Mayer, T.O. Harasym, P.G. Tardi, N.L. Harasym, C.R. Shew, S.A. Johnstone, E.C. Ramsay, M.B. Bally, and A.S. Janoff. Ratiometric dosing of anticancer drug combinations: Controlling drug ratios after systemic administration regulates therapeutic activity in tumor-bearing mice. Molecular Cancer Therapeutics. 5:1854-1863 (2006).

61. T.T. Dang, K.M. Bratlie, S.R. Bogatyrev, X.Y. Chen, R. Langer, and D.G. Anderson. Spatiotemporal effects of a controlled-release anti-inflammatory drug on the cellular dynamics of host response. Biomaterials. 32:4464-4470 (2011).

62. L.E. van Vlerken, Z. Duan, S.R. Little, M.V. Seiden, and M.M. Amiji. Augmentation of therapeutic efficacy in drug-resistant tumor models using

ceramide coadministration in temporal-controlled polymer-blend nanoparticle delivery systems. The AAPS Journal. 12:171-180 (2010).

63. F. Greco, M.J. Vicent, S. Gee, A.T. Jones, J. Gee, R.I. Nicholson, and R. Duncan. Investigating the mechanism of enhanced cytotoxicity of HPMA copolymer–Dox–AGM in breast cancer cells. Journal of Controlled Release. 117:28-39 (2007).

64. T. Minko. Soluble polymer conjugates for drug delivery. Drug Discovery Today: Technologies. 2:15-20 (2005).

65. A. Ponta, S. Akter, and Y. Bae. Degradable cross-linked nanoassemblies as drug carriers for heat shock protein 90 inhibitor 17-N-Allylamino-17-demethoxy-geldanamycin. Pharmaceuticals. 4:1281-1292 (2011).

66. H.C. Shin, A.W. Alani, H. Cho, Y. Bae, J.M. Kolesar, and G.S. Kwon. A 3-in-1 polymeric micelle nanocontainer for poorly water-soluble drugs. Molecular Pharmaceutics 8:1257-1265 (2011).

67. M.J.W. Johnston, S.C. Semple, S.K. Klimuk, K. Edwards, M.L. Eisenhardt, E.C. Leng, G. Karlsson, D. Yanko, and P.R. Cullis. Therapeutically optimized rates of drug release can be achieved by varying the drug-to-lipid ratio in liposomal vincristine formulations. Bba-Biomembranes. 1758:55-64 (2006).

68. M. Yokoyama, T. Okano, Y. Sakurai, H. Ekimoto, C. Shibazaki, and K. Kataoka. Toxicity and antitumor activity against solid tumors of micelle-forming polymeric anticancer drug and its extremely long circulation in blood. Cancer Research. 51:3229-3236 (1991).

69. J. Ma and D.J. Waxman. Modulation of the antitumor activity of metronomic cyclophosphamide by the angiogenesis inhibitor axitinib. Molecular Cancer Therapeutics. 7:79-89 (2008).

70. H.J. Lee, A. Ponta, and Y. Bae. Polymer nanoassemblies for cancer treatment and imaging. Therapeutic Delivery. 1:803-817 (2010).

71. M. Yokoyama, T. Sugiyama, T. Okano, Y. Sakurai, M. Naito, and K. Kataoka. Analysis of micelle formation of an Adriamycin-conjugated poly(ethylene glycol)-poly(aspartic acid) block copolymer by gel permeation chromatography. Pharmaceutical Research. 10:895-899 (1993).

72. Y. Masayuki, M. Mizue, Y. Noriko, O. Teruo, S. Yasuhisa, K. Kazunori, and I. Shohei. Polymer micelles as novel drug carrier: Adriamycin-conjugated poly(ethylene glycol)-poly(aspartic acid) block copolymer. Journal of Controlled Release. 11:269-278 (1990).

73. M. Howard, A. Ponta, A. Eckman, M. Jay, and Y. Bae. Polymer micelles with hydrazone-ester dual linkers for tunable release of dexamethasone. Pharmaceutical Research. 28:2435-2446 (2011).

74. M. Yokoyama, S. Inoue, K. Kataoka, N. Yui, and Y. Sakurai. Preparation of Adriamycin-conjugated poly(ethylene glycol)-poly(aspartic acid) block copolymer. A new type of polymeric anticancer agent. Die Makromolekulare Chemie, Rapid Communications. 8:431-435 (1987).

75. M. Yokoyama, G.S. Kwon, T. Okano, Y. Sakurai, T. Seto, and K. Kataoka. Preparation of micelle-forming polymer drug conjugates. Bioconjugate Chemistry. 3:295-301 (1992).

76. G. Kwon, M. Naito, M. Yokoyama, T. Okano, Y. Sakurai, and K. Kataoka. Block copolymer micelles for drug delivery: loading and release of Doxorubicin. Journal of Controlled Release. 48:195-201 (1997).

77. P. Cao, A. Ponta, J. Kim, and Y. Bae. Block copolymer crosslinked nanoassemblies co-entrapping acridine yellow and Doxorubicin for cancer theranostics. British Journal of Pharamceutical Research. 3:525-535 (2013).

78. A.M. Eckman, E. Tsakalozou, N.Y. Kang, A. Ponta, and Y. Bae. Drug release patterns and cytotoxicity of PEG-poly(aspartate) block copolymer micelles in cancer cells. Pharmaceutical Research. 29:1755-1767 (2012).

79. J.O. Kim, G. Sahay, A.V. Kabanov, and T.K. Bronich. Polymeric micelles with ionic cores containing biodegradable cross-links for delivery of chemotherapeutic agents. Biomacromolecules. 11:919-926 (2010).

80. Y. Bae, A.W.G. Alani, N.C. Rockich, T.S.Z.C. Lai, and G.S. Kwon. Mixed pH-sensitive polymeric micelles for combination drug delivery. Pharmaceutical Research. 27:2421-2432 (2010).

81. T. Etrych, L. Kovar, J. Strohalm, P. Chytil, B. Rihova, and K. Ulbrich. Biodegradable star HPMA polymer-drug conjugates: Biodegradability, distribution and anti-tumor efficacy. Journal of Controlled Release. 154:241-248 (2011).

82. L.E. van Vlerken, T.K. Vyas, and M.M. Amiji. Poly(ethylene glycol)-modified nanocarriers for tumor-targeted and intracellular delivery. Pharmaceutical Research. 24:1405-1414 (2007).

83. K. Kazunori, K. Glenn S, Y. Masayuki, O. Teruo, and S. Yasuhisa. Block copolymer micelles as vehicles for drug delivery. Journal of Controlled Release. 24:119-132 (1993).

84. H. Suzuki, D. Nakai, T. Seita, and Y. Sugiyama. Design of a drug delivery system for targeting based on pharmacokinetic consideration. Advanced Drug Delivery Reviews. 19:335-357 (1996).

85. T. Nakanishi, S. Fukushima, K. Okamoto, M. Suzuki, Y. Matsumura, M. Yokoyama, T. Okano, Y. Sakurai, and K. Kataoka. Development of the polymer micelle carrier system for Doxorubicin. Journal of Controlled Release. 74:295-302 (2001).

86. Y. Bae, N. Nishiyama, S. Fukushima, H. Koyama, M. Yasuhiro, and K. Kataoka. Preparation and biological characterization of polymeric micelle drug carriers with intracellular pH-triggered drug release property: tumor permeability, controlled subcellular drug distribution, and enhanced in vivo antitumor efficacy. Bioconjugate Chemistry. 16:122-130 (2004).

87. Y. Yamamoto, Y. Nagasaki, Y. Kato, Y. Sugiyama, and K. Kataoka. Long-circulating poly(ethylene glycol)-poly(D,L-lactide) block copolymer micelles with modulated surface charge. Journal of Controlled Release. 77:27-38 (2001).

88. Y. Bae, S. Fukushima, A. Harada, and K. Kataoka. Design of environment-sensitive supramolecular assemblies for intracellular drug delivery: polymeric micelles that are responsive to intracellular pH change. Angewandte Chemie International Edition. 42:4640-4643 (2003).

89. T. Kaneko, D. Willner, I. Monkovic, J.O. Knipe, G.R. Braslawsky, R.S. Greenfield, and D.M. Vyas. New hydrazone derivatives of Adriamycin and their immunoconjugates - a correlation between acid stability and cytotoxicity. Bioconjugate Chemistry. 2:133-141 (1991).

90. S. Binauld and M.H. Stenzel. Acid-degradable polymers for drug delivery: a decade of innovation. Chemical Communications. 49:2082-2102 (2013).

91. E.H. Cordes and W.P. Jencks. The mechanism of hydrolysis of Schiff bases derived from aliphatic amines. Journal of the American Chemical Society. 85:2843-2848 (1963).

92. E.H. Cordes and W.P. Jencks. On the mechanism of Schiff base formation and hydrolysis. Journal of the American Chemical Society. 84:832-837 (1962).

93. K. Koehler, W. Sandstrom, and E.H. Cordes. Concerning the mechanism of the hydrolysis and aminolysis of Schiff bases. Journal of the American Chemical Society. 86:2413-2419 (1964).

94. F. Kratz, U. Beyer, and M.T. Schutte. Drug-polymer conjugates containing acid-cleavable bonds. Critical Reviews in Therapeutic Drug Carrier Systems. 16:245-288 (1999).

95. A.A. Kale and V.P. Torchilin. Design, synthesis, and characterization of pH-sensitive PEG-PE conjugates for stimuli-sensitive pharmaceutical nanocarriers: the effect of substitutes at the hydrazone linkage on the ph stability of PEG-PE conjugates. Bioconjugate Chemistry. 18:363-370 (2007).

96. E.S. Lee, Z. Gao, and Y.H. Bae. Recent progress in tumor pH targeting nanotechnology. Journal of Controlled Release. 132:164-170 (2008).

97. A.T. Jones, M. Gumbleton, and R. Duncan. Understanding endocytic pathways and intracellular trafficking: a prerequisite for effective design of advanced drug delivery systems. Advanced Drug Delivery Reviews. 55:1353-1357 (2003).

98. J. Callahan and J. Kopecek. Intracellular Trafficking and Subcellular Distribution of a Large Array of HPMA Copolymers. Biomacromolecules. 10:1704-1714 (2009).

99. J. Gong, M.W. Chen, Y. Zheng, S.P. Wang, and Y.T. Wang. Polymeric micelles drug delivery system in oncology. Journal of Controlled Release. 159:312-323 (2012).

100. T.A. Diezi, Y. Bae, and G.S. Kwon. Enhanced stability of PEG-block-poly(N-hexyl stearate l-aspartamide) micelles in the presence of serum proteins. Molecular Pharmaceutics. 7:1355-1360 (2010).

101. Y. Matsumura and K. Kataoka. Preclinical and clinical studies of anticancer agent-incorporating polymer micelles. Cancer Science. 100:572-579 (2009).

102. S.P. Egusquiaguirre, M. Igartua, R.M. Hernandez, and J.L. Pedraz. Nanoparticle delivery systems for cancer therapy: advances in clinical and preclinical research. Clinical & Translational Oncology. 14:83-93 (2012).

103. Y. Matsumura, T. Hamaguchi, T. Ura, K. Muro, Y. Yamada, Y. Shimada, K. Shirao, T. Okusaka, H. Ueno, M. Ikeda, and N. Watanabe. Phase I clinical trial and pharmacokinetic evaluation of NK911, a micelle-encapsulated Doxorubicin. British Journal of Cancer. 91:1775-1781 (2004).

104. S.B. La, T. Okano, and K. Kataoka. Preparation and characterization of the micelle-forming polymeric drug indomethacin-incorporated poly(ethylene oxide)-poly(beta-benzyl L-aspartate) block copolymer micelles. Journal of Pharmaceutical Sciences. 85:85-90 (1996).

105. N. Nishiyama and K. Kataoka. Current state, achievements, and future prospects of polymeric micelles as nanocarriers for drug and gene delivery. Pharmacology & Therapeutics. 112:630-648 (2006).

106. C. Allen, D. Maysinger, and A. Eisenberg. Nano-engineering block copolymer aggregates for drug delivery. Colloids and Surfaces B: Biointerfaces. 16:3-27 (1999).

107. Y. Bae, T.A. Diezi, A. Zhao, and G.S. Kwon. Mixed polymeric micelles for combination cancer chemotherapy through the concurrent delivery of multiple chemotherapeutic agents. Journal of Controlled Release. 122:324-330 (2007).

108. A.W. Alani, Y. Bae, D.A. Rao, and G.S. Kwon. Polymeric micelles for the pH-dependent controlled, continuous low dose release of paclitaxel. Biomaterials. 31:1765-1772 (2010).

109. W.H. Daly and D. Poché. The preparation of N-carboxyanhydrides of α-amino acids using bis(trichloromethyl)carbonate. Tetrahedron Letters. 29:5859-5862 (1988).

110. S. Cammas and K. Kataoka. Functional poly[(ethylene oxide)-co-(β-benzyl-L-aspartate)] polymeric micelles: block copolymer synthesis and micelles formation. Macromolecular Chemistry and Physics. 196:1899-1905 (1995).

111. K. Kataoka, T. Matsumoto, M. Yokoyama, T. Okano, Y. Sakurai, S. Fukushima, K. Okamoto, and G.S. Kwon. Doxorubicin-loaded poly(ethylene glycol)–poly(β-benzyl-l-aspartate) copolymer micelles: their pharmaceutical characteristics and biological significance. Journal of Controlled Release. 64:143-153 (2000).

112. E.M. Czekanska. Assessment of cell proliferation with resazurin-based fluorescent dye. In M.J. Stoddart (ed.), Mammalian Cell Viability: Methods and Protocols. 740:27-32 (2011).

113. P.W. Buehler, S.J. Robles, G.R. Adami, R. Gajee, and A. Negrusz. Analysis of Doxorubicin in cell culture media and human plasma using solid phase extraction and HPLC. Chromatographia. 49:557-561 (1999).

114. T. Etrych, P. Chytil, M. Jelinkova, B. Rihova, and K. Ulbrich. Synthesis of HPMA copolymers containing Doxorubicin bound via a hydrazone linkage. Effect of spacer on drug release and in vitro cytotoxicity. Macromolecular Bioscience. 2:43-52 (2002).

115. Y. Barenholz. Doxil (R) - The first FDA-approved nano-drug: Lessons learned. Journal of Controlled Release. 160:117-134 (2012).

116. K. Ulbrich and V. Subr. Polymeric anticancer drugs with pH-controlled activation. Advanced Drug Delivery Reviews. 56:1023-1050 (2004).

117. A.J. D'Souza and E.M. Topp. Release from polymeric prodrugs: Linkages and their degradation. Journal of Pharmaceutical Sciences. 93:1962-1979 (2004).

118. J. Kalia and R.T. Raines. Hydrolytic stability of hydrazones and oximes. Angewandte Chemie-International Edition. 47:7523-7526 (2008).

119. G. Gasparini, L.J. Prins, and P. Scrimin. Exploiting neighboring-group interactions for the self-selection of a catalytic unit. Angewandte Chemie-International Edition. 47:2475-2479 (2008).

120. B. Garcia, M.S. Munoz, M. Ibeas, and J.M. Leal. Hydrolysis mechanisms for the acetylpyridinephenylhydrazone ligand in sulfuric acid. Journal of Organic Chemistry. 65:3781-3787 (2000).

121. M. Yokoyama, S. Fukushima, R. Uehara, K. Okamoto, K. Kataoka, Y. Sakurai, and T. Okano. Characterization of physical entrapment and chemical conjugation of Adriamycin in polymeric micelles and their design for in vivo delivery to a solid tumor. Journal of Controlled Release. 50:79-92 (1998).

122. S. Zhang, J. Li, G. Lykotrafitis, G. Bao, and S. Suresh. Size-Dependent Endocytosis of Nanoparticles. Advanced Materials. 21:419-424 (2009).

123. R. Duncan and S.C. Richardson. Endocytosis and intracellular trafficking as gateways for nanomedicine delivery: opportunities and challenges. Molecular Pharmacology. 9:2380-2402 (2012).

124. M.P. Xiong, Y. Bae, S. Fukushima, M.L. Forrest, N. Nishiyama, K. Kataoka, and G.S. Kwon. pH-responsive multi-PEGylated dual cationic nanoparticles enable charge modulations for safe gene delivery. ChemMedChem. 2:1321-1327 (2007).

125. H. Hillaireau and P. Couvreur. Nanocarriers' entry into the cell: relevance to drug delivery. Cell Molecular Life Science 66:2873-2896 (2009).

126. L.M. Bareford and P.W. Swaan. Endocytic mechanisms for targeted drug delivery. Advanced Drug Delivery Reviews 59:748-758 (2007).

127. M.L. Forrest and D.W. Pack. On the kinetics of polyplex endocytic trafficking: implications for gene delivery vector design. Molecular Therapy. 6:57-66 (2002).

128. A.M. Funhoff, S. Monge, R. Teeuwen, G.A. Koning, N.M. Schuurmans-Nieuwenbroek, D.J. Crommelin, D.M. Haddleton, W.E. Hennink, and C.F. van Nostrum. PEG shielded polymeric double-layered micelles for gene delivery. Journal of Controlled Release. 102:711-724 (2005).

129. D.C. Drummond, C.O. Noble, M.E. Hayes, J.W. Park, and D.B. Kirpotin. Pharmacokinetics and in vivo drug release rates in liposomal nanocarrier development. Journal of Pharmaceutical Sciences. 97:4696-4740 (2008).

130. M.A. Baker, B.D. Gray, B.M. OhlssonWilhelm, D.C. Carpenter, and K.A. Muirhead. Zyn-Linked colchicines: c-release lipophilic prodrugs with enhanced antitumor efficacy. Journal of Controlled Release. 40:89-100 (1996).

131. F. Li, M. Danquah, and R.I. Mahato. Synthesis and characterization of amphiphilic lipopolymers for micellar drug delivery. Biomacromolecules. 11:2610-2620 (2010).

132. D. Sutton, S.H. Wang, N. Nasongkla, J.M. Gao, and E.E. Dormidontova. Doxorubicin and beta-lapachone release and interaction with micellar core materials: Experiment and modeling. Experimental Biology and Medicine. 232:1090-1099 (2007).

133. S.J. Lee, Y. Bae, K. Kataoka, D. Kim, D.S. Lee, and S.C. Kim. In vitro release and in vivo anti-tumor efficacy of Doxorubicin from biodegradable temperature-sensitive star-shaped PLGA-PEG block copolymer hydrogel. Polymer Journal. 40:171-176 (2008).

134. C. Washington. Evaluation of non-sink dialysis methods for the measurement of drug release from colloids: effects of drug partition. International Journal of Pharmaceutics. 56:71-74 (1989).

135. C. Washington. Drug release from microdisperse systems: a critical review. International Journal of Pharmaceutics. 58:1-12 (1990).

136. S. Modi and B.D. Anderson. Determination of drug release kinetics from nanoparticles: overcoming pitfalls of the dynamic dialysis method. Molecular Pharmaceutics. 10:3076-3089 (2013).

137. G. Moreno-Bautista and K.C. Tam. Evaluation of dialysis membrane process for quantifying the in vitro drug-release from colloidal drug carriers. Colloids and Surfaces A: Physicochemical and Engineering Aspects. 389:299-303 (2011).

138. P.K. Gupta, C.T. Hung, and D.G. Perrier. Quantitation of the release of Doxorubicin from colloidal dosage forms using dynamic dialysis. Journal of Pharmaceutical Sciences. 76:141-145 (1987).

139. O. Gavet and J. Pines. Progressive activation of CyclinB1-Cdk1 coordinates entry to mitosis. Developmental Cell. 18:533-543 (2010).

140. J. Rejman, V. Oberle, I.S. Zuhorn, and D. Hoekstra. Size-dependent internalization of particles via the pathways of clathrin- and caveolae-mediated endocytosis. The Biochemical Journal. 377:159-169 (2004).

141. D. Scott, J. Rohr, and Y. Bae. Nanoparticulate formulations of Mithramycin analogs for enhanced cytotoxicity. International Journal of Nanomedicine. 6:2757-2767 (2011).

142. S. Akter, B.F. Clem, H.J. Lee, J. Chesney, and Y. Bae. Block copolymer micelles for controlled delivery of glycolytic enzyme inhibitors. Pharmaceutical Research. 29:847-855 (2012).

143. F.M. Veronese, O. Schiavon, G. Pasut, R. Mendichi, L. Andersson, A. Tsirk, J. Ford, G.F. Wu, S. Kneller, J. Davies, and R. Duncan. PEG-Doxorubicin conjugates: Influence of polymer structure on drug release, in vitro cytotoxicity, biodistribution, and antitumor activity. Bioconjugate Chemistry. 16:775-784 (2005).

144. K.H. Min, H.J. Lee, K. Kim, I.C. Kwon, S.Y. Jeong, and S.C. Lee. The tumor accumulation and therapeutic efficacy of Doxorubicin carried in calcium phosphate-reinforced polymer nanoparticles. Biomaterials. 33:5788-5797 (2012).

145. P.J. Chikhale, E. Marvanyos, and N.S. Bodor. Improved delivery through biological membranes. LXI: Design, synthesis, and evaluation of a lipolol-based intradermal drug targeting system for 5-fluorouracil. Cancer Biotherapy. 9:245-252 (1994).

146. Y. Takakura and M. Hashida. Macromolecular carrier systems for targeted drug delivery: pharmacokinetic considerations on biodistribution. Pharmaceutical Research 13:820-831 (1996).

147. P. Cao and Y. Bae. Comparison between microplate spectrometry and LC/MS chromato-graphy for facile pilot pharmacokinetics and biodistribution studies of Doxorubicin-loaded nanoparticle drug carriers. Journal of Applied Pharmaceutical Science. 2:1-9 (2012).

148. Y. Tsukioka, Y. Matsumura, T. Hamaguchi, H. Koike, F. Moriyasu, and T. Kakizoe. Pharmaceutical and biomedical differences between micellar Doxorubicin (NK911) and liposomal Doxorubicin (Doxil). Japanese Journal of Cancer Research. 93:1145-1153 (2002).

149. M. Yokoyama, M. Miyauchi, N. Yamada, T. Okano, Y. Sakurai, K. Kataoka, and S. Inoue. Characterization and anticancer activity of the micelle-forming polymeric anticancer drug Adriamycin-conjugated poly(ethylene glycol)-poly(aspartic acid) block copolymer. Cancer Research 50:1693-1700 (1990).

150. R.L. Jones, C. Swanton, and M.S. Ewer. Anthracycline cardiotoxicity. Expert Opinion on Drug Safety. 5:791-809 (2006).

151. G. Minotti, P. Menna, E. Salvatorelli, G. Cairo, and L. Gianni. Anthracyclines: molecular advances and pharmacologic developments in antitumor activity and cardiotoxicity. Pharmacological Reviews. 56:185-229 (2004).

152. F. Danhier, O. Feron, and V. Preat. To exploit the tumor microenvironment: Passive and active tumor targeting of nanocarriers for anti-cancer drug delivery. Journal of Controlled Release. 148:135-146 (2010).

153. T.C. Lai, Y. Bae, T. Yoshida, K. Kataoka, and G.S. Kwon. pH-sensitive multi-PEGylated block copolymer as a bioresponsive pDNA delivery vector. Pharmaceutical Research. 27:2260-2273 (2010).

154. D. Putnam and J. Kopecek. Polymer conjugates with anticancer activity. Advances in Polymer Science. 122:55-123 (1995).

155. X. Yang, J.J. Grailer, S. Pilla, D.A. Steeber, and S. Gong. Tumor-Ttargeting, pH-responsive, and stable unimolecular micelles as drug nanocarriers for targeted cancer therapy. Bioconjugate Chemistry. 21:496–504 (2010).

156. M. Nogawa, T. Yuasa, S. Kimura, J. Kuroda, K. Sato, H. Segawa, A. Yokota, and T. Maekawa. Monitoring luciferase-labeled cancer cell growth and metastasis in different in vivo models. Cancer Letters. 217:243-253 (2005).

VITA

Andrei Gheorghe Ponta

Birthplace: Bucureşti, România

EDUCATION

2004 – 2008 B.S. Chemical Engineering, College of Engineering, The University of Alabama (Tuscaloosa, Alabama)

HONORS AND AWARDS

Dissertation Year Fellowship 2012 - 2013

Pre-Qual Graduate Student Scholarship Award 2010

PUBLICATIONS

6. P. Cao, **A. Ponta**, J. Kim, and Y. Bae. Block Copolymer Crosslinked Nanoassemblies Co-Entrapping Acridine Yellow and Doxorubicin for Cancer Theranostics. British Journal of Pharmaceutical Research. 3:525-535 (2013).

5. A. Eckman, E. Tsakalozou, N. Kang, **A. Ponta**, and Y. Bae. Drug Release Patterns and Cytotoxicity of PEG-poly(aspartate) Block Copolymer Micelles in Cancer Cells. Pharmaceutical Research. 29:1755-1767 (2012).

4. **A. Ponta**, S. Akter, and Y. Bae. Degradable Cross-Linked Nanoassemblies as Drug Carriers for Heat Shock Protein 90 Inhibitor 17-N-17-N-Allylamino-17-demethoxy-geldanamycin. Pharmaceuticals. 4:1281-1292 (2011).

3. M. Howard, **A. Ponta**, A. Eckman, M. Jay, and Y. Bae. Polymer Micelles with Hydrazone-Ester Dual Linkers for Tunable Release of Dexamethasone. Pharmaceutical Research. 28:2435-2446 (2011).

2. H.J. Lee, **A. Ponta**, and Y. Bae. Polymer nanoassemblies for Cancer Treatment and Imaging. Therapeutic Delivery. 1:803-817 (2010).

1. **A. Ponta** and Y. Bae. PEG-poly(amino acid) Block Copolymer Micelles for Tunable Drug Release. Pharmaceutical Research. 27:2330-2342 (2010).

INVITED TALKS

3. **A. Ponta** and Y. Bae. "Tunable Drug Release from Novel Polymer Micelles for Maximized Chemotherapeutic Efficacy." 4th Annual Biomaterials Day. September 22, 2012.

2. **A. Ponta** and Y. Bae. “Polymer Micelles Achieving Tunable Drug Release for Improved Cancer Chemotherapy.” Annual Symposium on Drug Discovery and Development. September 20, 2012.

1. **A. Ponta** and Y. Bae. “Polymer Nanoassemblies for Tunable Drug Release in Tumors.” Annual Symposium on Drug Discovery and Development. October 13, 2011.

PRESENTATIONS

National

11. **A. Ponta** and Y. Bae. “*In vitro* Efficacy of Doxorubicin Loaded Micelles Achieving Tunable Drug Release.” AAPS Annual Meeting and Exposition. October 18, 2012.

10. **A. Ponta** and Y. Bae. “*In vitro* Cytotoxicity of pH-Sensitive Micelles for Tunable Release of Doxorubicin.” The 38th Annual Meeting & Exposition of the Controlled Release Society. August 2, 2011.

9. **A. Ponta** and Y. Bae. “Micelle Forming PEG-poly(amino acid) Block Copolymers for Tunable pH-Sensitive Drug Release in Tumor Tissue.” AAPS Annual Meeting and Exposition. November 18, 2010.

8. M. Howard, **A. Ponta,** M. Jay, and Y. Bae. “pH-sensitive PEG-Poly(Amino Acid) Block Copolymer Micelles for Tumor-Targeted Delivery of Dexamethasone.” AAPS Annual Meeting and Exposition. November 15, 2010.

7. A. Eckman, **A. Ponta**, and Y. Bae. “Drug-loading Efficiency of PEG-poly(amino acid) Polymer Micelles with Different Core Environment.” AAPS Annual Meeting and Exposition. November 15, 2010.

6. **A. Ponta** and Y. Bae. “Block Copolymer Micelles as Tunable pH-Sensitive Drug Delivery Carriers.” The 37th Annual Meeting & Exposition of the Controlled Release Society. July 14, 2010.

5. **A. Ponta** and Y. Bae. “pH-Sensitive PEG-poly(amino acid) Block Copolymer Micelles for Tunable Drug Release.” AAPS National Biotechnology Conference. May 17, 2010.

4. **A. Ponta** and Y. Bae. “Tunable Release of Doxorubicin in Cancer Tumors Using Polymeric Micelles.” Society for Biomaterials Annual Meeting and Exposition. April 22, 2010.

3. **A. Ponta** and Y. Bae. “Polymeric Micelles for Tunable Combination Release of Multiple Drugs in Cancer Tumors.” AAPS Annual Meeting and Exposition. November 11, 2009.

2. D. Lindsay, **A. Ponta**, Z. Hilt, and Y. Bae. “Grafted Block Copolymer Nanoassembly Drug Carrier.” AIChE Annual Meeting. November 9, 2009.

1. **A. Ponta**, I. Ankareddi, and C.S. Brazel. “Mechanical Analysis of Thermosensitive Hydrogels for Drug Delivery.” AIChE Annual Meeting. November 17, 2007.

Local

11. **A. Ponta** and Y. Bae “PEG-poly(amino acid) Micelles Capable of Fine-Tuning Drug Release at the Tumor Site for Improved Cancer Chemotherapy.” Markey Cancer Center Research Day. April 15, 2013.

10. **A. Ponta** and Y. Bae. “Tunable Release of Doxorubicin from PEG-poly(amino acid) Micelles.” Center for Clinical and Translational Science Conference. April 21, 2011.

9. A. Eckman, **A. Ponta**, and Y. Bae. “Core Environment Influence of PEG-poly(Aspartate) Block Copolymer Micelles Entrapping Doxorubicin.” Center for Clinical and Translational Science Conference. April 21, 2011.

8. A. Eckman, **A. Ponta**, and Y. Bae. “Core Environment Influence of PEG-poly(Aspartate) Block Copolymer Micelles Entrapping Doxorubicin.” Markey Cancer Center Research Day. March 22, 2011.

7. **A. Ponta** and Y. Bae. “Tunable Release of Doxorubicin from PEG-poly(amino acid) Micelles.” Markey Cancer Center Research Day. March 22, 2011.

6. **A. Ponta** and Y. Bae. “Micelle Forming PEG-poly(amino acid) Block Copolymers for Tunable pH-Sensitive Drug Release in Tumor Tissue.” PWSC Congress for Students and Postdoctoral Fellows. November 13, 2010.

5. E. Tsakalozou, **A. Ponta**, M. Leggas, and Y. Bae. “Heat Shock Protein 90 Mediate Chemotherapeutic Synergy in Prostate Cancer.” Markey Cancer Center Research Day. April 14, 2010.

4. **A. Ponta** and Y. Bae. “Polymeric Micelles for Tunable Release of Doxorubicin in Cancer Tumors.” 1st Annual Biomaterials Day. September 25, 2009.

3. **A. Ponta**, I. Ankareddi, and C.S. Brazel. “Mechanical Analysis of Thermosensitive Hydrogels for Drug Delivery.” 1st Annual UA Undergraduate Research and Creative Activities Conference. April 21, 2008.

2. I. Ankareddi, A**. Ponta**, A. Shamsuzzoha, and C.S. Brazel. “Positive Thermoresponsive Grafted Hydrogels for Heating-Activated Drug Delivery.” ACS Spring National Meeting & Exposition. April 7, 2008.

1. **A. Ponta**, I. Ankareddi, and C.S. Brazel. “Mechanical Analysis of Thermosensitive Hydrogels for Drug Delivery.” AIChE Southern Regional Conference. April 5, 2008.